

AD-A198 686

2

MONTE CARLO ANALYSIS OF QUANTUM
TRANSPORT AND FLUCTUATIONS IN
SEMICONDUCTORS II

Final Technical Report

by

Prof. Carlo Jacoboni, Prof. Lino Reggiani,
Prof. Paolo Lugli, Dr. Rossella Brunetti

February 1988

United States Army
EUROPEAN RESEARCH OFFICE of the U.S. Army
London - England

Contract Number DAJA45-86-C-0004
Principal Investigator Prof. Carlo Jacoboni

Approved for Public Release, distribution unlimited

DTIC
ELECTE
S AUG 11 1988 D
E

1

UNCLASSIFIED
SECURITY CLASSIFICATION OF THIS PAGE

ADA198686

REPORT DOCUMENTATION PAGE				Form Approved OMB No 0704-0188 Exp Date Jun 30, 1986	
1a REPORT SECURITY CLASSIFICATION Unclassified			1b RESTRICTIVE MARKINGS		
2a SECURITY CLASSIFICATION AUTHORITY			3 DISTRIBUTION/AVAILABILITY OF REPORT Approved for public release; distribution unlimited		
2b DECLASSIFICATION/DOWNGRADING SCHEDULE					
4 PERFORMING ORGANIZATION REPORT NUMBER(S)			5 MONITORING ORGANIZATION REPORT NUMBER(S) R&D 5152-EE-01		
6a NAME OF PERFORMING ORGANIZATION Universita di Modena		6b OFFICE SYMBOL (if applicable)		7a NAME OF MONITORING ORGANIZATION USARDSG-UK	
6c ADDRESS (City, State, and ZIP Code) Dipartimento di Fisica, Via G. Campi 213/A, 41100 Modena, Italy/			7b ADDRESS (City, State, and ZIP Code) Box 65 FPO NY 09510 1500		
8a NAME OF FUNDING/SPONSORING ORGANIZATION USARDSG-UK ARO-E		8b OFFICE SYMBOL (if applicable)		9 PROCUREMENT INSTRUMENT IDENTIFICATION NUMBER DAJA45-86-C-0004	
8c ADDRESS (City, State, and ZIP Code) Box 65 FPO NY 09510-1500			10. SOURCE OF FUNDING NUMBERS		
			PROGRAM ELEMENT NO 61102A	PROJECT NO 1L161102BH	TASK NO 7 03
11 TITLE (Include Security Classification) (U) Monte Carlo Analysis of Quantum Transport and Fluctuations in Semiconductors					
12 PERSONAL AUTHOR(S) Professor C. Jacoboni					
13a. TYPE OF REPORT Final		13b TIME COVERED FROM Feb 85 TO Feb 88		14 DATE OF REPORT (Year, Month, Day) February 1988	
15 PAGE COUNT 99					
16. SUPPLEMENTARY NOTATION					
17. COSATI CODES			18 SUBJECT TERMS (Continue on reverse if necessary and identify by block number)		
FIELD	GROUP	SUB-GROUP	Elec Equip, Sol State Physics		
09	01				
20	12				
19. ABSTRACT (Continue on reverse if necessary and identify by block number)					
<p>>The first topic treated is quantum transport. Two major lines of research have been investigated: the first is based on the introduction of the joint spectral density into a traditional Monte Carlo simulation; the second regards the formulation of a fully quantum mechanical approach for electron transport based on the density matrix approach.</p> <p>The second deals with treats noise, diffucion, and autocorrelation functions both from a theoretical and a simulative point of view. Results have been obtained for both bulk systems and quantum wells.</p> <p>The third topic concerns with an analysis of the effect of phonon populations in excess with respect to their thermal equilibrium values. Numerical Monte Carlo simulations have been performed for both GaAs and GaAs-AlGaAs quantum wells.</p>					
20. DISTRIBUTION/AVAILABILITY OF ABSTRACT <input checked="" type="checkbox"/> UNCLASSIFIED/UNLIMITED <input checked="" type="checkbox"/> SAME AS RPT <input checked="" type="checkbox"/> DTIC USERS			21 ABSTRACT SECURITY CLASSIFICATION Unclassified		
22a NAME OF RESPONSIBLE INDIVIDUAL Dr. John M. Zavada			22b TELEPHONE (Include Area Code) 01-409 4423		22c OFFICE SYMBOL AMXSN-UK-RI

DD FORM 1473, 84 MAR

83 APR edition may be used until exhausted
All other editions are obsolete

SECURITY CLASSIFICATION OF THIS PAGE

Unclassified

ABSTRACT

The contents of this report concern with the work developed at the Department of Physics of the University of Modena under the Contract DAJA45-86-C-0004.

The first topic treated is quantum transport. Two major lines of research have been investigated: the first is based on the introduction of the joint spectral density into a traditional Monte Carlo simulation; the second regards the formulation of a fully quantum mechanical approach for electron transport based on the density matrix approach.

The second deals with treats noise, diffusion, and autocorrelation functions both from a theoretical and a simulative point of view. Results have been obtained for both bulk systems and quantum wells.

The third topic concerns with an analysis of the effect of phonon populations in excess with respect to their thermal equilibrium values. Numerical Monte Carlo simulations have been performed both for GaAs and for GaAs-AlGaAs quantum wells.

List of Keywords

Autocorrelation Function - Boltzmann equation - Collisional Broadening -
 Density Matrix - Diffusion Coefficient - Electron Photoexcitation -
 Electron Transport - Fluctuation - Hot Electrons - Hot Phonons -
 Intercollisional Field Effect - Liouville-von Neumann equation -
 Monte Carlo Simulations - Noise - Quantum Wells - Semiconductors -
 Spectral Density - Transient Transport -

Accession For	
NTIS GRA&I	<input checked="" type="checkbox"/>
DTIC TAB	<input type="checkbox"/>
Unannounced	<input type="checkbox"/>
Justification	
By _____	
Distribution/	
Availability Codes	
Dist	Avail and/or Special
A-1	



CONTENTS

1. INTRODUCTION	1
2. QUANTUM TRANSPORT	4
2.1 Inclusion of the Spectral Density in the conventional Monte Carlo Approach	4
2.1.1 Introduction	4
2.1.2 Model	5
2.1.3 The Spectral Density	7
2.1.4 Applications	7
2.1.4.1 Free Electrons with ICFE	8
2.1.4.2 Collisional Broadening	10
2.1.5 Numerical Calculations	12
2.1.6 Conclusions	14
2.2 A Monte Carlo Approach to the Solution of the Liouville- von Neumann Equation for Quantum Transport	15
2.2.1 Introduction	15
2.2.2 Physical System and Theoretical Approach	17
2.2.3 Numerical Procedure	22
2.2.4 Results	25
2.2.4.1 Analysis of the First and the Second Order in Presence of Electric Fields	25
2.2.4.2 Quantum Energy Relaxation of Photoexcited	

Carriers in Absence of Electric Fields	28
2.2.5 Semiclassical Limit: Backword Monte Carlo	
Procedure	30
2.2.5.1 The Method	31
2.2.5.2 Results	34
References	36
Figure Captions	38
Figures	41
Tables	41b
 3. CORRELATION FUNCTIONS OF HOT ELECTRONS	 42
3.1 Correlation Functions for Bulk Semiconductors	42
3.1.1 Introduction	42
3.1.2 Equations of Motion for a Closed Set of Correlation Functions	42
3.1.3 Numerical Results	45
3.1.4 Microscopic Expression of the Noise Temperature	47
3.2 Correlation Functions for Quantum Wells	48
3.2.1 Introduction	48
3.2.2 Autocorrelation Function, Diffusion, and Noise in	
Stationary Conditions	50
3.2.3 Autocorrelation Function and Diffusion in Transient Conditions	53
3.2.4 The Physical System and the Monte Carlo Procedure	54
3.2.5 Results for Stationary Conditions	55
3.2.6 Results for Transient Conditions	58
References	61
Figure Captions	63
Figures	65

4. MONTE CARLO STUDIES OF NON-EQUILIBRIUM	
PHONON EFFECTS	66
4.1 Introduction	66
4.2 The Transport Model and The Monte Carlo Algorithm	67
4.3 Applications	74
4.4 Conclusions	81
References	83
Figure Captions	85
Figures	87

1. INTRODUCTION

This report presents technical matter related to the research performed at the Department of Physics of the University of Modena for the Contract Number DAJA45-86-C-0004 "Monte Carlo Analysis of Quantum Transport and Fluctuations in Semiconductors". Such a Contract follows a similar Contract with the same title relative to the period 1983/85.

In the Final Technical Report of that first Contract we reported a general review of quantum approaches to charge transport in semiconductors; we therefore refer to that review for general references and for introductory treatment of quantum transport.

In the present report we shall limit ourselves to the results of the research performed under the Contract to which it relates. For the sake of completeness, however, we shall sometimes include some materials developed during the first part of this research.

In the presentation we shall follow the same order as in the Work Statement of the Contract. In particular, Chapters 2, 3, and 4 refer to the points 1, 2, and 3 listed as Objectives of the Research.

As it regards quantum transport, two major lines of activity have been followed. In one of them, described in Sec.2.1, the traditional Monte Carlo approach has been extended to include the quantum features that could be represented by the use of the joint spectral density in the transition probabilities. The theory at the basis of this extension has been developed to a certain level of detail in general, and in some special cases it has been fully developed up to the realization of Monte Carlo codes for simple-model semiconductors (Secs. 2.1.4, 2.1.5).

In the second approach a method is developed for the numerical solution of the Liouville-von Neumann equation that describes electron transport in

semiconductors in a fully quantum mechanical formulation. The problem has been solved in principle, but the amount of computations necessary to obtain the results for real cases of interest is still very large. The method is presented in Sec.2.2. Two applications have been considered in particular: the analysis of the effect of multiple collisions and of intra-collisional field effect in presence of high applied electric fields (Sec.2.2.4.1), and the analysis of the energy relaxation of photoexcited electrons in absence of external fields (Sec.2.2.4.2).

A comparison of the two approaches presented in this report should stress that the first one requires little modifications of the traditional Monte Carlo technique, but some more investigations are required to understand how much of the quantum features of electron transport it will be able to describe; the second approach is more rigorous, but further analytical developments are required if we want it to be useful for practical calculations.

As it regards the analysis of correlation functions of hot electrons (Chapter 3), two major lines of research have again been followed.

In the first work (Sec.3.1), explicit formulae have been obtained for the time evolution of the velocity correlation functions which generalize the linear-response theory to conditions far from equilibrium.

The second line of research (Sec. 3.2) has investigated the velocity correlation function of electrons in semiconductor quantum wells under high applied electric fields both in transient and in steady-state conditions.

Hot phonons, i.e. phonon populations in excess with respect to their thermal-equilibrium values, can be obtained by means of the application of strong electric fields or by photoexcited high-energy electrons with laser pulses. This subject has recently collected large interest and debates. Chapter 4 contains the description of the method developed by our group for a simultaneous

simulation of electron and phonon transport in bulk semiconductors and quantum wells. Several applications are discussed in details for bulk GaAs and for GaAs-AlGaAs quantum wells. Good qualitative agreement with Raman experimental data is obtained.

2. QUANTUM TRANSPORT

2.1 Inclusion of the Spectral Density in the conventional Monte Carlo Approach

2.1.1 Introduction

The fast development in the field of submicron devices has provided a renewed interest in the theory of electron transport beyond the free-particle approach based on the semiclassical Boltzmann equation. Indeed, quantum theory has indicated that a proper treatment of high-field transport in semiconductors should include the intra collisional field effect (ICFE) as well as collisional broadening (CB) [2.1].

ICFE accounts for the presence of the electric field in the collision operator of the kinetic equation. In other words, a scattering event does not occur between states described by the plane waves of a free electron, but between those of an electron in the field. Introduced by Levinson and Yasevichyute [2.2], ICFE has subsequently been investigated by many researchers [2.3 - 11].

Since the total Hamiltonian H is not the same as that of the perfect crystal, an electron in a state with wave vector \mathbf{k} is not in an eigenstate of H and does not correspond to a well defined energy $\hbar\omega$, but to a broad interval of energies associated to \mathbf{k} . The spectral function $A(\mathbf{k}, \omega)$ gives the probability that an electron in state \mathbf{k} is found with energy $\hbar\omega$. It is possible to show that $A(\mathbf{k}, \omega)$ represents also the probability that an electron with energy $\hbar\omega$ is found in state \mathbf{k} [2.12,13].

The effective mass model is recovered when $A(\mathbf{k}, \omega) = 2\pi\delta(\hbar^2 k^2/2m - \hbar\omega)$. CB in the context of high-field transport in semiconductors was described in detail by Barker [2.14] and its importance within a Monte Carlo simulation was firstly pointed out by Capasso et al [2.15].

Since then, several research groups [2.16 - 24] have attempted to estimate the importance of these effects by suitable generalizations of standard Monte Carlo algorithms. However, the technical details have been scarcely documented. As a consequence, it has been practically impossible for anyone outside a given research group to reproduce quantitatively the results obtained by other groups. This, in turn, has led to contradictory findings and difficulties in objectively assessing the significance of the various quantum effects, and in judging the relative merits of various calculations.

The main objective of this section is thus to present the theoretical framework and the details of two Monte Carlo algorithms which we have used to estimate ICFE and CB effects within a simple model semiconductor. Our scheme is based on a quantum kinetic equation we have recently derived [2.25], and which accounts for quantum effects through the introduction of the joint spectral density $K(\epsilon_i, \epsilon_f)$ describing the connection between the initial, ϵ_i , and final, ϵ_f , kinetic energy of the carrier during a single scattering process. (Let us remark that we are within the so called completed collision regime [2.11.25], which enables us to construct time-independent scattering rates). The joint spectral density reduces to the well known delta function behavior when ICFE or CB are neglected. Therefore, the present scheme yields the correct semiclassical Boltzmann limit. One of the objective of our study is to provide a first standard on the subject which hopefully will be of general use and open to further improvements.

2.1.2 Model

The theory is formulated in terms of the Generalized Kadanoff-Baym approach [2.26, 27]. Our physical model is based on the following assumptions:

- (i) One isotropic band;
- (ii) Time independent and space homogeneous conditions;

- (iii) An ansatz which links the single particle Wigner distribution function $f(\mathbf{k})$ to the full correlation function $G^<(\mathbf{k}, t)$ [2.28] ($G^<(\mathbf{k}, t) = iA(\mathbf{k}, t)f(\mathbf{k} - \frac{e\mathbf{E}}{2\hbar}|t|)$);
 (iv) Completed collisions limit.

Within this model, the quantum kinetic Boltzmann equation for $f(\mathbf{k})$ writes [2.25]:

$$f(\mathbf{k}) = \int d\mathbf{k}' \int_0^\infty dt \left[W^{QM}(\mathbf{k}' - e\mathbf{E}t/\hbar, \mathbf{k} - e\mathbf{E}t/\hbar) f(\mathbf{k}' - e\mathbf{E}t/\hbar) - W^{QM}(\mathbf{k} - e\mathbf{E}t/\hbar, \mathbf{k}' - e\mathbf{E}t/\hbar) f(\mathbf{k} - e\mathbf{E}t/\hbar) \right] \quad (2.1)$$

The scattering probability per unit time W^{QM} , for electron phonon interactions, is given by:

$$W^{QM}(\mathbf{k}_1, \mathbf{k}_2) = \sum_{\eta=\pm 1} |V(q)|^2 (N_q + \frac{1}{2} + \frac{1}{2}\eta) K(\mathbf{k}_1, \mathbf{k}_2) \quad (2.2)$$

where $K(\mathbf{k}_1, \mathbf{k}_2)$ is the joint spectral density of the quasi particle which, in the self-consistent Born approximation, is given by:

$$K(\mathbf{k}_1, \mathbf{k}_2) = \int_0^\infty dt' 2\text{Re} \left\{ A(\mathbf{k}_1 + \frac{e\mathbf{E}}{2\hbar}t', t') A(\mathbf{k}_2 + \frac{e\mathbf{E}}{2\hbar}t', -t') \exp(-i\eta\omega_q t') \right\} \quad (2.3)$$

The description of the physical processes is based on a quasi-particle picture, where \mathbf{k} and \mathbf{k}' are the quasi particle kinetic momenta before and after a scattering event, $q = |\mathbf{k} - \mathbf{k}'|$ is the transferred momentum, \mathbf{E} is the external applied electric field, $|V(q)|^2$ the square of the matrix element for electron phonon collision, N_q the equilibrium phonon population, $\hbar\omega_q$ the phonon energy involved in the collision, with $\eta = \pm 1$ referring respectively to emission and absorption processes.

The joint spectral density $K(\mathbf{k}_1, \mathbf{k}_2)$ is the central quantity in our approach, since it enables us to account for quantum corrections of the otherwise semiclassical free-particle picture.

2.1.3 The Spectral Density

In the framework of a many-body approach which uses a the Green function formalism [2.29], the spectral density is defined as:

$$A(\mathbf{k}, t) = i[G^r(\mathbf{k}, t) - G^a(\mathbf{k}, t)] \quad (2.4)$$

where $G^{r,a}(\mathbf{k}, t)$ is the retarded (advanced) Green function, respectively.

In the presence of a steady external electric field \mathbf{E} and of collisions, $G^r(\mathbf{k}, t)$ obeys the Dyson's equation which, when expressed in terms of gauge invariant variables, has the form:

$$G^r(\mathbf{k}, t) = G_E^r(\mathbf{k}, t) + \int \int dt_1 dt_2 G_E^r(\mathbf{k} - \frac{e\mathbf{E}}{2\hbar}(t - t_1), t_1) \times \\ \times \Sigma^r(\mathbf{k} - \frac{e\mathbf{E}}{2\hbar}(t_2 - t_1), t - (t_1 + t_2)) G^r(\mathbf{k} - \frac{e\mathbf{E}}{2\hbar}(t_2 - t), t_2). \quad (2.5)$$

$\Sigma^r(\mathbf{k}, t)$ is the retarded self energy. The field dependent retarded Green function $G_E^r(\mathbf{k}, t)$ is given by [2.26]:

$$G_E^r(\mathbf{k}, t) = -i\theta(t) \exp \left[-i \int_{-t/2}^{t/2} du \epsilon(\mathbf{k} - e\mathbf{E}u/\hbar) \right] \quad (2.6)$$

where $\theta(t)$ is the unit step function, and ϵ is the carrier kinetic energy.

An equivalent formulation of Eqs.(2.4-6) in the frequency domain can be easily obtained through a Fourier transformation.

2.1.4 Applications

In the following, the explicit expressions for $K(\mathbf{k}, \mathbf{k}') = K(\epsilon_i, \epsilon_f)$ will be given for the case of ICFE and CB.

2.1.4.1 Free Electrons with ICFE

For free electrons in the presence of an external electric field \mathbf{E} the joint spectral density is given by [2.30]:

$$K(\epsilon_i, \epsilon_f) = \left(\frac{\pi}{|Q|}\right)^{\frac{1}{2}} \left\{ \cos\left(\frac{P^2}{2|Q|}\right) \left[1 - 2C\left(\frac{PQ}{(2|Q|^3)^{\frac{1}{2}}}\right)\right] + \sin\left(\frac{P^2}{2|Q|}\right) \left[1 - 2S\left(\frac{PQ}{(2|Q|^3)^{\frac{1}{2}}}\right)\right] \right\} \quad (2.7)$$

with

$$P = \epsilon_f - \epsilon_i + \hbar\omega_q; \quad Q = -\frac{\hbar^2}{m} \mathbf{e}_q \cdot \mathbf{E}, \quad (2.8)$$

where $C = C(z)$ and $S = S(z)$ are the Fresnel integrals given by:

$$C(z) = \left(\frac{2}{\pi}\right)^{\frac{1}{2}} \int_0^z dt \cos(t^2); \quad S(z) = \left(\frac{2}{\pi}\right)^{\frac{1}{2}} \int_0^z dt \sin(t^2). \quad (2.9)$$

Because of the presence of fast oscillations associated to the Fresnel integrals in Eq. (2.9) $K(\epsilon_i, \epsilon_f)$ in the form of Eq.(2.7) cannot be used directly in a Monte Carlo scheme which requires a positive definite quantity. As suggested by Barker [2.3], a plausible way of suppressing the oscillations (whose tails integrate to zero) is to approximate the expression (2.7) with a Lorentzian function. In order to preserve normalization and control the low and high energy tails we use a truncation procedure: $K(\epsilon_i, \epsilon_f) = 0$ for $\epsilon_f \leq 0$ and $\epsilon_f \geq \bar{\epsilon}_f$, where $\bar{\epsilon}_f$ is a cut-off energy. Thus, Eq. (2.7) is approximated by the following expression:

$$K(\epsilon_i, \epsilon_f) = \frac{1}{|\beta|^{1/2}} \frac{A}{1 + (x_i - x_f - x_0 - \pi \frac{\beta}{|\beta|})^2} \quad (2.10)$$

where

$$A = [\arctg(\bar{x}_f - x_i + x_0 + \pi \frac{\beta}{|\beta|}) - \arctg(x_0 - x_i + \pi \frac{\beta}{|\beta|})]^{-1} \quad (2.11)$$

$$\beta = \frac{e\hbar E}{\pi(2m^*)^{1/2}} (x_f^{1/2} \cos\theta_f - x_i^{1/2} \cos\theta_i) \quad (2.12)$$

Here θ_i and θ_f are respectively the initial and final angles of \mathbf{k}_i and \mathbf{k}_f with respect to the electric field \mathbf{E} and we introduce dimensionless energies by $x_i = \epsilon_i/|\beta|^{1/2}$, $x_f = \epsilon_f/|\beta|^{1/2}$, $\bar{x}_f = \bar{\epsilon}_f/|\beta|^{1/2}$, $x_0 = \hbar\omega_0/|\beta|^{1/2}$. The final state x_f can be obtained by applying the direct technique [2.31] to Eq. (2.10). Once x_i , x_0 , \bar{x}_f and β are given, x_f is then found by generating random numbers r , evenly distributed between (0,1), and using:

$$x_f = (x_i - x_0 - \pi \frac{\beta}{|\beta|}) - \text{tg}[\text{arctg}(x_i - x_0 - \pi \frac{\beta}{|\beta|}) - \frac{r}{A}]. \quad (2.13)$$

Figures 2.1 - 2.3 show the joint spectral densities as obtained from Eq. (2.7) (continuous curves) and the approximate expression (2.10) (dashed curves). As is seen from Fig. 2.1 and 2.2, the presence of ICFE results in a broadening and skewing of the original delta function. The skewness depends on the direction of \mathbf{q} with respect to \mathbf{E} and the broadening can be so large that the final kinetic energy of a carrier may be greater than the initial one, even if a phonon emission process has occurred. (Note that for illustrative purposes in the figures we have chosen the maximum q available in the process.) By decreasing the electric field strength, the skewness and broadening reduce and the oscillations become faster. Both Eqs. (2.7) and (2.11) recover a delta function shape for $E = 0$. We point out that by generating 10^4 random numbers according to Eq.(2.13) the distribution of x_f is found to coincide with Eq. (2.11).

To introduce ICFE into a Monte Carlo program we suggest the following procedure:

If \mathbf{k}_i is the wave vector before scattering then:

- (a) generate the direction of the final \mathbf{k}_f assuming isotropic distribution;
- (b) evaluate the magnitude of k_f as in the absence of ICFE;
- (c) evaluate β using the k_f as in the absence of ICFE;
- (d) generate x_f from Eq. (2.13) and determine k_f in the presence of ICFE accordingly.

The above procedure contains two weak points. First, the k_f used to calculate β is not consistent with the final k_f and second, we must fix \bar{x}_f appropriately. The first point leads to an incorrect determination of the shift of $K(\epsilon_i, \epsilon_f)$ due to the electric field. However, since this shift is proportional to $q^{1/2}$ the error thus introduced should be practically irrelevant.

The second point is more serious. Allowing \bar{x}_f to approach infinity leads to carrier run-away and thus to a diverging mean kinetic energy, as evinced by our simulations. Since this point is common to CB as well, we will comment on it below.

2.1.4.2 Collisional Broadening

We shall confine our interest to the case where the scattering rate is a function of $\hbar\omega$ only, because this is the only case that can be handled analytically (scattering with non-polar optical, intervalley, and acoustic phonons under elastic and energy-equipartition approximations are the corresponding cases of interest [2.32]). By taking the self energy in the lowest order in the electron-phonon coupling [2.17] we find [2.30]:

$$K(\epsilon_i, \epsilon_f) = \frac{1}{(\pi\gamma)^2} \left\{ \int_{2y_0}^{\infty} dy \frac{(y - y_0)^{1/2} (y - 2y_0)^{1/2} \theta(y_i - y_0) \theta(y_f - y_0)}{[(y - y_i)^2 + (y - y_0)][(y - y_0 - y_f)^2 + (y - 2y_0)]} \right. \\ \left. + \pi \frac{y_f^{1/2} \theta(y_i - y_0) \theta(y_0 - y_f) \theta(y_f)}{(y_0 + y_f - y_i)^2 + y_f} + \pi^2 \delta(y_0 + y_f - y_i) \theta(y_0 - y_i) \theta(y_0 - y_f) \right\} \quad (2.14)$$

where we use dimensionless energies, $y = \hbar\omega/\gamma^2$, $y_i = \epsilon_i/\gamma^2$, $y_f = \epsilon_f/\gamma^2$, $y_0 = \hbar\omega_0/\gamma^2$, $\hbar\omega_0$ is the optical phonon energy. The parameter γ represents the coupling strength in energy units. It is related to the usual deformation

potential constant $D_t K$ [2.32] by $[\gamma = m^{3/2}(D_t K)^2 / (2^{5/2} \pi \rho \hbar^2 \omega_0)]$, where ρ is the density of the material.

The joint spectral density of Eq. (2.14) is positive definite but it exhibits a long tail for positive energies, where it decays as $\epsilon_f^{-3/2}$. An analytical expression which approximates Eq. (2.14) accurately for $y_i \gg y_0$ (typically $y_i \geq 5y_0$), and controls the low and high energy tails ($K(\epsilon_i, \epsilon_f) = 0$ for $y_f \leq 0$ and $y_f \geq \bar{y}_f$, $\bar{y}_f = \bar{\epsilon}_f / \gamma^2$) is given by:

$$K(\epsilon_i, \epsilon_f) = \frac{1}{\gamma^2} B \left[\frac{2y_i^{1/2}}{(y_i - y_f - y_0)^2 + 4y_i} \right] \quad (2.15)$$

with

$$B = \left[\arctg\left(\frac{y_i - y_0}{2y_i^{1/2}}\right) - \arctg\left(\frac{y_i - \bar{y}_f - y_0}{2y_i^{1/2}}\right) \right]^{-1} \quad (2.16)$$

We find the final state y_f , once y_i , y_0 and \bar{y}_f are given, by generating y_f as:

$$y_f = y_i - y_0 + 2y_i^{1/2} + \left[\frac{r}{B} - \arctg\left(\frac{y_i - y_0}{2y_i^{1/2}}\right) \right] \quad (2.17)$$

where r is a random number uniformly distributed between (0,1).

Figures 2.4 - 6 show the joint spectral densities as obtained from Eq. (2.14) (continuous curves) and the approximate expression (2.15) (dashed curves). As a general trend the approximation improves for increasing values of the initial kinetic energy (see Figs. 2.4 and 2.5). As can be seen from Figs. 2.5 and 2.6, the broadening increases for increasing γ values, and it gives rise to carrier run-away as in the case of ICFE. We point out that by generating 10^4 random numbers according to Eq. (2.17) the distribution of y_f is found to coincide with Eq. (2.16).

To introduce CB into a Monte Carlo program we suggest the following procedure.

If k_i is the wave vector before scattering, then:

- (i) generate the direction of the final \mathbf{k}_f assuming isotropic distribution;
- (ii) generate y_f from Eq. (2.17) and determine k_f accordingly.

The above procedure requires an appropriate choice for \bar{y}_f just as was the case of ICFE.

2.1.5 Numerical Calculations

To investigate the main features of ICFE and CB we have performed Monte Carlo simulations using 10^4 electrons for the simple model semiconductor characterized by the three parameters $m = 0.3m_0$ (m_0 is the free electron mass), $\hbar\omega_0 = 40\text{meV}$ and $\gamma^2 = 1.1\text{meV}$. The choice of these values can be considered as typical for several cubic semiconductors. As a plausible choice, we have taken the cut-off energy in dimensionless units as $\bar{x}_f = 2x_i$ for ICFE and $\bar{y}_f = 2y_i$ for CB, respectively.

Figures 2.7 to 2.10 display the energy distribution functions as obtained in the presence of ICFE alone and CB alone for various different electric field strengths. For the sake of comparison, we have also given the results for the semiclassical case (SC) obtained by using a delta function for the joint spectral density. (In order to facilitate a detailed comparison all the curves show the direct Monte Carlo results).

For the high electric fields (500 and 100 kV/cm) the presence of ICFE and CB is found to strongly increase the number of carriers in the high energy tail of the electron distribution with respect to the SC case. We have also found that, in general, CB is responsible for an increase in the population of the lower energy region of the distribution function, while ICFE evidences an opposite effect. At these high fields, the SC model is characterized by a heated Maxwell-Boltzmann distribution, as expected within the quasi elastic regime [2.32]. In particular, we notice that, for the present choice of parameters, ICFE gives a slightly larger effect than CB.

For the low electric fields (10 and 5 kV/cm), the calculations show that the effect of ICFE and CB becomes negligible (see Figs. 2.9 and 2.10), apart for some minor effects of ICFE in the lower energy tail of the distribution probably due to the approximate expression (2.13) used. At these low fields, the SC model approaches the streaming motion regime [2.32], where the distribution function sharply drops to zero for kinetic energies larger than the optical phonon energy.

Figure 2.11 shows the distribution of the energy difference between states before and after a scattering event ($\Delta\epsilon = \epsilon_i - \epsilon_f$). With respect to the SC case, for which $\Delta\epsilon = \hbar\omega_0$, both ICFE and CB exhibit a broadened distribution which reflect the joint-spectral-density model used in the simulation. In particular, the two peaks for the case of ICFE are correlated to the skewness associated with the forward and backward directions of q with respect to E .

Table 2.1 summarizes the values of the mean kinetic energy, the drift velocity, and the maximum kinetic energy achievable by a carrier during a simulation for the different cases. At low fields SC and CB give the same results, within the numerical uncertainty, while ICFE gives a value which deviates for about 20%, with a larger mean energy and a smaller drift velocity than the SC case. These deviations should be attributed to the scarce reliability of the model spectral density at the lowest energies. At high fields the mean energy for ICFE and CB is significantly larger (over 50% at 500 kV/cm) than for the SC case, reflecting a higher population of the high energy tail of the distribution. Conversely, the drift velocity change is limited to slight deviations, about 15%. However, an increase in the value of the high energy cut-off $\bar{\epsilon}_f$ of the joint spectral density has been found to be responsible for a systematic increase in the mean kinetic energy. As a consequence, the maximum kinetic energy achievable by a carrier during a simulation also increases together with its numerical uncertainty, and it is clear that the computer time necessary for a simulation becomes unacceptably

long. This effect is shown in Table 2.2 for the case of ICFE at $E = 100kV/cm$. Analogous results have been found for the case of CB as well. Clearly this increase of the mean kinetic energy is associated with a larger population of the high energy tail of the distribution function. Therefore, we conclude that the choice of the high energy cut-off is important for a quantitative evaluation of the effects of both ICFE and CB. This is a crucial point for the present modeling and, in our opinion, it has affected all previous calculations [2.16 - 24]. Thus, physical justifications, which are outside the scope of this paper, are needed to overcome this drawback.

2.1.6 Conclusions

We have presented a theoretical framework which enables one to account for genuine quantum effects for the case of hot-electron transport in semiconductors. The main quantities of interest are the spectral density and the associated joint spectral density which can include ICFE as well as CB. After providing the general theory, analytical models for these quantities have been obtained in some cases of interest. When quantum effects are neglected, that is carriers behave as a free particle between two scatterings, the semiclassical Boltzmann picture with the collision term determined from the golden rule is recovered. We have presented two algorithms, compatible to standard Monte Carlo codes, for estimating quantum effects, such as intra-collisional field effects and collisional broadening, in semiconductor high-field transport. The basic feature of these algorithms is to model joint spectral densities replacing the Dirac function which, within a semiclassical approach, conserves the kinetic energy within a scattering event. The methodology chosen by us has been given with details, so that it may constitute a first standard which can be easily reproduced and/or improved by other research groups. The broadening of the final energy after

a scattering event, which is associated to these models, yields in general a significant increase of the population in the high energy region of the distribution function. Accordingly, the concept of a broadening assisted run-away effecty has been introduced. However, because of their long tails at high energies, these joint-spectral density models need an "ad hoc" truncation to avoid an unpractical (and unphysical) blowing up of the mean kinetic energy. Because of this, in turn, the quantitative results may depend on the choice of the empirical cut-off energy. To overcome this drawback, which has received some attention in the recent literature [2.33], more appropriate physical models, such as relaxing the simple effective mass model for the density of states [2.34], should be introduced. We shall address this issue in our further research.

2.2 A Monte Carlo Approach to the Solution of the Liouville-von Neumann equation for quantum transport

2.2.1 Introduction

In the last decades the Monte Carlo method [2.31] has proved to be a formidable tool for the solution of charge-transport problems in semiconductors. It provides a simple way to solve the semiclassical Boltzmann transport equation once the band structure and the scattering mechanisms are sufficiently well known. From its original formulation [2.35] it has been greatly improved in efficiency and it has been extended to cover a large variety of problems such as space or time-dependent systems, interacting electrons, degenerate statistics or even device modelling.

However, the very fast evolution of miniaturization techniques for semiconductor technology is leading very rapidly towards experimental conditions where typical lengths are of the order of the De Broglie wavelenght of the carriers, and typical times are comparable with carrier relaxation times [2.1]. In particular,

in modern laser spectroscopy a time resolution has been achieved of the order of 10^1 femtoseconds. If the system is observed at a time of this order after it has been "prepared", transitions may be observed that would not be allowed by energy conservation. In other words, the quantum interference phenomena that produce the δ of energy conservation are not yet complete at so short observation times.

It is clear that the classical transport theory, based on Boltzmann equation, is not adequate for the description of the physical processes that are taking place on this time scale. In fact, semiclassical transport is based on the hypothesis, among others, that each scattering event is completed when the next one starts. For the validity of such an assumption it is necessary that the coupling between electrons and the scattering agents is sufficiently weak so that a first-order perturbation theory can be applied, and this must be done in the limit of "completed collisions" so that energy conservation holds at each interaction process.

Several possible approaches have been presented for attacking the problem of quantum charge transport [2.1].

A new Quantum Monte Carlo (QMC) procedure has been recently developed [2.36] for the solution of the Liouville equation for the electronic density matrix in semiconductors. The principles of the method will be summarized in Sects. 2.2.2 and 2.2.3.

In Sec. 2.2.4.1 we present an analysis of the first two perturbative corrections in presence of an arbitrary high electric field, and in Sec. 2.2.4.2 the method is applied to the problem of energy relaxation of photoexcited electrons in GaAs in absence of electric field.

In the semiclassical limit our quantum equation recovers the semiclassical Boltzmann equation, and the numerical procedure results to be a new formulation of the traditional Monte Carlo procedure [2.37]. The semiclassical limit of the procedure is described in Sec. 2.2.5.

The method allows to evaluate the electronic density matrix as a function of time without any assumptions on the intensity and the duration of the electron-phonon interaction. The quantum equation is solved through a random generation of all possible quantum interactions at the various perturbative orders, in the same way as the usual Classical Monte Carlo (CMC) generates classical scattering events [2.36].

2.2.2 Physical System and Theoretical Approach

In order to study the properties of charge transport in a quantum scheme, let us consider an ensemble of electrons in a semiconductor crystal, coupled to the phonon gas. Carriers are assumed to be not interacting with each other, so that the interaction of one carrier with the phonons will represent the behaviour of the whole electron gas. The electron band structure is introduced in the effective-mass approximation, with a simple spherical and parabolic band.

The Hamiltonian of the system is given by

$$H = H_e + H_E + H_p + H_{ep} \quad (2.18)$$

where $H_e = -\frac{\hbar^2}{2m} \nabla^2$ is the term corresponding to an electron in a perfect crystal (m = effective mass); $H_E = e\mathbf{E} \cdot \mathbf{r}$ describes the electric field turned on at $t=0$; $H_p = \sum \hbar\omega_q a_q^\dagger a_q$ describes the free-phonon system in the second-quantization formalism (a_q^\dagger and a_q are the creation and annihilation operators of a phonon mode q). The electron-phonon interaction Hamiltonian H_{ep} , turned on at $t = 0$, depends on the scattering mechanisms included in the model.

We have not explicitly introduced any interactions among phonons and between phonons and the thermal bath. In the numerical procedure, however, we will assume that these interactions can maintain an equilibrium phonon population during the evolution of the system.

In order to work in the interaction representation, we use the set of basis functions

$$| \mathbf{k}, \{n_q\}, t \rangle = \frac{1}{\sqrt{V}} e^{i(\mathbf{k}(t) \cdot \mathbf{r})} \cdot e^{-i \int_0^t d\tau \omega(\mathbf{k}(\tau))} \cdot \Phi(\{n_q\}, t) \quad (2.19)$$

that include the time dependence due to the unperturbed Hamiltonian $H_e + H_p + H_E$. They are direct products of electronic accelerated plane waves, with $\mathbf{k}(t) = \mathbf{k}_0 - \frac{e\mathbf{E}}{\hbar}t$, normalized to 1 over the crystal, and the phonon states $\Phi(\{n_q\})$ with n_q phonons in mode \mathbf{q} with frequency ω_q . The state $|\Psi\rangle$ of the system can be expanded over this set as:

$$|\Psi\rangle = \sum_{\mathbf{k}} \sum_{\{n_q\}} c(\mathbf{k}, \{n_q\}, t) | \mathbf{k}, \{n_q\}, t \rangle \quad (2.20)$$

If we now consider to the density matrix of the system in the representation of the set in Eq.(2.19):

$$\rho(\mathbf{k}, \{n_q\}, \mathbf{k}', \{n'_q\}, t) = \langle c(\mathbf{k}, \{n_q\}, t) c^*(\mathbf{k}', \{n'_q\}, t) \rangle, \quad (2.21)$$

the Liouville-Von Neumann equation that describes its time evolution contains only the perturbation Hamiltonian:

$$i\hbar \frac{\partial}{\partial t} \rho(X, X', t) = [H_{ep}, \rho](X, X', t), \quad (2.22)$$

where we have used the symbolic compact notation $X = (\mathbf{k}, \{n_q\})$

A formal integration leads to

$$\rho(X, X', t) = \rho(X, X', 0) + \int_0^t dt_1 [\mathcal{H}_{ep}, \rho](X, X', t_1), \quad (2.23)$$

where $\mathcal{H}_{ep} = \frac{1}{i\hbar} H_{ep}$. If we are interested in the evaluation of expectation values of electron quantities which are diagonal in the electronic part of the states in Eq.(2.19), we can focus our attention on the diagonal elements $\rho(X, t)$ of ρ .

Furthermore, we will assume a diagonal initial condition for ρ decoupled in electron and phonon coordinates. This is justified by the fact that the interaction is turned on at $t=0$. The electronic part is taken as some distribution function f_0 , while the phonon part is assumed as the probability $P_{eq}(\{n_q\})$ of finding each mode q occupied by n_q phonons at equilibrium:

$$\rho(\mathbf{k}, \{n_q\}, 0) = f_0(\mathbf{k}) \cdot P_{eq}(\{n_q\}) \quad (2.24)$$

A perturbative expansion of Eq.(2.23) is easily obtained by iterative substitution of its right-hand side into the equation itself:

$$\begin{aligned} \rho(X, t) &= \rho(X, 0) + \int_0^t dt_1 [\mathcal{H}_{ep}(t_1), \rho(0)](X) + \\ &+ \int_0^t dt_1 \int_0^{t_1} dt_2 [\mathcal{H}_{ep}(t_1), [\mathcal{H}_{ep}(t_2), \rho(0)]](X) + \dots = \\ &= \rho^{(0)}(X, t) + \Delta\rho^{(1)}(X, t) + \Delta\rho^{(2)}(X, t) + \dots \end{aligned} \quad (2.25)$$

The zero-order term in the expansion corresponds to the case of no coupling between electrons and phonons, and it is equal to the initial condition for ρ .

In order to proceed with the theory we note that the perturbation Hamiltonian has the form

$$H_{ep} = \sum_q F(q) \{a_q e^{i\mathbf{q} \cdot \mathbf{r}} - a_q^\dagger e^{-i\mathbf{q} \cdot \mathbf{r}}\} = H_{ab} + H_{em}, \quad (2.26)$$

where H_{ab} and H_{em} refer to phonon absorption and emission, respectively. The matrix element of H_{ep} between X and X' contains only the mode q related to \mathbf{k} and \mathbf{k}' by momentum conservation and it is different from zero only if the

number of phonons in the mode q is changed by a unity going from X to X' , since it contains only linear terms in a_q e a_q^\dagger .

The explicit form of the first-order correction is:

$$\Delta\rho^{(1)}(X,t) = \int_0^t dt_1 \{ \mathcal{H}_{ep}(X, X', t_1) \rho^{(0)}(X', 0) - \mathcal{H}_{ep}(X, X', t_1) \rho^{(0)}(X, 0) \}. \quad (2.27)$$

From what we have seen about the matrix elements of H_{ep} , it is clear that the above first-order term gives no contribution to the diagonal elements of ρ since we assumed diagonal initial conditions. It can be shown that the same is true for all odd-order corrections.

The second-order term can be rewritten, using the property

$$\mathcal{H}_{ep}(X, X', t) = -\mathcal{H}_{ep}^*(X', X, t), \quad (2.28)$$

as

$$\begin{aligned} \Delta\rho^{(2)}(X,t) = & \sum_{X'} \int_0^t dt_1 \int_0^{t_1} dt_2 \{ \mathcal{H}_{ep}(X, X', t_1) \mathcal{H}_{ep}(X', X, t_2) \rho(X, 0) \\ & + \mathcal{H}_{ep}^*(X, X', t_1) \mathcal{H}_{ep}^*(X', X, t_2) \rho(X, 0) + \mathcal{H}_{ep}^*(X, X', t_1) \mathcal{H}_{ep}(X, X', t_2) \rho(X', 0) \\ & + \mathcal{H}_{ep}(X, X', t_1) \mathcal{H}_{ep}^*(X, X', t_2) \rho(X', 0) \} \end{aligned} \quad (2.29)$$

There is a simple and useful way of reading the above equation. At $t = 0$ the two arguments of ρ are equal; by application of \mathcal{H}_{ep} (or \mathcal{H}_{ep}^*) the first (or the second) argument of ρ is changed from the second argument of \mathcal{H}_{ep} to the first one; at t the two arguments of ρ are again equal (to X). Since each application of \mathcal{H}_{ep} changes the phonon state of one unity, in order to start from a diagonal element and end up to another diagonal element a mode q absorbed (or emitted) by one argument is to be absorbed (or emitted) also by the other argument or reemitted (or reabsorbed) by the same argument. Using the language of the

field theory, we refer to the first kind of processes as to "real" emissions and absorptions, while the other ones are "virtual processes".

Thus, the contributions to be included in the second order in \mathcal{H}_{ep} are those illustrated in Fig. 2.12.

With the above interpretation it is very simple to generalize the results to higher-order terms of the perturbative expansion. For example, Fig.2.13 is the diagramatic representation of the following contribution to the fourth-order term:

$$\mathcal{H}_{em}^*(X, X', t_1) \mathcal{H}_{ab}(X, X''', t_2) \mathcal{H}_{em}(X''', X'', t_3) \mathcal{H}_{em}(X'', X', t_4) \rho(X', 0) \quad (2.30)$$

Each "process" in these graphs corresponds to a single scattering event in classical transport. To recover the classical golden rule it should be necessary to integrate one of the two times of the process, without interfering with other processes, over an interval large enough to obtain the δ of energy conservation.

From the analysis of these graphs of the perturbation expansion for ρ , we can focus our attention to some important aspects of the quantum description. The quantum transitions have a finite duration, during which carriers experience the action of the electric field (ICFE). This effect is obviously not present in the semiclassical description where collisions are point-like. Only after a certain time we obtain again a diagonal state that corresponds to a semiclassical state of the system; during the interaction the system is in a quantum state given by a superposition of k states which does not correspond to any semiclassical situation. Furthermore, while one process is happening, a new one can start, giving rise to multiple collisions and vertex corrections.

Let us now introduce the reduced electronic density matrix, which is the quantity of interest in charge-transport phenomena and it can be considered the

quantum analogue of the classical distribution function. It is defined as the contraction over phonon states of the total density matrix:

$$\rho^{(e)}(\mathbf{k}, \mathbf{k}', t) \equiv \sum_{\{n_q\}} \rho(\mathbf{k}, \{n_q\}, \mathbf{k}', \{n_q\}, t) \quad (2.31)$$

The evolution equation for $\rho^{(e)}$ still contains the dynamical variables of the many-body system. In fact it is not possible to obtain a closed equation for $\rho^{(e)}$ by taking the trace of Eq.(2.23) for the full density matrix since the trace operation does not commute with the interaction Hamiltonian. The reduction of the total density matrix to the electron density matrix can instead be easily performed in the numerical QMC procedure introduced in the following section in order to evaluate the series in Eq.(2.25).

2.2.3 Numerical Procedure

The numerical QMC algorithm devised for the solution of Eq.(2.22) is essentially based on random generations of all possible processes associated with the different perturbative corrections.

From the fundamentals of the Monte Carlo technique [2.38] it is known that for the evaluation of a sum $S = \sum_i x_i$, one can consider the estimator $\frac{x_i}{p_i}$, where p_i 's are arbitrary probabilities between zero and one normalized to unity, and average it over random selections of the i index, made with probabilities p_i . This procedure is here used to obtain an estimate of Eq.(2.25): random selections with suitable probabilities determine

- i. the order of the perturbative correction to be estimated;
- ii. one of the possible contributions to the corresponding integrand;
- iii. the wavevectors \mathbf{q} of the phonons involved in the quantum interactions of that contribution. Due to momentum conservation of the H_{ep} matrix elements, these selections determine the argument \mathbf{k}_{in} of ρ at $t=0$.

The quantity:

$$\frac{\int_0^t dt_1 \dots \int_0^{t_{n-1}} dt_n \mathcal{H}_{ep}(t_1) \dots \mathcal{H}_{ep}(t_n)}{\mathcal{P}} \cdot \rho(k_{in}, t=0), \quad (2.32)$$

where \mathcal{P} is the total probability of all the selections that have been made, is then averaged over many generations and it gives an estimate of ρ at time t .

In this way we obtain the density matrix and the average values of the physical quantities of interest for our system through a random generation of quantum processes as we obtain the carrier distribution function and transport quantities from a random choice of carrier histories in the traditional Monte Carlo technique.

There is however a crucial point that requires to be analysed, which is how we perform the average over the phonon variables. As we already pointed out, we assume an initial condition for ρ which is the product of an electron distribution function times the equilibrium phonon distribution; furthermore the interaction Hamiltonian is linear in the creation and annihilation operators of the modes q .

In the numerical procedure we saw that a sequence of process is generated starting from an initial state $(k_{in}, \{n_{qin}\}, 0)$ which terminates on the state $(k, \{n_q\}, t)$. This sequence corresponds to a sequence of phonon wavevectors q which are absorbed or emitted on the first or on the second index of the density matrix. We can assume that each phonon mode is chosen only once in a given process, i.e. the electron always interacts with an equilibrium phonon bath. If a phonon q is absorbed in a certain transition and the corresponding occupation number at time t is n_q , the occupation number of the initial state is $n_q + 1$, and the interaction hamiltonian \mathcal{H}_{ep} must contain the factor $\sqrt{(n_q + 1)}$ because it contains the operator a_q . In order to finish the process \mathcal{H}_{ep} must act two times, and the numerical estimator will contain the multiplicative factor $n_q + 1$.

In the same way, if we have the emission of a mode q , and the corresponding final occupation number is n_q , then the initial occupation of this mode must be $n_q - 1$, and the numerical estimator will contain a factor n_q .

At the end of the random generation we obtain for the $2n$ -order correction $\Delta\rho^{(e)(2n)}(k, t)$ an estimator of the form

$$\Delta\rho^{(e)(2n)}(k, t) = (\text{constant}) \cdot f_o(k_{in}) \cdot \sum_{\{n_q\}} \langle \prod_{q^*} N_{q^*} \cdot \prod_q P_{eq}(n_{q_{in}}) \rangle \quad (2.33)$$

where $n_{q_{in}}$ is the occupation number of the mode q in the initial state and N_{q^*} is the multiplicative factor generated by the interaction hamiltonian for the phonon modes q^* involved into the generated sequence. The average $\langle \dots \rangle$ is performed over several generations of terms for a given perturbative order $2n$.

If a phonon q is not chosen, then the sum over all possible occupation numbers n_q of $P(n_q)$ must be equal to unity:

$$\sum_{n_q} P(n_{q_{in}}) = 1 \quad (2.34)$$

and this factor does not contribute to the product in Eq. (2.33).

If instead we consider a q^* chosen in the random generation, we have two possible case. In the case of absorption:

$$\sum_{n_{q^*}} \langle (n_{q^*} + 1) P(n_{q^*} + 1) \rangle = n_{q^*})_{Bose} \quad (2.35)$$

where $n_{q^*})_{Bose}$ is the equilibrium occupation number given by the Bose distribution.

In the case of emission:

$$\sum_{n_{q^*}} \langle (n_{q^*}) P(n_{q^*} - 1) \rangle = n_{q^*})_{Bose} + 1 \quad (2.36)$$

In both cases we have finally to use the Bose distribution for the evaluation of the term without introducing any approximations on the electron-phonon coupling, but for the assumption that the phonon gas is constantly kept in equilibrium conditions.

2.2.4 Results

2.2.4.1 Analysis of First and Second Orders in Presence of Electric Fields

The second order perturbative correction in the interaction hamiltonian involves only one of the processes discussed above. The explicit form of the corresponding integrals in Eq.(2.25) is of the type:

$$\int_0^t dt_1 \int_0^t dt_2 e^{i b(t_1 - t_2) + a(t_1^2 - t_2^2)}$$

$$a = \frac{e}{2m^*} (\mathbf{k}_f - \mathbf{k}_i) \cdot \mathbf{E}$$

$$b = \frac{1}{2} (\omega_f - \omega_i - \omega_q) \quad (2.37)$$

Here i and f refer to the interacting initial and final electron states and ω_q is the phonon frequency. This simple expression allows a direct analytical integration in terms of Fresnel integrals. The final expression of the second order correction after integration is:

$$\frac{\pi}{4a} \left\{ \left[C\left(\frac{at+b}{a}\right) - C\left(\frac{b}{a}\right) \right]^2 + \left[S\left(\frac{at+b}{a}\right) - S\left(\frac{b}{a}\right) \right]^2 \right\} \quad (2.38)$$

In the above equations the coefficient a accounts for the effect of the field during the finite duration of the collision, while b is related to the energy of the quantum states involved in the transition.

This formulation allows us to investigate separately the new features introduced by the quantum treatment of the interactions. In particular, we can

turn off the ICFE by neglecting the effect of the field between two vertices of the process.

Results for the first two perturbative terms have been obtained starting from equilibrium conditions for the electron and phonon system, and both electric field and electron-phonon coupling are turned on at $t=0$. In Fig.2.14 we compare the absolute value of the second order correction as given from Eq.(2.38) with the same contribution without ICFE. In the same figure we report also the corresponding classical contribution to the perturbative expansion of the classical integral equation for the distribution function obtained from the Boltzmann equation [2.37]. This classical correction comes from "one-scattering" trajectories and the corresponding contribution is always negative, due to the prevailing scattering out. These numerical results have been obtained for a simple-model semiconductor (relative effective mass $m^*=0.295$, crystal density $d=2.33 \text{ g/cm}^3$, one optical phonon scattering with $T_{ph} = 350 \text{ K}$, and coupling constant $D=2.5 \cdot 10^9 \text{ eV cm}^{-1}$). The working conditions ($T=20 \text{ K}$, $E=150 \text{ kV/cm}$, $t=5 \cdot 10^{-14} \text{ s}$) have been chosen in such a way that quantum effects can be easily detectable.

When we neglect the ICFE, we get a higher effect of the "quantum one-collision" trajectories. In fact the ICFE, by changing the energy of the carrier during the collision, reduces the efficiency of the scattering since it reduces the time of positive interference which occurs when the energy difference between initial and final states is equal to the phonon energy [2.39]. The classical contribution is even higher; such effect can be interpreted by noting that the field is so high that even at such short times the electrons can reach enough energy for classical instantaneous phonon emissions, while the time is so short that quantum transitions, with finite durations, are not yet fully developed.

An improvement in the efficiency of the method can be obtained also at higher orders by integrating over time every other vertex between the two adjacent vertices. The result is again expressed in terms of Fresnel integrals.

If we allow only processes that do not overlap (the two vertices of one given processes correspond to adjacent times) we neglect multiple collisions, and by comparison we may analyse their effect.

Finally we may neglect the effect of the field in the interference exponentials and analyse in this way the ICFE in the two-scattering trajectories. In this last case the integration of one vertex leads to the functions like $\frac{\sin(bt)}{b}$ which would lead to the delta of energy conservation for large times; in our case however the completion of the transition is not necessarily reached if the time interval considered is very short.

We show in Fig.2.15 the quantum corrections of the fourth perturbative order (which is now larger than zero) compared with the classical two-scattering contribution for the same model as in Fig.2.14. The quantum result is lower than the classical term as for the second order contribution, due again to the short time available for the interaction. When we allow only separate collisions (Fig.2.15c), the corresponding term appears somewhat higher. This result can be due to the fact that the two separate collisions allow for a higher contribution of transitions which do not conserve energy, even though the phenomenon still requires further investigation.

If we turn off the ICFE, we see that the whole curve is still higher and much closer to the classical one, as it happens for the second order term.

Finally in Fig.2.16 we report results for the density matrix in the case of a more realistic set of parameters that gets closer to a simplified silicon model. We changed the phonon temperature ($T=450$ K) and the coupling constant ($D=.8 \times 10^9$ eV/cm). The electric field is $E=15$ kV/cm and the time is $t=.5$ ps.

In this case we found that the ICFE is much lower than in the previous case due to the lower field strength.

Since the time is larger, the effect of multiple collisions is also lowered, and we expect that this effect influences higher order corrections.

2.2.4.2 Quantum Energy Relaxation of Photoexcited Carriers in Absence of Electric Fields

When electric fields are absent ($H_E = 0$) time integrations can be performed analytically. For example, the second-order contribution due to a real emission of a phonon in mode q is given by the first two graphs on the left in Fig.2.12, which are complex conjugate of each other. The integration yields

$$\begin{aligned} & 2\mathcal{R} \int_0^t dt_1 \int_0^{t_1} dt_2 \langle X, t_1 | \mathcal{H}_E | X', t_1 \rangle \langle X, t_2 | \mathcal{H}_E | X', t_2 \rangle^* \\ &= 2\mathcal{R} \left\{ \frac{1}{\hbar^2} \int_0^t dt_1 \int_0^{t_1} dt_2 |F(q)|^2 (n_q + 1) e^{i\delta\omega t_1} e^{-i\delta\omega t_2} \right\} \\ &= \frac{2 |F(q)|^2 (n_q + 1)}{\hbar^2 (\delta\omega)^2} (1 - \cos(\delta\omega t)), \end{aligned} \quad (2.39)$$

where \mathcal{R} indicates the real part, and $\delta\omega = \omega(k) - \omega(k') + \omega_q$. Similar results are obtained for other contributions and for higher-order terms. It is not easy to give general formula since the form of the result depends on the particular diagram considered.

The method described in the previous sections has been applied to the case of photoexcited electrons in bulk GaAs. The semiconductor model has been simplified to a single spherical, parabolic band. The interaction Hamiltonian includes only polar coupling to optical phonons; for such a case

$$|F(q)|^2 = \frac{2\pi e^2 \hbar \omega_o}{V q^2} \left(\frac{1}{\epsilon_\infty} - \frac{1}{\epsilon_o} \right), \quad (2.40)$$

where ω_o is the frequency of the optical phonons, assumed constant, V is the volume of the crystal, ϵ_∞ and ϵ_o are the high frequency and the static dielectric constants.

Electrons are generated at $t = 0$ according to a distribution proportional to $\exp(-|\epsilon - \epsilon_o|^2 / (K_B T_i))$, where ϵ is the electron energy and ϵ_o and T_i are appropriate constants

Terms up to fourth order have been included in the numerical computations. For such a reason the simulation time has been kept $\leq 100ps$. For longer times, higher perturbative orders would have been necessary.

For comparison results have been obtained for the same model at the same times in semiclassical transport, using an Ensemble Monte Carlo (EMC) technique.

The following parameters have been used: $m = 0.063m_o$; $\hbar\omega_o/K_B = 410K$; $T = 10K$; $T_i = 10K$; $\epsilon_\infty = 10.92$; $\epsilon_o = 12.9$; $\epsilon_o/K_B = 1000K$

Fig.2.17 shows the results obtained with EMC at $t = 0.1ps$ after excitation. The echos are clearly seen corresponding to electrons having emitted one or two optical phonons. About 30 % of the particles have left the original peak.

Fig.2.18 shows the corresponding result obtained with quantum transport theory (note the scale change). The initial distribution is diminished of a quantity very similar to that of the classical case. However, electrons can be found, at $t = 0.1ps$, in a very wide range of energies, since energy needs not to be conserved. The secondary peaks are not yet well formed. High energies are in fact favored in the distribution at time t by the larger density of states and by the q^{-2} factor in Eq.(2.40). Thus the energy relaxation predicted by quantum transport theory is less than that predicted by classical transport for $t \leq 0.1ps$ as shown in Fig.2.19.

2.2.5 Semiclassical Limit: Backward Monte Carlo Procedure

The semiclassical limit of the theoretical approach described in the previous sections is obtained when: i) we neglect ICFE; ii) we assume that the time between two collisions is much longer than the collision duration, so that during each collision energy is conserved; iii) the phonon population is always maintained at equilibrium, and the average occupation number is given by the Bose distribution.

Under these conditions the integral perturbative equation for the density matrix reduces to the Boltzmann equation written in an analogous integral form with the collision term expanded at the same perturbative order.

The semiclassical limit of the Quantum Monte Carlo gives a basically new M.C. method for the solution of the Boltzmann equation, which results as the classical limit of the method developed for the solution of the Liouville equation for quantum transport [2.36].

The technique described here differs from the traditional M.C. method in two major respects: 1). The occurrence of particular electron histories with given scattering events is arbitrarily selected in the procedure and appropriately weighted in the estimator. 2). The electron state k at which the distribution function is evaluated at time t is chosen at the beginning of the procedure and the electron paths are generated backward in time from t to the time $t=0$ of the (known) initial condition. This second feature seems to be not inherent to the method which should be suitable also for a normal forward simulation. However the fact that the value of k at which f is evaluated is fixed arbitrarily makes the method particularly appealing for problems where rare regions of f are of particular interest. The two features indicated above may suggest the names "weighted M.C." or "backward M.C." for the procedure introduced here.

2.2.5.1 The Method

Let us start from the standard form of the B.E. For simplicity we shall consider here a homogeneous system, with a homogeneous and constant applied field E , but the method should be easily generalizable to space and time dependent phenomena.

$$\begin{aligned} \frac{\partial}{\partial t} f(\mathbf{r}, \mathbf{k}, t) + \frac{\partial \mathbf{k}}{\partial t} \cdot \mathbf{k} f(\mathbf{r}, \mathbf{k}, t) = \frac{V}{(2\pi)^3} \int d\mathbf{k}_1 P_i(\mathbf{k}_1, \mathbf{k}) f(\mathbf{r}, \mathbf{k}_1, t) - \\ - \frac{V}{(2\pi)^3} \int d\mathbf{k}_1 P_o(\mathbf{k}, \mathbf{k}_1) f(\mathbf{r}, \mathbf{k}, t) \end{aligned} \quad (2.41)$$

Here P_i and P_o indicate the same transition probability from a state \mathbf{k} to state \mathbf{k}_1 ; the suffixes i and o are intended to specify IN or OUT scattering, respectively, for future reference. If the path variables $\mathbf{k}^* = \mathbf{k} - \frac{eE}{\hbar}t$ are used and a formal integration is performed, the Boltzman Equation takes the form of an integrál equation that can be iteratively expanded in powers of the scattering probability.

$$f(\mathbf{k}, t) = f^0 + f^1 + f^2 + \dots \quad (2.42)$$

$$f^0(\mathbf{k}, t) = f(\mathbf{k}(0), 0)$$

$$f^1(\mathbf{k}, t) = \int dt_1 \frac{V}{(2\pi)^3} \int d\mathbf{k}_1 P_i(\mathbf{k}_1, \mathbf{k}(t_1)) f(\mathbf{k}_1(0), 0) -$$

$$\frac{V}{(2\pi)^3} \int dt_1 \int d\mathbf{k}_1 P_o(\mathbf{k}(t_1), \mathbf{k}_1) f(\mathbf{k}(0), 0)$$

$$f^2(\mathbf{k}, t) = \int dt_1 \frac{V}{(2\pi)^3} \int d\mathbf{k}_1 P_i(\mathbf{k}_1, \mathbf{k}(t_1))$$

$$\int dt_2 \frac{V}{(2\pi)^3} \int d\mathbf{k}_2 P_i(\mathbf{k}_2, \mathbf{k}_1(t_2)) f(\mathbf{k}_2(0), 0)$$

$$\int dt_1 \frac{V}{(2\pi)^3} \int d\mathbf{k}_1 P_i(\mathbf{k}_1, \mathbf{k}(t_1)) \int dt_2 \frac{V}{(2\pi)^3} \int d\mathbf{k}_2 P_o(\mathbf{k}_1(t_2), \mathbf{k}_2) f(\mathbf{k}_1(0), 0)$$

$$\int dt_1 \frac{V}{(2\pi)^3} \int d\mathbf{k}_1 P_o(\mathbf{k}(t_1), \mathbf{k}_1) \int dt_2 \frac{V}{(2\pi)^3} \int d\mathbf{k}_2 P_i(\mathbf{k}_2, \mathbf{k}(t_2)) f(\mathbf{k}_2(0), 0)$$

$$+ \int dt_1 \frac{V}{(2\pi)^3} \int dk_1 P_o(k(t_1), k_1) \int dt_2 \frac{V}{(2\pi)^3} \int dk_2 P_o(k(t_2), k_2) f(k(0), 0) \quad (2.43)$$

Here $k(t)$ is the value of k moved back to time t .

The zero order term, f^0 , which corresponds to the absence of interaction, is the ballistic translation of f during the interval $(0, t)$, due to the action of the external electric field. The first order term f^1 represents the contribution of electrons that suffered one scattering event between $t=0$ and $t=t$. Here, the first integral, or 'IN' term, is due to electrons that at time t_1 have a collision from k_1 to $k(t_1)$ at time t . The second integral or 'OUT' term, is due to electrons that are scattered out from the ballistic trajectory and do not reach the state (k, t) and reach k at time t . An interpretation like this can be carried on to all the other terms. An example of a third order term is shown in Fig. (2.20).

Eq. (2.20) gives f formally as an infinite sum. A possible M.C. technique for the evaluation of a sum $S = \sum x_i$ is the following: we select values of i at random with arbitrary probabilities p_i such that $p_i > 0$ and $\sum p_i = 1$ and make the estimator x_i/p_i so we have

$$\left\langle \frac{x_i}{p_i} \right\rangle = \sum p_i \frac{x_i}{p_i} = S \quad (2.44)$$

The method can be extended to the evaluation of an integral: if we consider a multiple integral like those in Eq (2.20) then

$$\int dt_1 \int \dots \int dt_n f(t_1, t_2, \dots, t_n) = v \langle f \rangle = \frac{1}{n!} t^n \langle f(t_1, \dots, t_n) \rangle \quad (2.45)$$

where the mean value is evaluated over the possible choices of the set (t_1, t_2, \dots, t_n) and v is the volume of integration.

If we apply the above method for the evaluation of the sum in Eq (2.20) the following procedure could result: 1) the perturbative order n of the term to be evaluated is chosen first; 2) n times, between $t = 0$ and the time t of simulation,

are then generated ; 3) then, starting from the final state (\mathbf{k}, t) we have to move \mathbf{k} backward in time with free flights from each t_i to the previous one ; 4) at each t_i we choose between scattering IN or OUT and the scattering mechanism (for example, in our case where we consider only scattering by one optical mode, we chose between emission or absorbtion ; 5) if at time t_i an OUT scattering is chosen the integration over the final states is performed analytically, and the current \mathbf{k} is kept to continue the simulation; if an IN scattering is chosen an initial state is chosen, at random in the surface of energy conservation, and this new \mathbf{k} is used to continue the simulation; 6) the previous two points are repeated until $t = 0$; 7) the initial distribution is evaluated at $\mathbf{k}_i(0)$ and multiplied by the product of the transition rates for the simulated path and divided by the probabilities of the choices selected in the simulation.

However, a change can be introduced in the above algorithm giving a more physical and fast evaluation of f . In fact all terms containing any number of OUT scattering events between two given IN scattering can be summed up analitically. Let us consider, for example, the term containing two OUT scattering events :

$$\int dt_1 \int d\mathbf{k}_1 P_o(\mathbf{k}(t_1), \mathbf{k}_1) \int dt_2 \int d\mathbf{k}_2 P_o(\mathbf{k}(t_2), \mathbf{k}_2) f(\mathbf{k}(0), 0) \quad (2.46)$$

Since the integrals are symmetric with respect to the echange of the time variables, Eq (2.26) can be reduced to :

$$\begin{aligned} f(\mathbf{k}(0), 0) \frac{1}{2!} \int dt_1 \int d\mathbf{k}_1 P_o(\mathbf{k}(t_1), \mathbf{k}_1) \int dt_2 \int d\mathbf{k}_2 P_o(\mathbf{k}(t_2), \mathbf{k}_2) \\ = f^0 \frac{1}{2!} \left[\int dt_1 P_o(\mathbf{k}, t_1) \right]^2 \end{aligned}$$

where $P_o(\mathbf{k}, t_1)$ is the scattering probability integrated over all possible final states.

If we sum all such contribution the result is the exponential series:

$$\begin{aligned}
 f^0 - \{f^0 \int dt_1 P_o(k, t_1)\} + \{f^0 \frac{1}{2!} [\int dt_1 P_o(k, t_1)]^2 \dots = \\
 = f^0 \exp\{-\int dt_1 P_o(k_1, t)\} \quad (2.47)
 \end{aligned}$$

Where now $\exp \int dt_1 P_o(k, t_1)$ is the probability of no scattering between the times 0 and t. new term is the ballistic term multiplied by the probability that an electron has not had a scattering in the time interval (0,t).

The same argument can be applied to sum up analytically all OUT terms between two given IN events. The result is that for any pair of IN terms at times t_1 and t_2 the estimator must be multiply by the probability $\exp\{-\int dt P_o(k, t)\}$, that an electron is not taken away from the trajectory by an OUT scattering.

The procedure sketched above is then to be modified in that only IN scattering events are to be considered and the no-scattering probabilities due to out scattering added to the estimator. Such a change results in an enormous improvment of the convergence since we move from a series with alternate signs to a series of positive terms.

2.2.5.2 Results

The above method has been applied, for testing purposes, to a simple model semiconductor based on silicon. A simple spherical parabolic band is used and only one optical phonon scattering is considered. For such a model the integral in equation (2.47) can be easily performed analytically. The following physical parameters have been used: effective mass=.295, phonon temperature= 450° K, coupling constant $0.8 \cdot 10^9$ V/cm, density= 2.329 cm^{-3} . Figs (2.21) and (2.22) show the results.

Fig (2.21) shows the distribution function obtained at different times at the initial application of the electric field $E= 10 \text{ KV/cm}$. While for $t = 0.5 \text{ ps}$ the

curve is complete with terms up to fifth order, for $t = 1.5ps$ we had to include, for convergence, terms up to the 12th order. (path with up to 12 scattering events contribute to the distribution function) In Fig (2.22) the distribution function is shown as a function of energy. A sampling of final k values in the energy sphere had to be performed. Results of the new method are compared with a traditional (EMC) performed with $2.4 \cdot 10^6$ particles. The curves in the figure show how many orders contribute to the final shape of the distribution function.

Several problems could be discussed about the efficiency of the method proposed here. In particular it is to be considered that if the probabilities (the p_i 's that appear in Eq (2.22)) are not appropriately chosen the advantage of selecting the final k is lost by the fact that most of the times the initial k_i , where the source function $f(k_i(0), 0)$ is to be evaluated, falls into regions where f is very small and the variance would result very large. A smart choice of the p_i 's for every particular problem will greatly improve the efficiency of the method.

Finally we would like to remind that the method should be applicable also to space dependent problems; in particular it could be very useful to analyse the problem of electrons injected into the semiconductor material from a metallic contact. In the traditional M.C. very long paths (and computations) correspond to electrons wandering around in the metal before entering the semiconductor space. On the contrary, with the present procedure only paths ending in the desired region are analysed.

References

- [2.1] For a recent review on the subject see L. Reggiani, *Physica* **134B**, 123 (1985)
- [2.2] I.B. Levinson and Ya. Yasevichyute, *Sov. Phys. JETP* **35**, 991 (1972)
- [2.3] J.R. Barker, *Solid State Electron.* **21**, 267 (1978).
- [2.4] K.K. Thornber, *Sol. State Electron.* **21**, 259 (1978)
- [2.5] D.C. Herbert and S.J. Till, *J. Phys. C*, **15**, 5411 (1982)
- [2.6] N. Pottier and D. Calecki *Physica* **110A**, 471 (1982)
- [2.7] V.P. Seminozhenko, *Phys. Repts.* **3**, 103 (1982)
- [2.8] A.C. Marsh and J.C. Inkson, *J. Phys. C: Solid State Phys.* **17**, 4501 (1984)
- [2.9] D.J. Lowe, *J. Phys. C: Solid State Phys.* **18**, L209 (1985).
- [2.10] S.K. Sarker, J.H. Davies, F.S. Khan and J.W. Wilkins, *Phys. Rev.* **B33**, 7263 (1986)
- [2.11] F.S. Khan, J.H. Davies and J.W. Wilkins, *Phys. Rev.* **B36**, 2578 (1987)
- [2.12] G.D. Mahan in "Polarons in ionic crystals and polar semiconductors" Ed. J.T. Devreese, North-Holland (Amsterdam, 1972) p. 554
- [2.13] G.D. Mahan "Many-particle Physics" (Plenum, New York, 1981)
- [2.14] J.R. Barker, *J. Phys. C: Solid State Phys.* **6**, 2663 (1973)
- [2.15] F. Capasso, T.P. Pearsall and K.K. Thornber, *IEEE EDL-2*, 295 (1981)
- [2.16] J.Y. Tang, H. Shichijo, K. Hess and G.J. Iafrate, *Journal de Physique Coll.* - **C7, 42**, 63 (1981).
- [2.17] Y.C. Chang, D.Z.Y. Ting, J.Y. Tang and K. Hess, *Appl. Phys. Lett.* **42**, 76 (1983)
- [2.18] J.Y. Tang and K. Hess, *J. Appl. Phys.* **54**, 5139 (1983)
- [2.19] K. Brennan and K. Hess, *Solid State Electron.* **27**, 347 (1984)
- [2.20] K. Brennan and K. Hess, *Phys. Rev.* **B29**, 5581 (1984)

- [2.21] S.D. Brorson, D.J. DiMaria, M.V. Fischetti, F.L. Pesavento, P.M. Solomon and D.W. Dong, *J. Appl. Phys.* **58**, 1902 (1985)
- [2.22] M. Artaki and K. Hess, *Superlattices and Microstructures* **1**, 489 (1985)
- [2.23] W. Porod and D.K. Ferry, *Physica* **134B**, 137 (1985)
- [2.24] P. Lugli, L. Reggiani and C. Jacoboni, *Superlattices and Microstructures* **2**, 143 (1986)
- [2.25] L. Reggiani, P. Lugli and A.P. Jauho, *Phys. Rev.* **B36**, 6602 (1987)
- [2.26] A.P. Jauho and J.W. Wilkins, *Phys. Rev.* **29B**, 1919 (1984).
- [2.27] D. Langreth and J. Wilkins, *Phys. Rev.* **6B**, 3189 (1972); D.C. Langreth, in "Linear and Nonlinear Electron Transport in Solids", Eds. J.T. Devreese and E. Van Doren (Plenum, New York, 1976).
- [2.28] P. Lipavsky, V. Spicka and B. Velicky, *Phys. Rev.* **34B**, 6933 (1986)
- [2.29] G.D. Mahan, *Phys. Rep.* **110**, 321 (1984); *ibidem* **145**, 235 (1987)
- [2.30] A.P. Jauho and L. Reggiani, *Solid State Electron.* to be published
- [2.31] C. Jacoboni and L. Reggiani, *Rev. Mod. Phys.*, **55**, 645 (1983)
- [2.32] L. Reggiani, "Hot electron transport in semiconductors", *Topics in Applied Physics* **58**, Springer Verlag (Heidelberg, 1985)
- [2.33] J. Liu and L.C. Chin, *Appl. Phys. Lett.* **47**, 1304 (1985)
- [2.34] K. Kim, B.A. Mason and K. Hess, *Phys. Rev.* **B36**, 6547 (1987)
- [2.35] T. Kurosawa, *J. Phys. Soc. Japan*, suppl.21, 424 (1966)
- [2.36] R. Brunetti and C. Jacoboni, *Proc. Int. Conference on Ho Carriers in semiconductors*, Boston (1987), in press.
- [2.37] C. Jacoboni, P. Poli, and L. Rota, *Proc. Int. Conference on Hot Carriers in semiconductors*, Boston (1987), in press.
- [2.38] J.M. Hammersley and D.C. Handscombe, "Monte Carlo Methods", Methuen and Co., London (1964)
- [2.39] J.R. Barker, *Sol. State Electron.* **21**, 267 (1978)

Figure Captions

Fig. 2.1 - Joint spectral density accounting for ICFE as a function of the kinetic energy after a scattering event. Continuous and dashed lines refer respectively to the exact and approximated expressions reported in the text for an initial energy $\epsilon_i = 1\text{eV}$, with $E = 500\text{kV/cm}$, and q antiparallel to E .

Fig. 2.2 The same as Fig. 2.1 with q parallel to E .

Fig. 2.3 The same as Fig. 2.1 with $E = 100\text{kV/cm}$, and q parallel to E .

Fig. 2.4 - Joint spectral density accounting for CB as a function of the kinetic energy after a scattering event. Continuous and dashed lines refer respectively to the exact and approximated expressions reported in the text with $\gamma^2 = 1.1\text{meV}$, and for an initial energy $\epsilon_i = 1\text{eV}$.

Fig. 2.5 - The same as Fig. 2.4 with $\epsilon_i = 0.2\text{eV}$.

Fig. 2.6 - The same as Fig. 2.5 with $\gamma^2 = 0.11\text{meV}$.

Fig. 2.7 - Distribution function of the carrier kinetic energy at $E = 500\text{kV/cm}$. Dashed curve refers to a semiclassical (SC) simulation, continuous curve to a simulation which includes collisional broadening (CB) only, and dot-dashed curve to a simulation which includes intra-collisional field effects (ICFE) only.

Fig. 2.8 - The same as Fig. 2.7 at $E = 100\text{kV/cm}$.

Fig. 2.9 - The same as Fig. 2.7 at $E = 10\text{kV/cm}$.

Fig. 2.10 - The same as Fig. 2.7 at $E = 5\text{kV/cm}$.

Fig. 2.11 - Distribution function of the difference between the initial and final kinetic energy after a scattering event ($\Delta\epsilon = \epsilon_i - \epsilon_f$) as obtained from Monte Carlo simulations for the case $E = 500\text{ kV/cm}$. The vertical line at $\Delta\epsilon = \hbar\omega_0$ represents the delta distribution of the semiclassical case. The continuous (dashed) curves refer to CB and (ICFE), respectively.

Fig. 2.12 - Diagrams representing the second order contributions to the density matrix. The horizontal axes represent the time for the two arguments of the density matrix and arrows indicate phonon absorption and emission processes.

Fig. 2.13 - Diagram representing the fourth-order contribution to the density matrix shown in Eq.(2.30).

Fig. 2.14 - Absolute value of quantum corrections at the second perturbative order compared with the absolute value of the classical one-scattering correction for the model semiconductor (see text). (a) classical one-scattering contribution; (b) quantum correction of the second perturbative order; (c) the same as in (b) without ICFE.

Fig. 2.15 - Quantum corrections at the fourth perturbative order compared with the classical two-scattering correction for the model semiconductor (see text). (a) classical two-scattering contribution; (b) quantum correction of the fourth perturbative order; (c) the same as in (b) with separate collisions; (d) the same as in (c) without ICFE.

Fig. 2.16 - Density matrix to zero-order (a), to second-order (c), and to fourth-order (b) perturbative correction for the silicon-like model (see text).

Fig. 2.17 - Classical distribution function of electrons as a function of energy at a time $t = 0.1ps$ after excitation. The highest peak at $1000K$ is the initial distribution at $t = 0$.

Fig. 2.18 - Quantum distribution function of electrons as a function of energy at a time $t = 0.1ps$ after excitation.

Fig. 2.19 - Mean electron energy as a function of time, obtained with quantum transport theory (continuous line) and classical theory (dashed line).

Fig. 2.20 - A possible trajectory of third order with two IN scatterings and one OUT scattering.

Fig. 2.21 - Electron distribution as a function of wavevector k at different times after the application of the electric field (a: $t=0$; b: $t=0.1$ ps; c: $t=0.5$ ps; d: $t=1$ ps; e: $t=1.5$ ps).

Fig. 2.22 - Electron distribution as a function of energy obtained at time $t=1$ ps after the application of the electric field. Continuous curves represent results obtained by summing orders up to 10th (a), 13th (b), 16th (c), 19th (d), 25th (e). $E = 10^5$ V/cm.

Figures

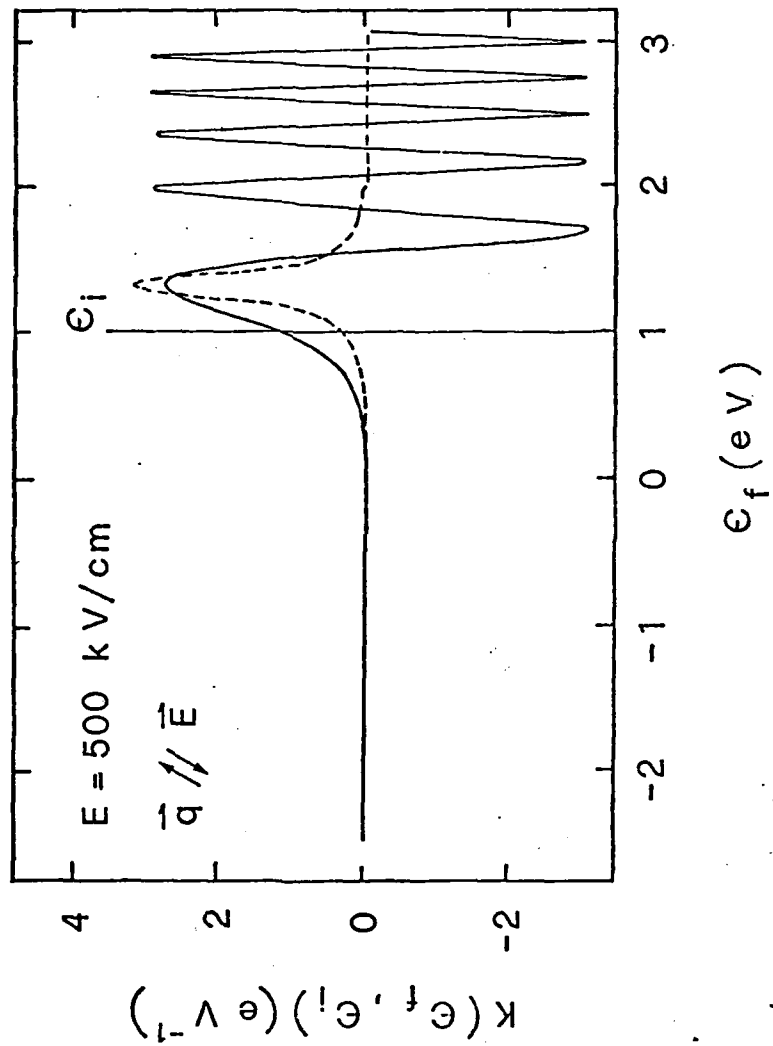


FIG. 2.1

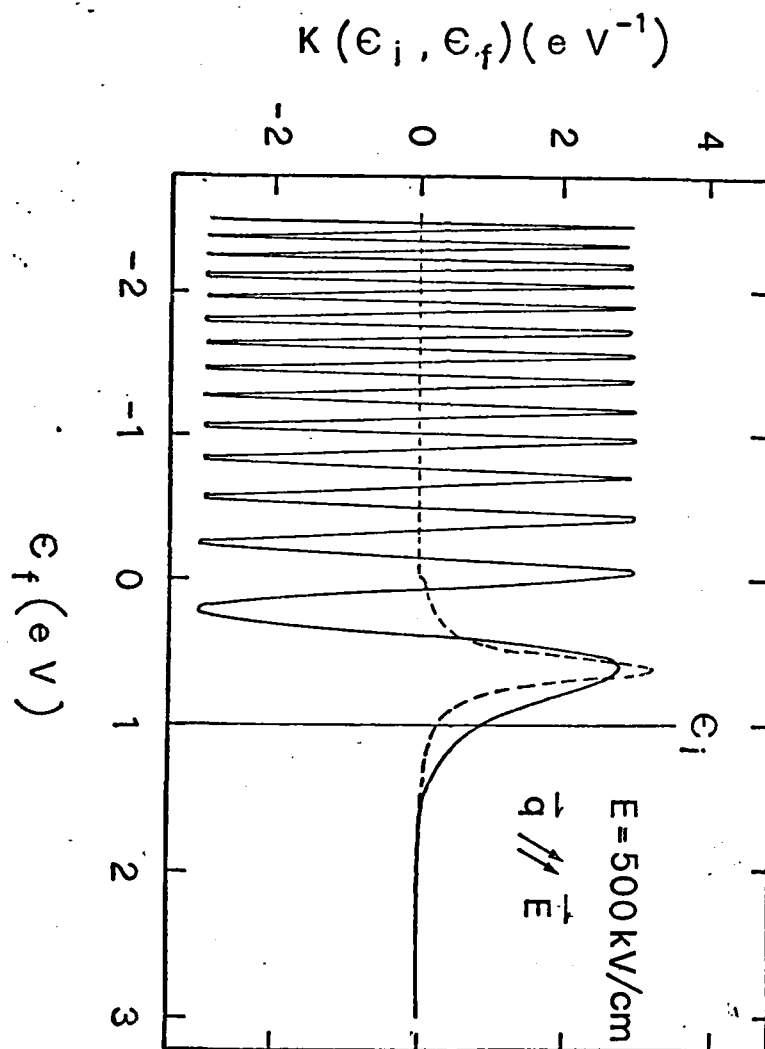


FIG. 2.2

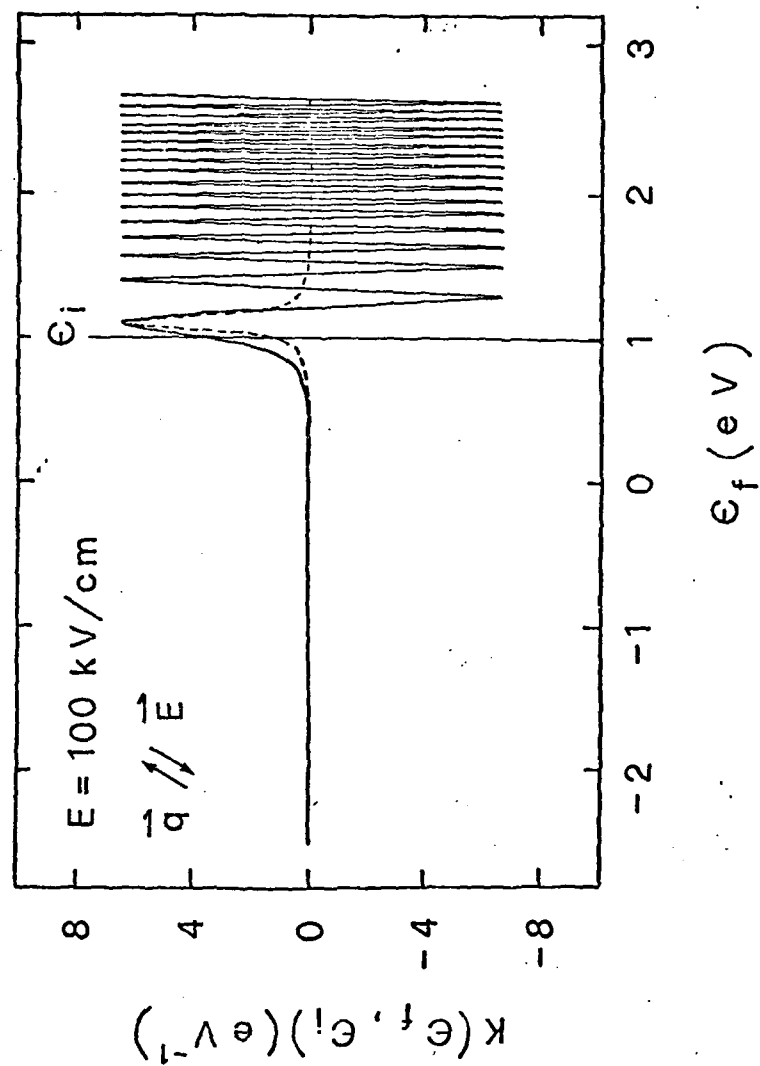


FIG. 2.3

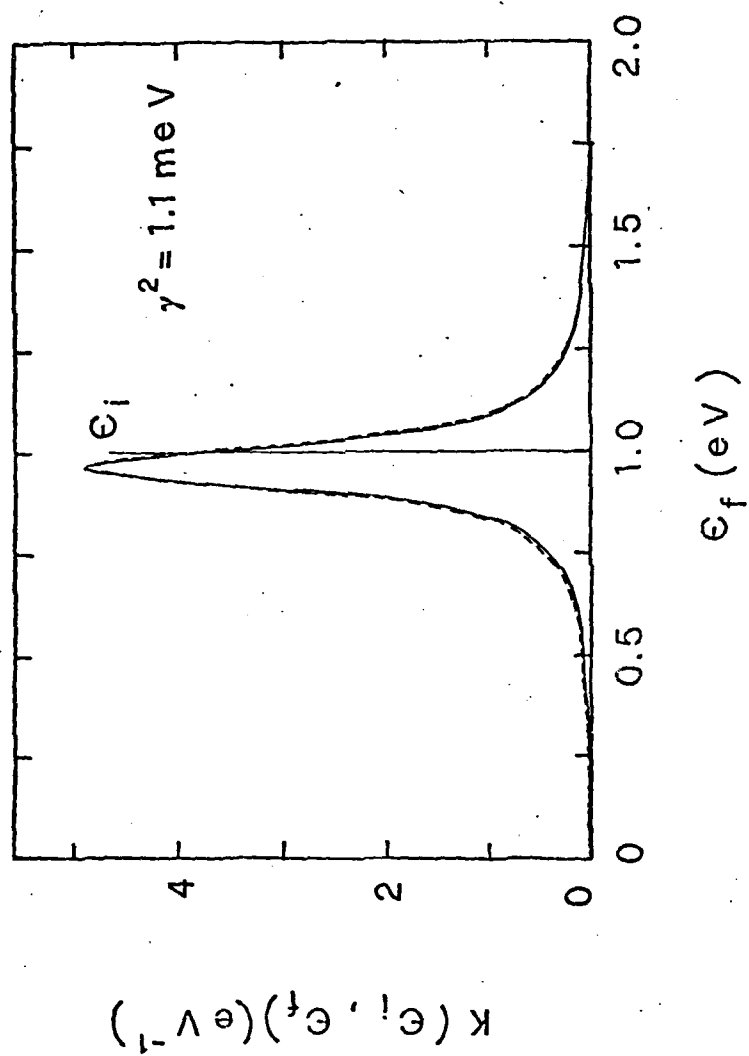


FIG. 2.4

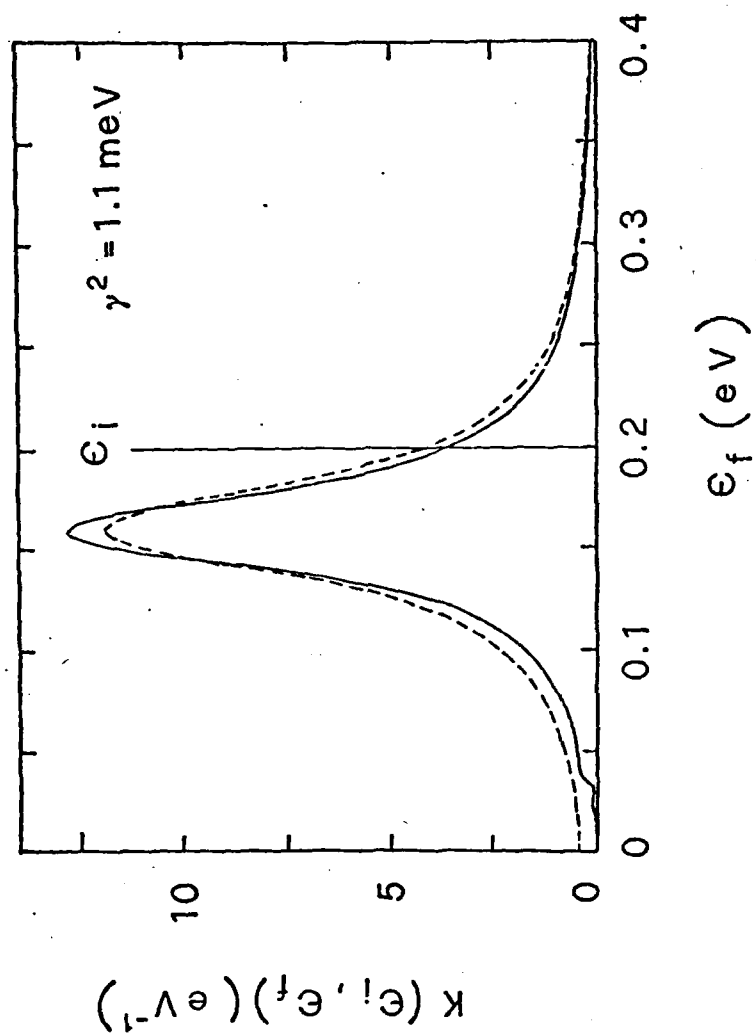


FIG. 2.5

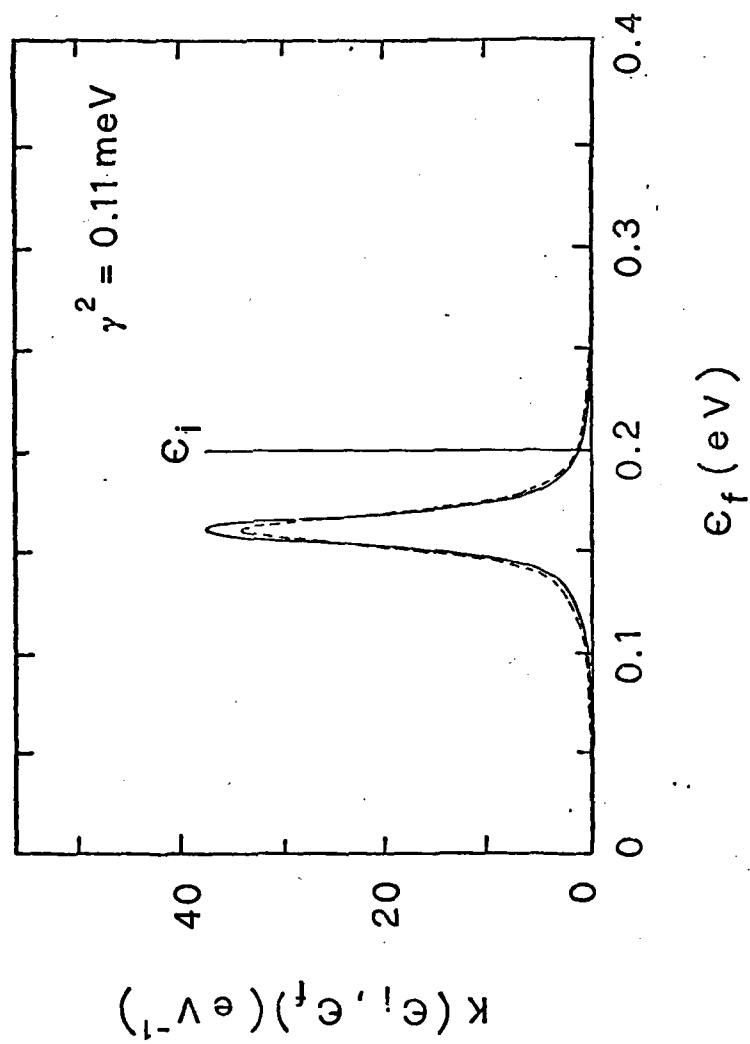


FIG. 2.6

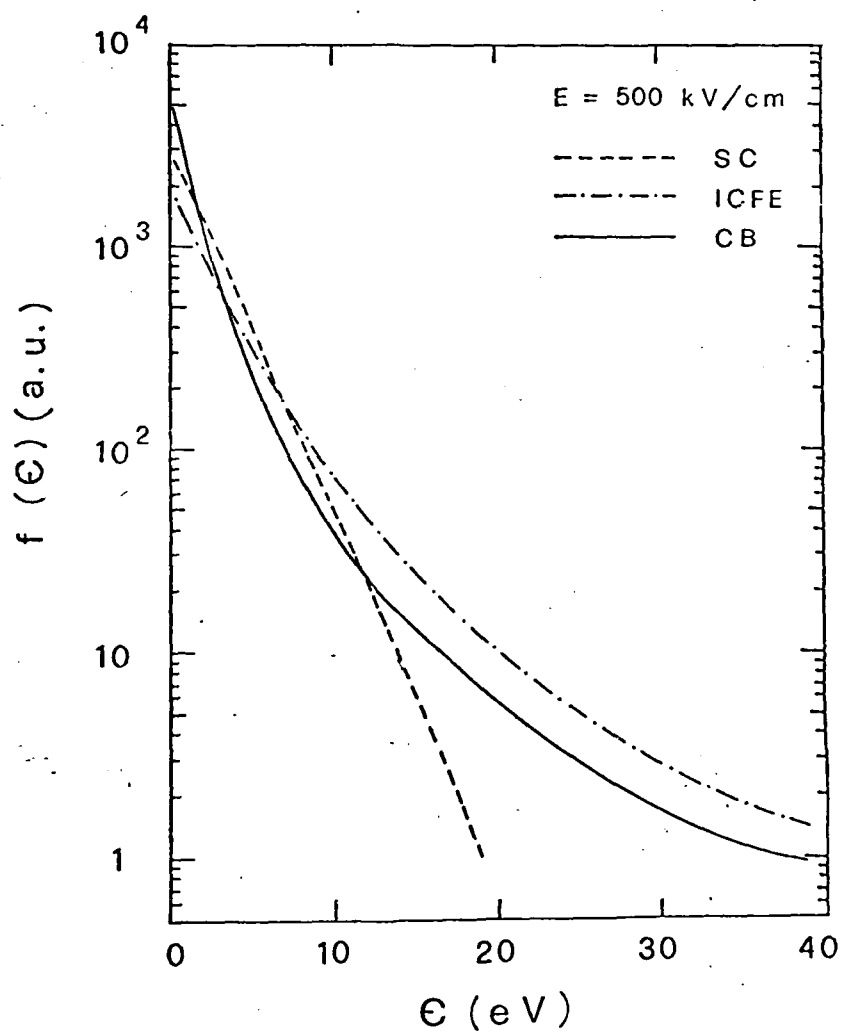


FIG. 2.7

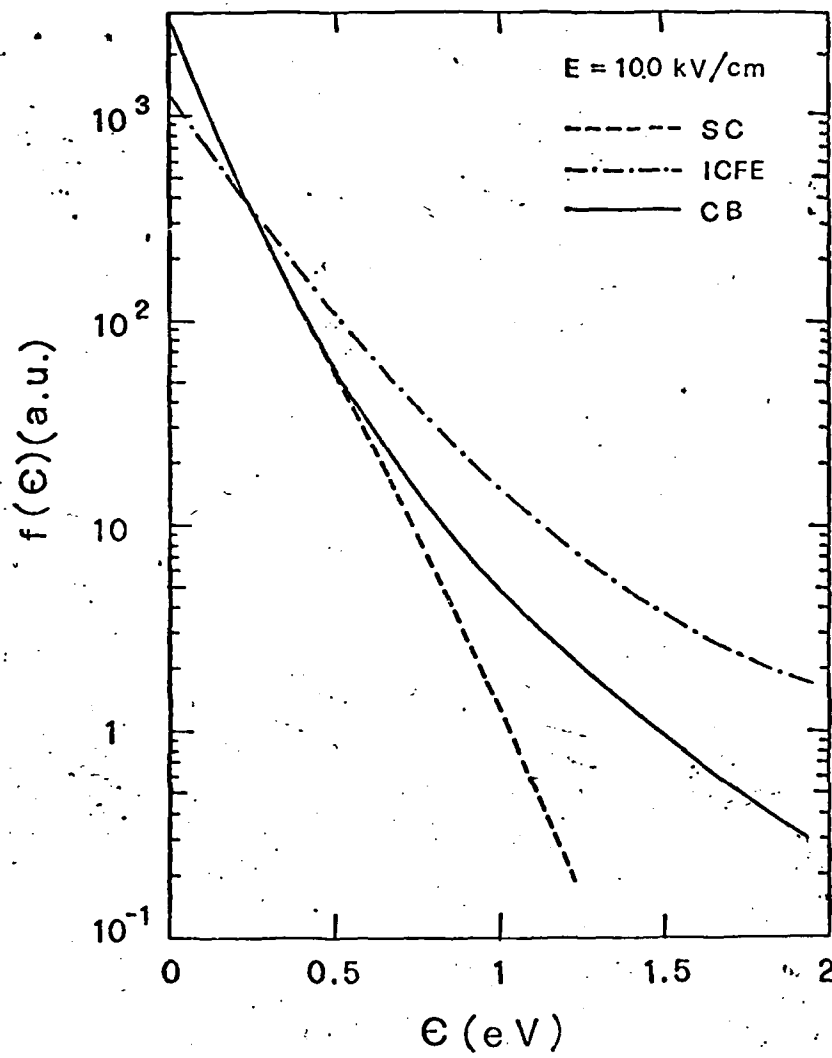


FIG. 2.8

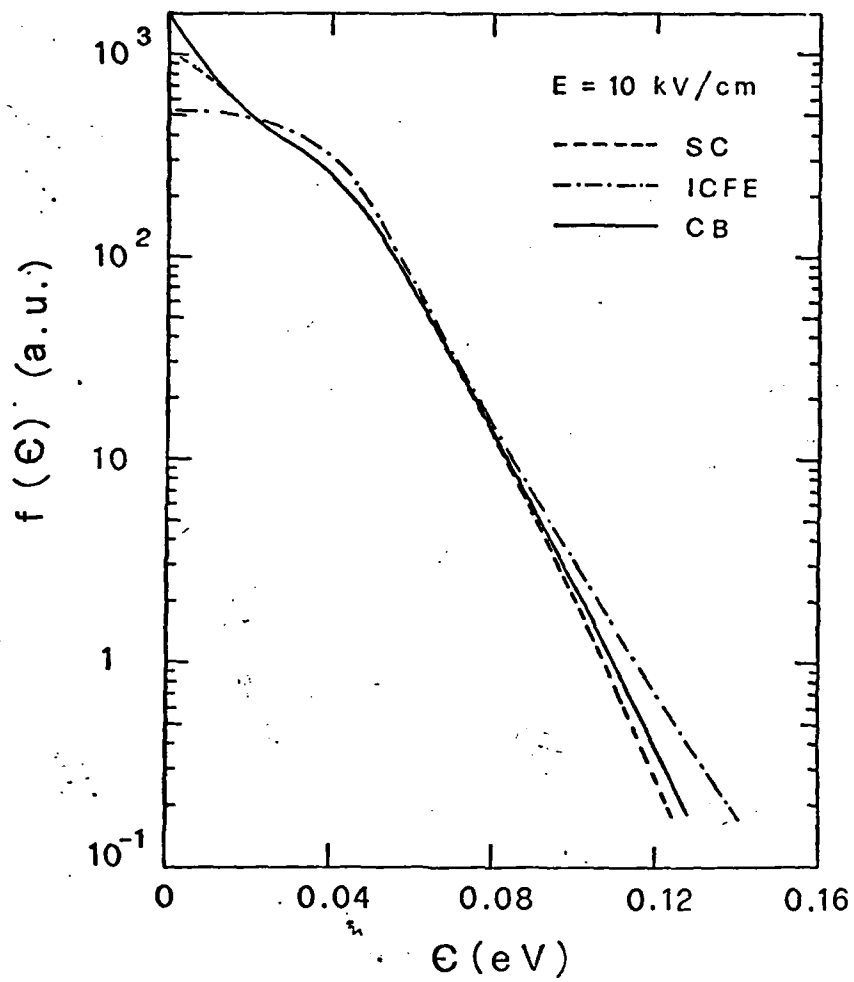


FIG. 2.9

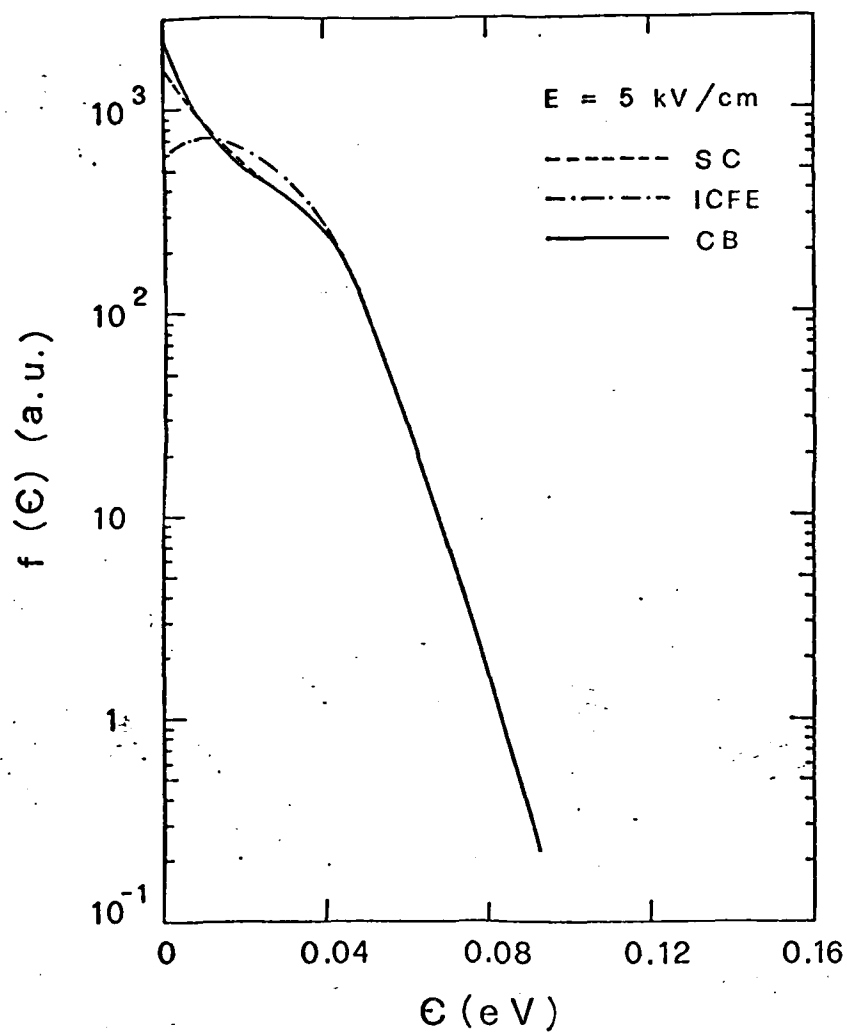


FIG. 2.10

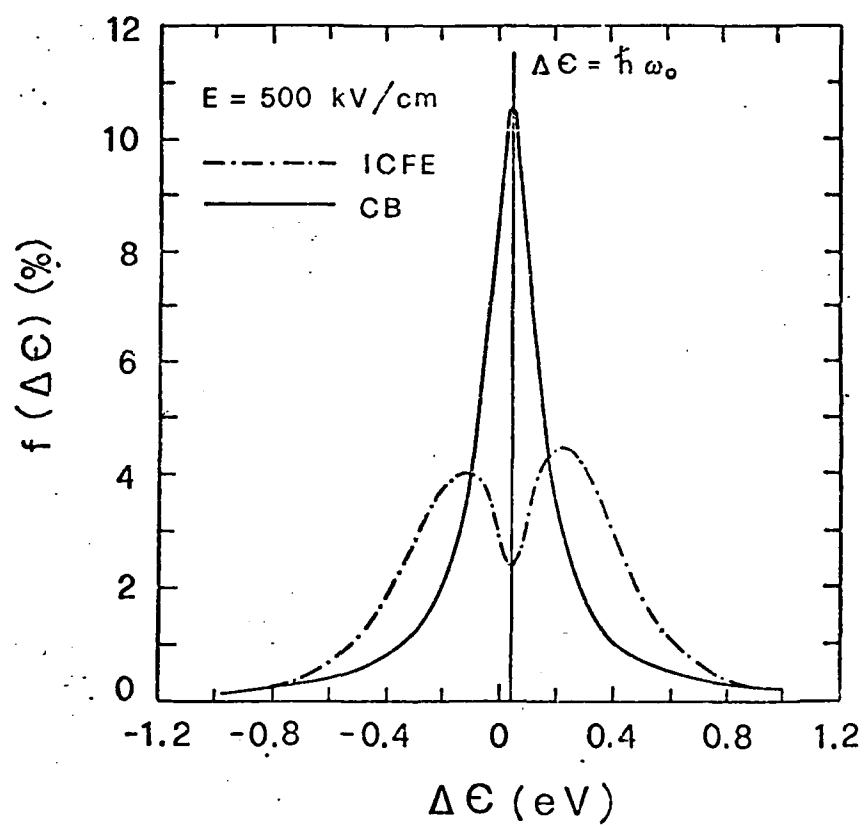


FIG. 2.11

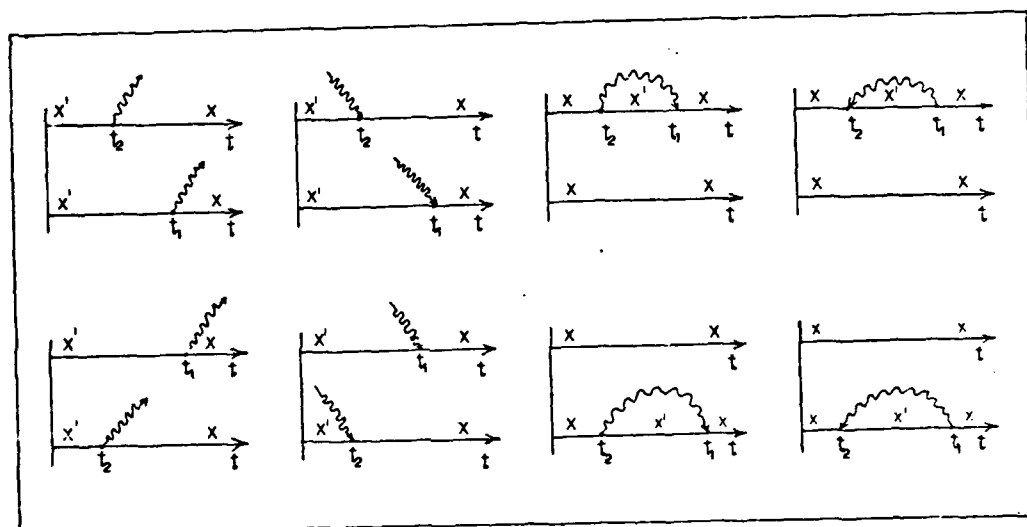


FIG. 2.12

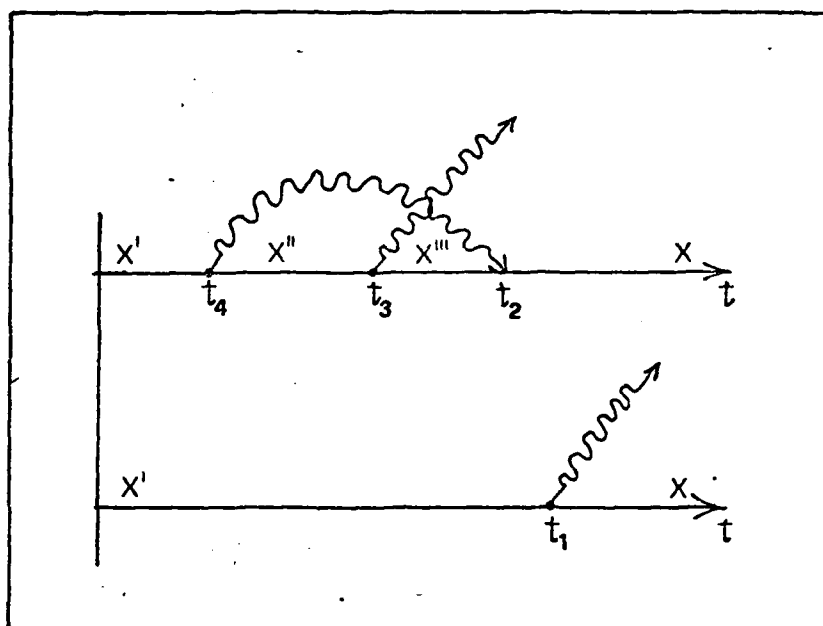


FIG. 2.13

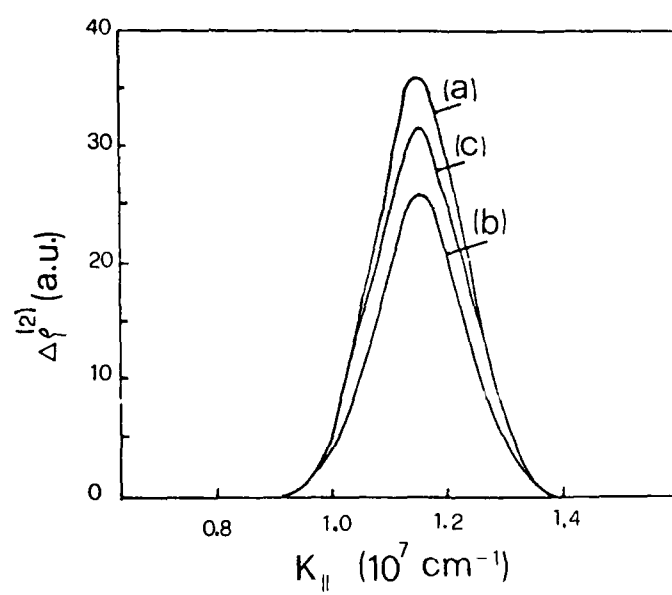


FIG. 2.14

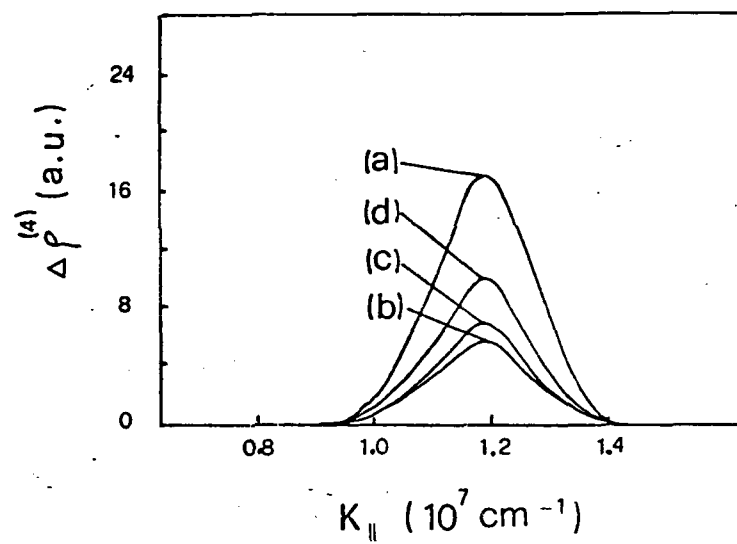


FIG. 2.15

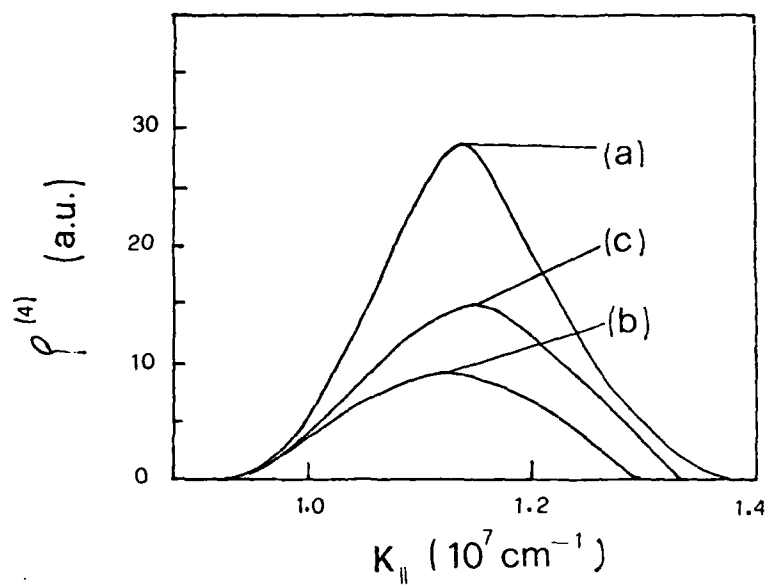


FIG. 2.16

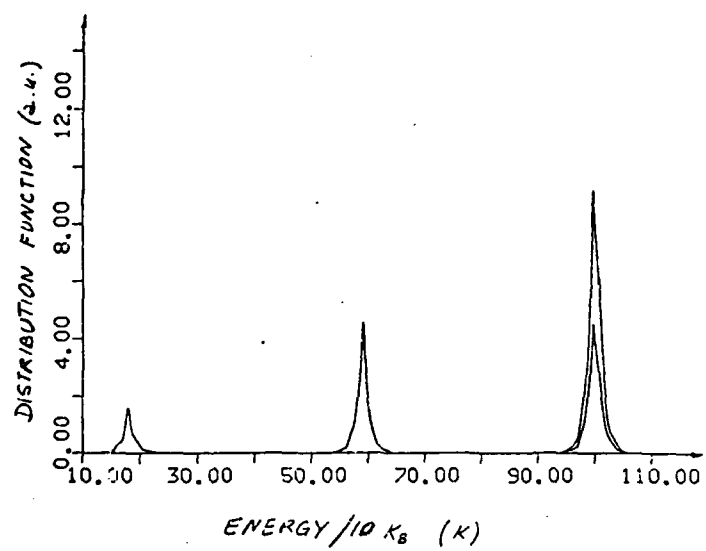


FIG. 2.17

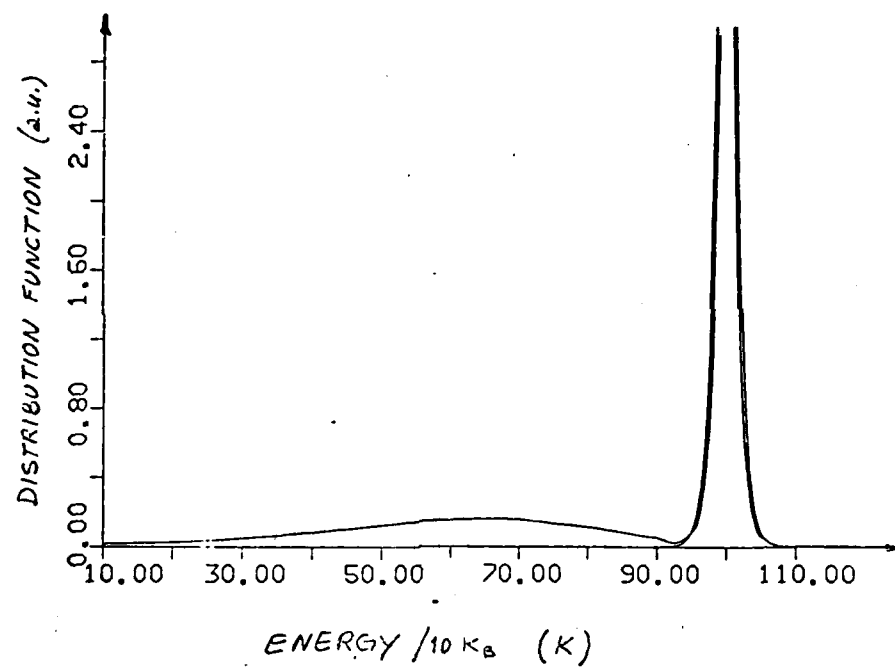


FIG. 2.18

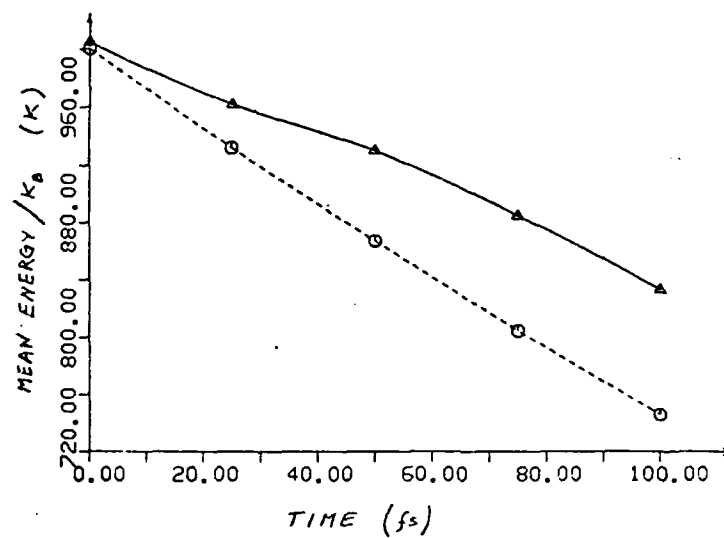


FIG. 2.19

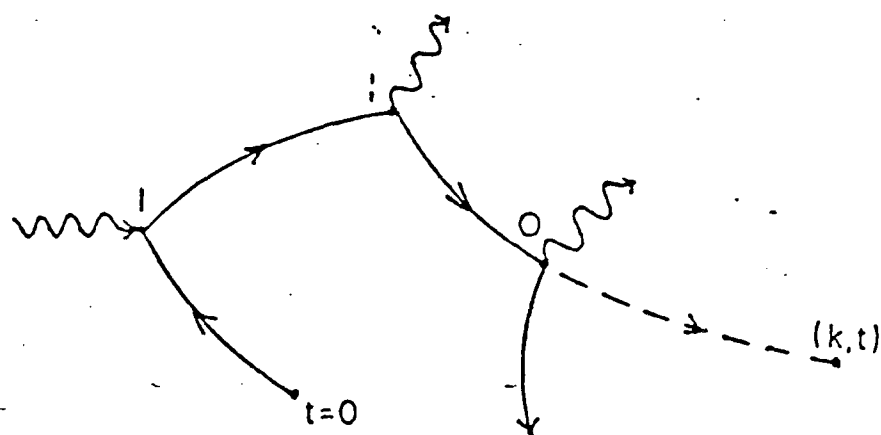


FIG. 2.20

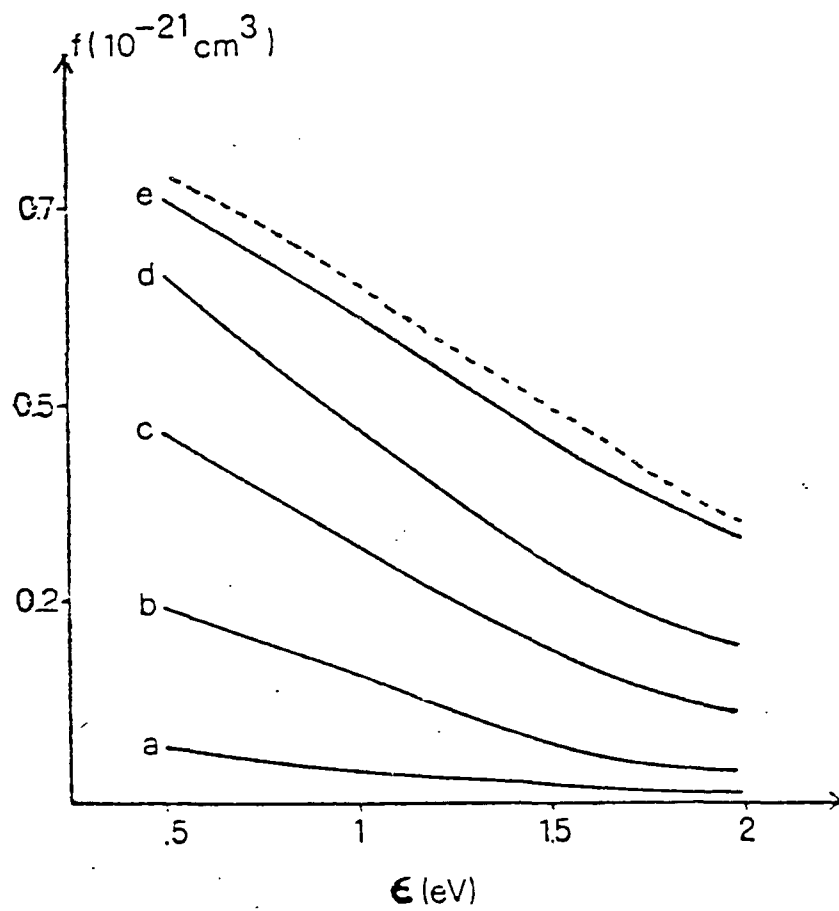


FIG. 2.21

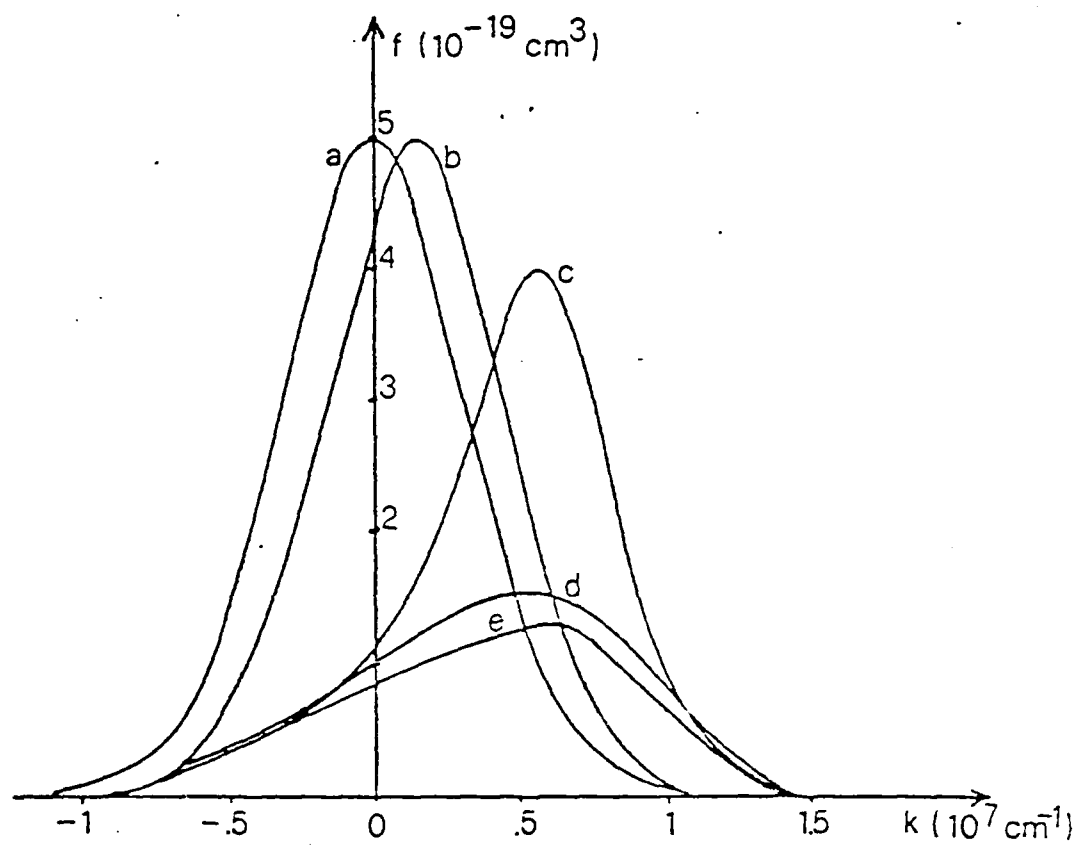


FIG. 2.22

Tables

TABLE 2.1

E (kV/cm)	$\langle \epsilon \rangle$ (eV)	v_d (10^7 cm/s)	ϵ_{max} (eV)	
5	0.015	1.05	< 1	SC
	0.018	0.86	< 1	ICFE
	0.015	1.06	< 1	CB
10	0.019	1.06	< 1	SC
	0.022	0.86	< 1	ICFE
	0.019	1.08	< 1	CB
100	0.13	1.33	49	SC
	0.020	1.07	59 ± 1	ICFE
	0.15	1.38	$110 \pm 13\%$	CB
500	2.5	1.41	$1200 \pm 5\%$	SC
	4.7	1.23	$2200 \pm 40\%$	ICFE
	3.9	1.65	$3850 \pm 13\%$	CB

Table 2.1 - Summary of the carrier mean kinetic energy $\langle \epsilon \rangle$, drift velocity v_d , and the maximum kinetic energy achievable by a carrier during a simulation ϵ_{max} corresponding to the various joint spectral density models at different electric field strengths. The uncertainty of the numerical results is within $\pm 2\%$ if not stated otherwise.

TABLE 2.2

x_f	$\langle \epsilon \rangle$ (eV)	v_d ($10^7 cm/s$)	ϵ_{max} (eV)
$2x_i$	0.20	1.07	59
$4x_i$	0.29	0.98	121
$8x_i$	0.54	0.93	508

Table 2.2 - Dependence of the mean values and of the maximum kinetic energy achievable by a carrier during a simulation ϵ_{max} upon different values of the cut-off energy for the case of ICFE at $E = 100 kV/cm$

3. CORRELATION FUNCTIONS OF HOT-ELECTRONS

3.1 Correlation Functions for Bulk Semiconductors

3.1.1 Introduction

Since the work of Green and Kubo, the use of the velocity autocorrelation function has been proven to be a fundamental tool for the description of the kinetic coefficients under linear response condition in an applied external field. Near equilibrium, the velocity autocorrelation function represents the microscopic quantity which unifies the physical interpretation of both the mobility μ and diffusivity D (fluctuation-dissipation theorem). This is no longer the case under far from equilibrium conditions, when a static electric field E externally applied is sufficiently high to produce hot-electron effects.

Under far from equilibrium conditions it is possible to introduce a set of correlation functions which still enables a unified interpretation of the transport coefficients. In the following sections we will present theoretical developments and results for bulk materials.

3.1.2 Equations of Motion for a Closed Set of Correlation Functions

Following the results of Niez [3.1-3] we use a first principle Heisenberg picture to write the equations of motion for the required quantities, in our case energy and momentum. By a projection operator technique, the thermodynamical motion is separated from the fluctuations. Taking for simplicity a single spherical and parabolic band model semiconductor, it has been proven [3.3] that four correlation functions, which couple velocity and energy fluctuations, are needed. These can be written in matrix notation as:

$$\begin{pmatrix} \phi_{vv}(t) & \phi_{ve}(t) \\ \phi_{ev}(t) & \phi_{ee}(t) \end{pmatrix} = \begin{pmatrix} \langle \delta v \delta v(t) \rangle & \langle \delta v \delta e(t) \rangle \\ \langle \delta e \delta v(t) \rangle & \langle \delta e \delta e(t) \rangle \end{pmatrix} \quad (3.1)$$

The set in Eq. (3.1) is found to satisfy the following closed system of coupled

first order differential equations:

$$\begin{cases} \frac{d}{dt}\phi_{vv} = -\alpha_{11}\phi_{vv} - \alpha_{12}\phi_{ve} \\ \frac{d}{dt}\phi_{ve} = -\alpha_{21}\phi_{vv} - \alpha_{22}\phi_{ve} \end{cases}, \quad \begin{cases} \frac{d}{dt}\phi_{ev} = -\alpha_{11}\phi_{ev} - \alpha_{12}\phi_{ee} \\ \frac{d}{dt}\phi_{ee} = -\alpha_{21}\phi_{ev} - \alpha_{22}\phi_{ee} \end{cases} \quad (3.2)$$

where the coefficients α_{ij} (which depend on the external field but not on time) describe the microscopic properties of the physical system. These coefficients come from the general theory [3.3] when the relaxation time approximation is used. Then, all the slow components of the system dynamics, such as the total energy and momentum, are taken care of by the projection operator used. The kernels of the Langevin-like convolution integrals obtained in this framework are rapidly varying functions [3.4], and the α_{ij} are just their time integrals. The physical meaning of the diagonal terms α_{11} and α_{22} is related to the momentum and energy relaxations rates. The off-diagonal terms α_{12} and α_{21} are zero at equilibrium ($E = 0$) when, as known, the relaxation of momentum and energy are independent. Under hot electron conditions these rates are no longer independent and the off-diagonal terms describe the coupling between them. A microscopic determination of the α_{ij} coefficients remains a formidable problem which has not been yet considered. The analytical solution of Eqs. (3.2) in normalized form is given by:

$$\begin{array}{c} \dots\dots\dots \\ \omega_0^2 \geq 0 \\ \dots\dots\dots \end{array}$$

$$\begin{aligned}
\phi_{vv}(t) &= \frac{e^{-\lambda t}}{\tilde{\alpha}_{21}\omega_0} \{ \tilde{\alpha}_{21}[\omega_0 ch(\omega_0 t) + (\lambda - \alpha_{11})sh(\omega_0 t)] + [(\lambda - \alpha_{11})^2 - \omega_0^2]sh(\omega_0 t) \} \\
\phi_{ve}(t) &= \frac{e^{-\lambda t}}{\omega_0} \{ \omega_0 ch(\omega_0 t)[(\lambda - \alpha_{11}) + \tilde{\alpha}_{21}]sh(\omega_0 t) \} \\
\phi_{ev}(t) &= \frac{e^{-\lambda t}}{\tilde{\alpha}_{21}\omega_0} \{ \tilde{\alpha}_{21}[\omega_0 ch(\omega_0 t) + (\lambda - \alpha_{11})sh(\omega_0 t)] + [(\lambda - \alpha_{11})^2 - \omega_0^2]sh(\omega_0 t) \} \\
\phi_{ee}(t) &= \frac{e^{-\lambda t}}{\omega_0} \{ \omega_0 ch(\omega_0 t)[(\lambda - \alpha_{11}) + \tilde{\alpha}_{21}]sh(\omega_0 t) \}
\end{aligned} \tag{3.3a}$$

$$\begin{aligned}
&\dots\dots\dots \\
&\omega_0^2 < 0 \\
&\dots\dots\dots
\end{aligned}$$

$$\begin{aligned}
\phi_{vv}(t) &= \frac{e^{-\lambda t}}{\tilde{\alpha}_{21}\omega_0} \{ \tilde{\alpha}_{21}[\omega_0 cos(\omega_0 t) + (\lambda - \alpha_{11})sin(\omega_0 t)] + [(\lambda - \alpha_{11})^2 - \omega_0^2]sin(\omega_0 t) \} \\
\phi_{ve}(t) &= \frac{e^{-\lambda t}}{\omega_0} \{ \omega_0 cos(\omega_0 t)[(\lambda - \alpha_{11}) + \tilde{\alpha}_{21}]sin(\omega_0 t) \} \\
\phi_{ev}(t) &= \frac{e^{-\lambda t}}{\tilde{\alpha}_{21}\omega_0} \{ \tilde{\alpha}_{21}[\omega_0 cos(\omega_0 t) + (\lambda - \alpha_{11})sin(\omega_0 t)] + [(\lambda - \alpha_{11})^2 - \omega_0^2]sin(\omega_0 t) \} \\
\phi_{ee}(t) &= \frac{e^{-\lambda t}}{\omega_0} \{ \omega_0 cos(\omega_0 t)[(\lambda - \alpha_{11}) + \tilde{\alpha}_{21}]sin(\omega_0 t) \}
\end{aligned} \tag{3.3b}$$

where $\lambda = 1/2(\alpha_{11} + \alpha_{22})$, $\omega_0^2 = \frac{1}{4} (\alpha_{11} - \alpha_{22})^2 + \alpha_{12}\alpha_{21}$, $\beta = < \delta v \delta \epsilon > / < \delta v^2 >$; $\gamma = < \delta v \delta \epsilon > / < \delta \epsilon^2 >$; $\tilde{\alpha}_{21} = \alpha_{21}/\beta$; $\tilde{\alpha}_{21} = \alpha_{21}\gamma$. We notice that λ and ω_0 are two frequencies which characterize the main features of the time evolution of the correlation functions. As a matter of fact λ , which is always real, is responsible for a damping , while ω_0 , when imaginary, determines an oscillatory behaviour.

3.1.3 Numerical Results

To check the reliability of the functional form given by Eqs. (3.3), we have prepared an Ensemble Monte Carlo simulation for the two following cases of interest.

(i) **Quasi elastic regime:** This condition corresponds to a carrier momentum distribution function with the even part dominating over the odd part. We have considered here scatterings with acoustic and non-polar optical (or intervalley) phonons at 300 K for a simple model semiconductor (Si-like with $E // < 111 >$ [3.5]).

(ii) **Streaming motion regime:** In this condition the odd part of the distribution strongly prevails over the even part. To this purpose, with respect to the previous case, the optical phonon coupling has been arbitrarily increased (by a factor 5) at 77 K.

The results for the above regimes are shown in Figs. 3.1,2, where the data obtained from the simulation are found to agree quite satisfactorily with the analytical curves (we notice that a similar agreement has been obtained at various field strengths from 5 to 200 kV/cm). In particular the quasi elastic regime is characterized by $\lambda > |\omega_0|$, while the streaming motion regime by $\lambda < |\omega_0|$. In the latter case, in agreement with the expectations [3.6], the relationship $\omega_0 = (2\pi/e)E(2m\hbar\omega_{op})^{-1/2}$, $\hbar\omega_{op}$ being the optical phonon energy and m a carrier effective mass, has been verified within the numerical uncertainty. Figure 3.3 shows the dependence with electric field of the α_{ij} coefficients for the case of quasi elastic regime.

Having succeeded in deriving a set of equations describing the evolution of the correlation functions of the thermodynamical variables (v, ϵ) , we consider now, in the same theoretical framework, the basic ideas which underlie the linear response theory around the steady state. We thus apply to the system an extra perturbative electric field $E_1(t)$. The Hamiltonian is now time dependent,

and we focus on the thermodynamical differences between the steady state values of our variables and their values induced by $E_1(t)$. By repeating for the present case the calculations that led to Eqs. (3.3), it appears that the equation which drives the momentum of the system gives, as it is well known, the first fluctuation-dissipation theorem only when $E = 0$, i.e. in the near equilibrium situation. If $E = 0$ one comes with the so-called "dressing term" T_E [3.5], which characterizes the dissipative nature of the steady state. We have been able to evaluate T_E and to give its expressions in terms of the coefficients driving the dynamics of the correlation functions of the thermodynamical variables only. After some delicate algebra (which will be published later), one can write :

$$(-i\omega + \alpha) \begin{pmatrix} \delta < v > (\omega) \\ \delta < \epsilon > (\omega) \end{pmatrix} = eNE_1(\omega) \left\{ \begin{pmatrix} 1/m \\ v_d \end{pmatrix} - \frac{eE}{m} \left[((P;P)_L^{-1})_{2,1} + v_d((P;P)_L^{-1})_{2,2} \right] \sum_{i=1}^2 (\alpha^{-1})_{1,i} \begin{pmatrix} \gamma(1,i) \\ \gamma(2,i) \end{pmatrix} \right\} \quad (3.4)$$

where the notation of Niez [3.3] has been used. In Eq. (3.4) the indices 1 and 2 correspond respectively to the velocity and the energy of the electronic system; furthermore v_d is the steady-state drift velocity. The α coefficients are the same as in Eq. (3.2). The dressing term (second term in the squared braces) has been evaluated taking into account that the collision time τ_c is much shorter than any time describing the dynamics of the relevant variables. In T_E , the $(P;P)_L$ correlation functions of energy and momentum at time $t = 0$ are defined through the displaced Maxwellian distribution of the problem. The γ coefficients in T_E are directly related (through a mass factor m) to the first moments of the collision kernels [3.3] for their definition):

$$\gamma(i,j) \sim \int_0^\infty dt \, t [G_0(t)(1 - \Pi_s) \dot{P}_{i,L} ; (1 - \Pi_s) \dot{P}_{j,L}]_s \quad (3.5)$$

Thus from Eq. (3.4) it is possible to give the complex differential mobility $\mu'(\omega)$ of the system through information coming from the correlation functions of the

thermodynamical variables only. While an explicit formula for μ' from Eq. (3.4) is currently in progress, its expression when the dressing term is neglected (i.e. under warm electron conditions) is given by:

$$\mu'(\omega) = \frac{e}{m} \left[\frac{2\lambda - \alpha_{11} - i\omega}{(\lambda^2 - i\omega) - \omega_0^2} \right] \quad (3.6)$$

3.1.4 Microscopic Expression of the Noise Temperature

Under far from equilibrium conditions due to the presence of a uniform electric field E , the noise associated with velocity fluctuations is commonly described by the noise equivalent temperature T_n , a physical quantity which can be easily measured [3.6]. When two particle interactions are neglected and the system is electrically stable (i.e. $\mu' > 0$, μ' being the differential mobility), a generalized Einstein relationship was proven to hold for T_n [3.7]:

$$T_n = \frac{eD}{K_B \mu'} \quad (3.7)$$

Here e is the unit charge, K_B the Boltzmann constant and D the diffusion coefficient.

The objective of this section is to provide for the first time a microscopic expression for T_n . The essence of our result relies on the proof that both D and μ' , and therefore T_n , can be defined from the same set of correlation functions describing the system under far from equilibrium conditions.

To this end we shall consider Eq. (3.6) in the limit $\omega \rightarrow 0$ and obtain:

$$\mu' = \frac{e}{m} \left(\frac{2\lambda - \alpha_{11}}{\lambda^2 - \omega_0^2} \right) \quad (3.8)$$

We recall that Eq. (3.8) is still an approximation since it neglects the so-called "dressing term" of Ref. [3.3], which comes from the dissipative nature of the steady-state. This limits the reliability of the present theory to fields below 20 kV/cm.

From the definition of D in terms of ϕ_{vv} [3.6] we obtain the desired definition of the noise temperature in terms of the α_{ij} coefficients as:

$$T_n = \frac{e}{K_B \mu'} \int_0^\infty \phi_{vv}(t) dt \quad (3.9)$$

Figure 3.4 shows the comparison between this theory and experiments [3.8] of the excess noise temperature for the case of electrons in Si. The agreement found is good and supports the present interpretation of the noise temperature in terms of correlation functions.

In summary, explicit formulae have been obtained for the time evolution of a closed system of correlation functions which generalized the linear response theory to the far from equilibrium case (hot electrons). This theory provides a unified microscopic interpretation of both diffusion (given by the Fourier transform of $\phi_{vv}(t)$) and mobility. At zero field our formulation coincides with the first form of the fluctuation-dissipation theorem. Therefore, the present theory can be viewed as a generalization of the Kubo formalism under far from equilibrium conditions. As such, we have proven that this formalism consistently interprets numerical simulations, as obtained through standard Monte Carlo procedure, for a variety of physical situations and experimental results.

3.2 Correlation Functions for Quantum Wells

3.2.1 Introduction

A theoretical analysis of velocity fluctuations can yield relevant information on the microscopic interpretation of transport coefficients as well as on the detailed features of the scattering sources. This analysis becomes even more important if submicrometer devices are considered, where ultrafast transport processes are usually involved and a deeper insight into the physics of transport phenomena is required. Furthermore fluctuations can play an important role in

the design and characterization of the device itself.

Several papers have appeared in the literature on this subject for bulk materials, while very scarce theoretical investigations have been done so far in this field for 2D systems, and few experimental data is available for noise properties in quantum wells.

The theoretical problem can be approached through a unified theory formulated in terms of the autocorrelation function, a quantity directly related to diffusivity and noise. This method can be used to describe both steady-state (Sec.3.2.2) and transient (Sec.3.2.3) situations, and also to analyse the different contributions due to the different physical sources of fluctuations which arise in the presence of an applied electric field.

In order to obtain results for realistic structures, a Monte Carlo simulation of the quantum well has been used, that allows to obtain an exact solution of the transport problem in hot electron conditions (i.e. out of equilibrium, in presence of high electric fields), where analitical techniques cannot be succesfully applied without introducing severe approximations. Furthermore, a direct simulation of the dynamics of charge carriers inside the crystal enables us to extract any required physical information while the solution of the transport equation is being built up and the simulation can be easily modeled in order to reproduce particular experimental conditions.

The physical system and the details of the Monte Carlo procedure used for the simulation of the 2D electron gas in the quantum well are presented in Sec.3.2.4. Results for autocorrelation function, diffusivity, and noise at room temperature are discussed in Sec. 3.2.5 and 3.2.6 for stationary conditions and transient conditions, respectively, together with a comparison between 2D and 3D data.

Few syntetic conclusive statements are given in Sec.3.2.7 together with possible developments of this research for the future.

3.2.2 Autocorrelation Function, Diffusion and Noise in Stationary Conditions

Let us consider an ensemble of electrons in a crystal semiconductor subject to an external electric field \mathbf{E} and to the action of scattering agents (phonons, impurities, etc). If the electrons have any nonuniform distribution in space the phenomenon of diffusion occurs, tending to make the concentration uniform through the spreading out of the carriers.

Diffusion is described, at a phenomenological level, by the equation [3.9]:

$$\mathbf{J}_i = e\{n(\mathbf{r})v_{di} - D_{ij} \frac{\partial n(\mathbf{r})}{\partial x_j}\} \quad (3.10)$$

In the above equation e is the electron charge, \mathbf{r} is the space position with components x_i , $n(\mathbf{r})$ and \mathbf{J} the particle density and current density, respectively, D_{ij} is the diffusion coefficient tensor ($i,j=1,2,3$, the sum over repeated indices is implied), v_d the drift velocity of the carriers in absence of diffusion.

If \mathbf{E} is applied along a high symmetry direction of a cubic crystal, then D_{ij} reduces to a diagonal form, with a longitudinal component D_l and two transverse components D_t . In the following we will analyze diffusivity and fluctuations along the field direction; consequently we will use a simplified scalar notation where all the vector quantities are substituted with their longitudinal components.

For vanishing small electric-field strengths, diffusivity D and mobility μ are field independent and verify the Einstein relation:

$$D = \frac{\mu K_B T}{e} \quad (3.11)$$

where T is the crystal temperature and K_B the Boltzmann constant.

At high fields the Einstein relation fails and the study of diffusion is generally performed through the introduction of a field-dependent D [3.10].

If the concentration gradients are small, in absence of carrier-carrier interactions $D(E)$ can be obtained from the following equation:

$$\frac{d\langle(x - \langle x \rangle)^2\rangle}{dt} = 2D \quad (3.12)$$

where x is the displacement along the field direction and brackets represent ensemble average. The quantity on the right hand side is the second central moment of the distribution $n(r)$ (SCM); eq.(3.12) is valid at times longer than both the transient transport time and the time necessary for setting up the correct space-velocity correlations at the basis of diffusivity effects.

The diffusion phenomenon is strictly related to velocity fluctuations and noise. The mathematical quantity that describes the common origin of diffusion and noise is in fact the autocorrelation function of velocity fluctuations, which carries the information on how large the fluctuations are and how they decay in time:

$$C(t) = \langle \delta v(\tau) \delta v(\tau + t) \rangle \quad (3.13)$$

(the mean value in steady state conditions is independent of τ). $C(t)$ is related to the diffusion D through [3.9]:

$$D = \int_0^\infty dt C(t) \quad (3.14)$$

Thus D can be evaluated from $C(t)$, which is of interest in itself since it gives important physical information on the time evolution of the dynamics of the carriers.

Finally, we introduce the noise spectrum $S_v(\omega)$:

$$S_v(\omega) = \lim_{T \rightarrow \infty} \langle \left| \int_0^T \delta v(t) e^{i\omega t} dt \right|^2 \rangle \quad (3.15)$$

Another well-known relation between $C(t)$ and the noise spectrum is given by the Wiener-Kintchine theorem [3.9]:

$$S_v(\omega) = 2 \int_0^\infty dt C(t) e^{i\omega t} \quad (3.16)$$

From this last equation and eq.(3.14) extended to non-zero frequencies, we have:

$$D(\omega) = \frac{1}{2} S_v(\omega) \quad (3.17)$$

Different physical sources contribute to fluctuations and diffusion of carriers in quantum wells. As it happens in bulk materials, fluctuations in carrier momentum produce the so called "thermal" velocity fluctuations [3.9]; energy fluctuations are associated with "convective" velocity fluctuations and noise [3.11], and valley fluctuations bring about "intervalley" velocity fluctuations [3.12], when, as in our case, two or more non equivalent valleys exist. In the case of quantum wells, however, the existence of several subbands with different average velocities implies the appearance of a new source of velocity fluctuations and noise, that is produced by the fluctuation of the subband occupied by the electrons during their motion in the quantum well. In the following we will refer to these fluctuations as to "intersubband" velocity fluctuations.

Following a decomposition procedure already applied to bulk structures [3.13,3.14] let us consider an electron that, at time t , is in a subband of type $B(t)$ and in a valley of type $V(t)$ (the indices V and B depend on time because carriers during their motion change both valley and subband because of scattering); let also $v_{\epsilon VB}(t)$ be the mean velocity of electrons in valley V and subband B with energy between ϵ and $\epsilon + d\epsilon$.

The instantaneous velocity of each electron $v(t)$ can then be written as the drift velocity plus a number of fluctuating terms:

$$\begin{aligned} v(t) &= v_d + [v_B(t) - v_d] + [v_{VB}(t) - v_B(t)] + [v_{\epsilon VB}(t) - v_{VB}(t)] + [v(t) - v_{\epsilon VB}(t)] \\ &= v_d + \delta v_B(t) + \delta v_V(t) + \delta v_\epsilon(t) + \delta v_\kappa(t), \end{aligned} \quad (3.18)$$

$\delta v_B(t)$ and $\delta v_V(t)$ are the fluctuations associated with the drift velocity of the subband and the valley in which the electron is at time t , respectively; $\delta v_\epsilon(t)$

is the velocity fluctuation associated to the fluctuation of electron energy, and $\delta v_{\kappa}(t)$ is the velocity fluctuation associated with the fluctuation of the electron momentum.

By using the definition in Eq.(3.13), the steady-state autocorrelation function becomes

$$C(t) = \sum_{i,j} \langle \delta v_i(t') \delta v_j(t' + t) \rangle = \sum_{i,j} C_{ij}(t), \quad (3.19)$$

where

$$C_{ij}(t) = \langle \delta v_i(t') \delta v_j(t' + t) \rangle, \quad (3.20)$$

and $i, j = B, V, \epsilon, k$. The total autocorrelation function of velocity fluctuations contains four "diagonal" contributions $C_{ii}(t)$ in Eq.(3.19), at the origin of interband (C_{BB}), intervalley (C_{VV}), convective ($C_{\epsilon\epsilon}$), and thermal ($C_{\kappa\kappa}$) noise, respectively. In general, however, off-diagonal terms C_{ij} also contribute to the autocorrelation of velocity fluctuations [3.13,3.14]. Only when the relaxation times of the various fluctuating terms have well different values, in calculating the "off-diagonal" terms one of the two fluctuations can be assumed as constant, while the other fluctuation averages to zero.

Owing to the linearity of Eqs.(3.14) and (3.16) we can also associate specific terms contributing to the autocorrelation function with corresponding terms contributing to diffusivity and noise, thus making explicit their physical origins.

3.2.3 Autocorrelation Function and Diffusion in Transient Conditions

The diffusion process of a carrier ensemble comes from the particle space-velocity correlations which arise during the evolution in time of the system. Starting from an initial condition in which the particle positions and velocities are totally uncorrelated, the process which occurs during the time necessary for setting up the correlations will be defined as correlation transient. Furthermore, when a high electric field is applied at a certain time to the electron ensemble,

the transport process itself must pass through a transient region which is necessary for attaining the stationary distribution $f(\mathbf{k})$ in \mathbf{k} space. This process is the transport transient.

The definition of the transient diffusion coefficient has been given by a generalization of Eq. (3.12) to arbitrary small times [3.15-3.17]:

$$D(t) = \frac{1}{2} \frac{d}{dt} \langle [z(t) - \langle z(t) \rangle]^2 \rangle, \quad (3.21)$$

where $z(t)$ is the space position of a carrier at time t along the z direction parallel to v_d .

This generalization can be put in an equivalent form in terms of the two-time transient autocorrelation function. If there is no correlation between the initial positions and velocities of the particles we have [3.16]:

$$D(t) = \int_0^t d\tau C_t(\tau), \quad (3.22)$$

with

$$C_t(\tau) = \langle \delta v(t) \delta v(t - \tau) \rangle, \quad 0 \leq \tau \leq t \quad (3.23)$$

Eq.(3.22) reduces to Eq.(3.14) in steady-state conditions ($t \rightarrow \infty$).

By comparing these two equations, we see that in transient cases (i) the integration interval ranges from $t=0$ (initial conditions) up to t (observation time); (ii) the autocorrelation function to be integrated in the transient analysis is not time independent; it is given by the specific ensemble average at a particular time, and its shape provides information about the transport transient.

3.2.4. The Physical System and The Monte Carlo Procedure

Electrons are simulated in a square well representing the effective 1D potential arising from the band offset between *GaAs* and *Al_xGaAs* ($x=.23$). The solutions of the wave equation for this potential give rise to a series of 2D subbands which are used in calculating the scattering rates for electronic motion

parallel to the well, modeled using an Ensemble Monte Carlo simulation. We treat both intra- and intersubband scattering of the 2D electrons by bulk longitudinal optical phonons; intervalley scattering to the satellite L-valleys is also included. Details of the physical model and of the Monte Carlo code for the quantum well can be found in Refs.3.18 and 3.19.

From the time evolution of the electron ensemble, we calculate the second central moment of the carrier displacement as a function of time and the transient autocorrelation function $C_t(\tau)$ [3.14]. The transient diffusion coefficient can be evaluated from them in two independent ways using eq.(3.21) and eq.(3.22).

The analysis of the various contributions to the stationary autocorrelation function requires a previous MC evaluation of the mean velocities in eq.(3.18). The stationary diffusion coefficient is determined both from the SCM following eq.(3.12) and from the ACF using eq.(3.14). The stationary noise spectral density is evaluated through eq.(3.16).

In order to compare 2D results with 3D results an Ensemble Monte Carlo program for bulk GaAs has also been used [3.14]. The physical model for GaAs includes the same intravalley and intervalley scattering sources as the 2D program, and the input parameters of the material have been consistently chosen.

3.2.5 Results for Stationary Conditions

Results have been obtained at 300 K for a 100 Å well for different applied electric fields. Fig.3.4 and Fig.3.5 report the longitudinal diffusion coefficient and the drift velocity of electrons as functions of field strength for both the 2D system and bulk GaAs. The absence of dissipative scattering mechanisms below the optical phonon energy does not permit the simulation of ohmic conditions. However the extrapolation to the low-field limit of the data for v_d and D satisfies

the Einstein relation within the Monte Carlo accuracy.

The ohmic mobility in the two cases is not significantly different because the 2D polar optical scattering rate is very close to the same curve for 3D. Consequently the equilibrium D is also close for 2D and 3D.

Negative differential mobility is present in both curves, and the threshold field for electron transfer to the upper valley and bands in 2D is lower than in 3D. At room temperature, for fields lower than the threshold, the dominant scattering is essentially given by intravalley polar optical interaction. When the electron energy is high enough to allow transfer to upper valleys and upper subbands mobility decreases with field.

The diffusion coefficient is found to decrease monotonically in both cases at increasing fields. At low and intermediate fields D is larger in 2D than in 3D because carrier random velocities are larger in the quantum well than in 3D. At higher fields the difference between 2D and 3D is reduced and finally it disappears when the electron energy is high enough to guarantee full randomization of electron paths in k space.

Our results differ from the theoretical data of van Rhee *et al.* [3.20,3.21], who found large difference between 2D and 3D results for both drift velocity and diffusivity vs. field, while the present Monte Carlo data seem to show better agreement with experiments [3.21], even though a direct comparison would require the knowledge of accurate values of both experimental and theoretical low-field diffusivity.

As a further confirmation of the above interpretation, Fig. 3.7 shows the normalized ACF of velocity fluctuations as a function of time for $E=2,6,10$ kV/cm for the 2D case. A negative tail is present at 6 and 10 kV/cm which is due to the dynamical effect of the transfer back and forth from upper valleys. Furthermore the time necessary to cancel the correlations between velocity fluctuations is larger at fields close to the threshold field, and then it decreases at

increasing fields.

A comparison of the data at 10 kV/cm with the 3D data at the same field reported in Ref.3.14 shows that the decay time of the ACF is slightly shorter in the 2D case. The presence of different subbands in fact tends to destroy the strong correlation which sets in at fields above threshold for upper-valley transfer between large positive k values (before intervalley transfer), and large negative k values (after intervalley transfer) [3.22].

Fig. 3.8 shows the ACF of velocity fluctuations and the different diagonal contributions, as analysed in Sec. 2.2.2, for $E=7$ kV/cm. Within this analysis it is seen that the thermal fluctuations are in this conditions, much larger than the other fluctuations, like it happens in bulk GaAs [3.14], owing to the high electron energy, and they practically determine the value of the autocorrelation function at short times .

The diagonal terms C_{ee} and C_{VV} are smaller for an order of magnitude. They are almost equal in value at short times, but the intervalley term slowly decays to zero in about 3 ps, while the convective term vanishes in less than 1 ps. The intervalley term is responsible for the long-time tail of the total autocorrelation function.

We can notice that the decay time of C_{kk} is longer than the decay time of C_{ee} ; this fact is related again to the strong correlation between k values above threshold discussed above, that is peculiar of polar materials.

The new term C_{BB} not present in 3D system is negligible in these conditions because the drift velocities in different subbands are very close to each other. We expect to see an appreciable contribution only when the 1D levels are well separated in energy. Finally we can say that the overall contribution of off-diagonal terms C_{ij} is also negligible due to the difference in characteristic decay times associated to the different sources of fluctuation (0.6 ps for C_{ee} , 1.8 ps for C_{kk} , 2.5 ps for C_{VV}).

Fig.3.9 shows the power spectral density of velocity fluctuations as a function of frequency at $E=2, 5$, and 10 kV/cm. This quantity exhibits the same qualitative behaviour of the 3D case [3.14]. The bump at frequencies around 10^3 GHz is due to the presence of the negative part in the ACF. The maximum is shifted towards higher frequencies as the field increases because the negative correlations appear at shorter times the higher the field.

3.2.6 Results for Transient Conditions

Fig.3.10 shows the transient ACF $C_t(\tau)$ as evaluated from the Monte Carlo simulation using eq.(3.23) for $E=7$ kV/cm at different times t . The evolution in time of the shape of this curve allows us to verify directly how the scattering agents act during the very transient evolution of the system.

The first curve at $t=0.5$ ps shows a very large negative part at τ between .3 and .5 ps. At these short times the strong negative correlation of the values of electron wavevector due to the cycling motion in k space between central and upper valley is setting in. At longer times it is smoothed down because electrons progressively visit larger zones of k space.

At intermediate observation times ($t=2, 3$ ps) this correlation becomes, at the longest τ 's, even positive before stabilizing approximately over the steady-state value at $t=4$ ps.

The initial values of the transient ACF at very low τ 's first increase because of the initial overshoot in carrier velocity at observation times of .5 and 1 ps, and then they decrease monotonically towards the steady-state value.

Fig.3.11 shows the transient diffusion coefficient as a function of time for the same fields of Fig. 3.7. For the lowest field ($E=2$ kV/cm) below threshold for intervalley transfer D reaches monotonically the steady-state value. At 5 and 10 kV/cm D first increases rapidly, then it decreases to values lower than the steady-state value, and finally it reaches the stationary value. In 3D GaAs

D is found to be even negative because of the same effect, i.e. the electron cloud after a first initial spread, for a short time shrinks, and then it is blown around again. This peculiar behaviour of polar materials is related to the decrease in velocity during the transient, when the electron cloud begins the transfer to upper valleys and bands.

In 2D systems the presence of upper subbands seems to smooth the strong negative correlation of the dynamical picture described above, and D is always found positive.

Finally Fig.3.12 shows the transient evolution of the diffusion coefficient for two different carrier initial conditions. Curve (a) describes carriers starting from an equilibrium thermal distribution in the central valley of the lower subband, while curve (b) corresponds to an initial monoenergetic carrier distribution in the upper valley of the second subband, with energy much larger than both equilibrium and steady-state mean energy, that may roughly describe the initial condition of optically excited carriers.

From the comparison of the two cases it can be seen that the overshoot of D is strongly enhanced in the second case (for about a factor 3), but the undershoot is not strongly changed in value, even though the minimum is shifted at longer times. Even in this case transient D is never found negative.

In summary, a theoretical analysis of velocity fluctuations in GaAs-AlGaAs quantum wells both in steady-state and in transient conditions has been performed. Different contributions to velocity fluctuations and diffusion are analysed separately in a 2D system and, in particular, the contribution of inter-subband fluctuations, a new source not present in bulk system, is estimated. This study allows to acquire a deeper insight into the microscopic details of the transport picture in these structures.

A theoretical analysis of the transient properties of fluctuations and diffusivity of electrons in quantum wells is presented for the first time. Results

show that the transient features are strongly dependent on initial conditions, and that, for initial hot carrier distributions, D can be three times larger than for the case of equilibrium distributions. These results are important particularly in connection with the realization of submicrometer devices, for which the transit time can be comparable with the time required to attain steady-state conditions, and the distance travelled by carriers during the transient can be a significant portion of the device length.

This analysis will be extended in the future to quantum wells of different depths, and to more realistic models including real-space transfer, electron-electron and electron-hole interactions.

References

- [3.1] J.J. Niez and D.K. Ferry, Phys. Rev. B28, 889 (1985).
- [3.2] J.J. Niez , K.S. Yi and D.K. Ferry, Phys. Rev. B28, 1988 (1985).
- [3.3] J.J. Niez, Superlattices and Microstructures 2, 219 (1986).
- [3.4] D. Foster "Hydrodynamics fluctuations, broken symmetry and correlation functions" Benjamin (Reading, 1975).
- [3.5] P. Lugli, Ph. D. Dissertation, Colorado State University, (1985) unpublished.
- [3.6] L. Reggiani "Hot electron transport in semiconductors" Topics in Applied Physics, Vol. 58, Springer (Heidelberg, 1985).
- [3.7] P.J. Price, in "Fluctuation Phenomena in Solids" Ed. R.E. Burges, Academic Press, (New York, 1965) p. 335.
- [3.8] D. Gasquet, Doctorat d'Etat Dissertation, University of Montpellier (1984) unpublished.
- [3.9] F. Reif, "Fundamentals of Statistical and Thermal Physics", Mc Graw Hill, New York, 1965.
- [3.10] C. Jacoboni and L. Reggiani, Advances in Physics 28(4), 493 (1979).
- [3.11] P.J. Price, in "Fluctuation Phenomena in Solids", R.E. Burgess ed., Chapter 8, Academic Press, New York (1965).
- [3.12] W. Shockley, J.A. Copeland, and R.P. James, "Quantum Theory of Atoms, Molecules, and The Solid State", Academic Press, New York (1966).
- [3.13] R. Brunetti and C. Jacoboni, Phys. Rev. Lett. 50 (15), 1164 (1983).
- [3.14] R. Brunetti and C. Jacoboni, Phys. Rev. B15, 29(10), 5739 (1984).
- [3.15] A. Alberigi Quaranta, V. Borsari, C. Jacoboni, and G. Zanarini, Appl. Phys. Lett., 22, 103 (1973).
- [3.16] D.K. Ferry and J.R. Barker, J. Appl. Phys. 52, 818 (1981).

- [3.17] R. Brunetti and C. Jacoboni, in "Semiconductors Probed by Ultrafast Laser Spectroscopy", R.J.J. Alfano ed., vol.1,p.367 (1984).
- [3.18] L. Reggiani, R. Brunetti, and C. Jacoboni, Proc. III Int. Conference on Hot Carriers in Semiconductors, J. Phys. Colloques 42, C7-73 (1981).
- [3.19] S. M. Goodnick and P. Lugli Proc. Int. Conference on High Speed Electronics, Ed. Kallback and Beneking, Springer Series in Electronics and Photonics, Vol.22, 116 (1986).
- [3.20] S. M. Goodnick and P. Lugli, Phys. Rev. B, to be published.
- [3.21] A.D. van Rheenen and G. Bosman, Proc. Int. Conf. on Noise in Physical Systems and 1/f Noise, p.163, North Holland (1985).
- [3.22] C. Whiteside, G. Bosman and H. Morkoc, Proc. Int. Conf. on Noise in Physical Systems and 1/f Noise, Montreal, 1987 to be published.
- [3.23] W. Fawcett, D.A. Boardman, and S. Swain, J. Phys. Chem. Solids 31, 1963 (1970).

Figure Captions

Fig. 3.1 - Normalized correlation functions as a function of time for the case of electrons in Si at $T = 300$ K and $E = 10$ kV/cm. Continuous and dashed curves refer to present theory and Monte Carlo calculations, respectively.

Fig. 3.2 - The same as Fig. 3.1 for the case of "streaming motion regime"

Fig. 3.3 - Set of α_{ij} coefficients as a function of the electric field for the case of quasi elastic regime.

Fig. 3.4 - Excess noise temperature as a function of the electric field in Si at $T = 300$ K. The points refer to experiments of Ref. [3.8] and the curve to present theory. The error bars indicate the uncertainty of the calculations.

Fig. 3.5 - Longitudinal diffusion coefficient as a function of field strength for 2D and 3D cases. Horizontal lines indicate equilibrium values for the two cases.

Fig. 3.6 - Drift velocity as a function of field strength for bulk GaAs and the 2D quantum well at room temperature.

Fig. 3.7 - 2D autocorrelation function of velocity fluctuations as a function of time for $E=2,6$, and 10 kV/cm.

Fig. 3.8 - Autocorrelation function of velocity fluctuations at 7 kV/cm and its diagonal associated terms as functions of time for the 2D case (see text) .

Fig. 3.9 - Power spectral density of velocity fluctuations as a function of frequency at room temperature for $E=2,5$ and 10 kV/cm for the 2D case.

Fig. 3.10 - Transient autocorrelation function of velocity fluctuations for the 2D system as a function of τ evaluated at different times t indicated by the numbers on each curve.

Fig. 3.11 - Transient diffusion coefficient as a function of time for the 2D system

at the same fields shown in Fig.3. Electrons are at $t=0$ in equilibrium conditions.

Fig. 3.12 - Transient diffusion coefficient as a function of time for the 2D system.

a) refers to equilibrium initial conditions, b) refers to an initial monoenergetic carrier distribution at 10^3 K.

Figures

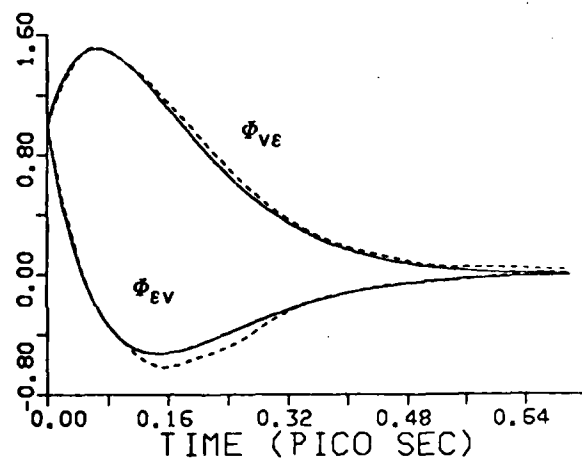
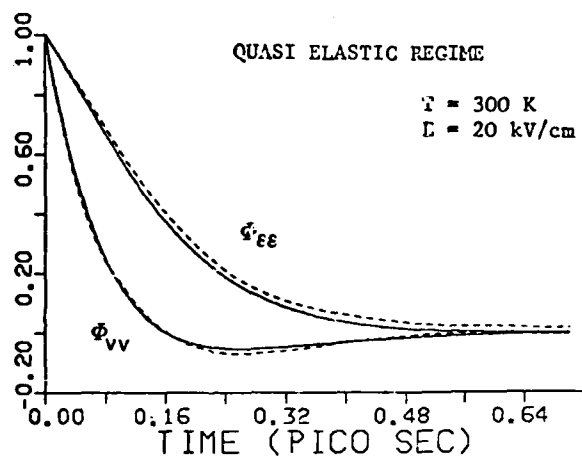


FIG. 3.1

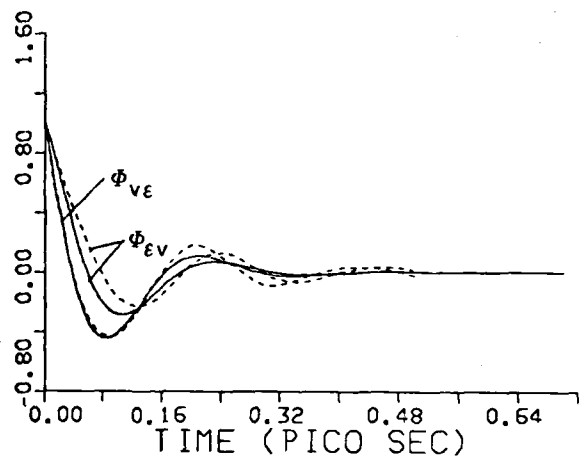
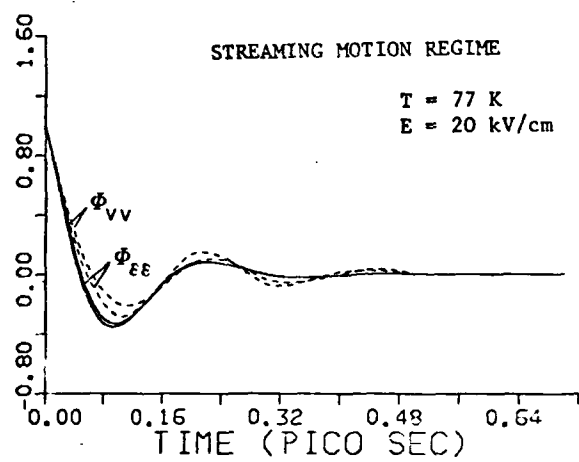


FIG. 3.2

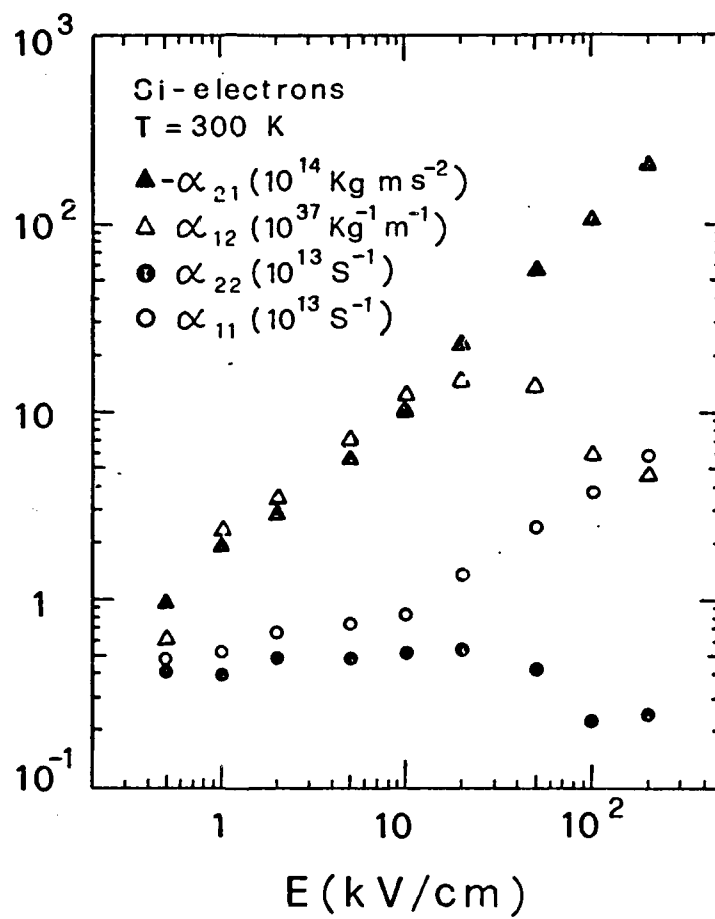


FIG. 3.3

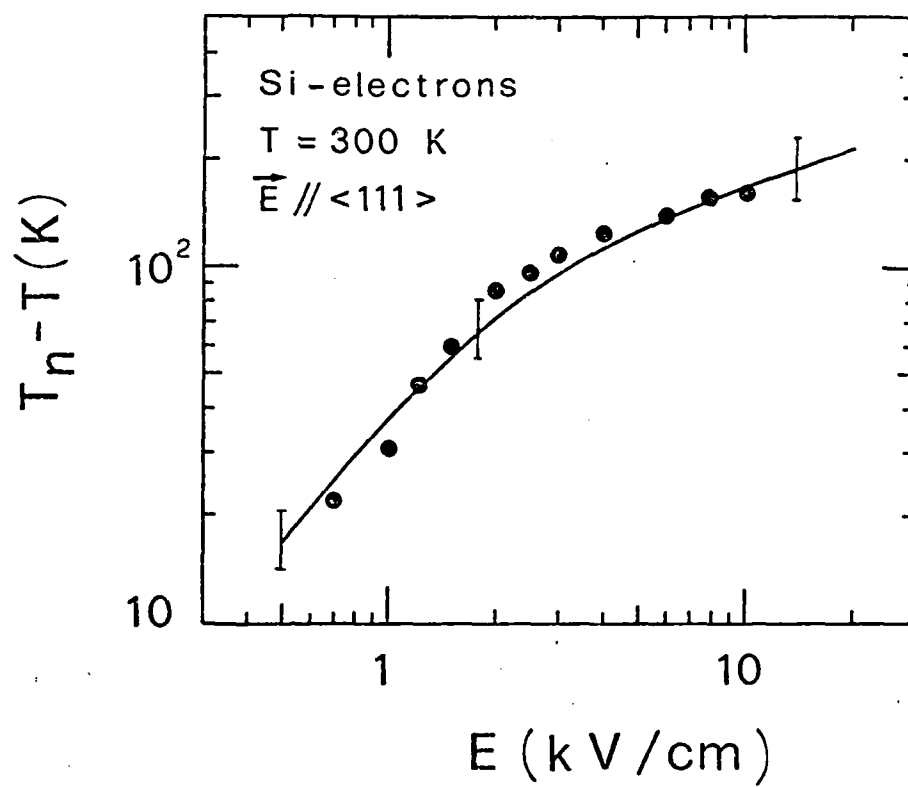
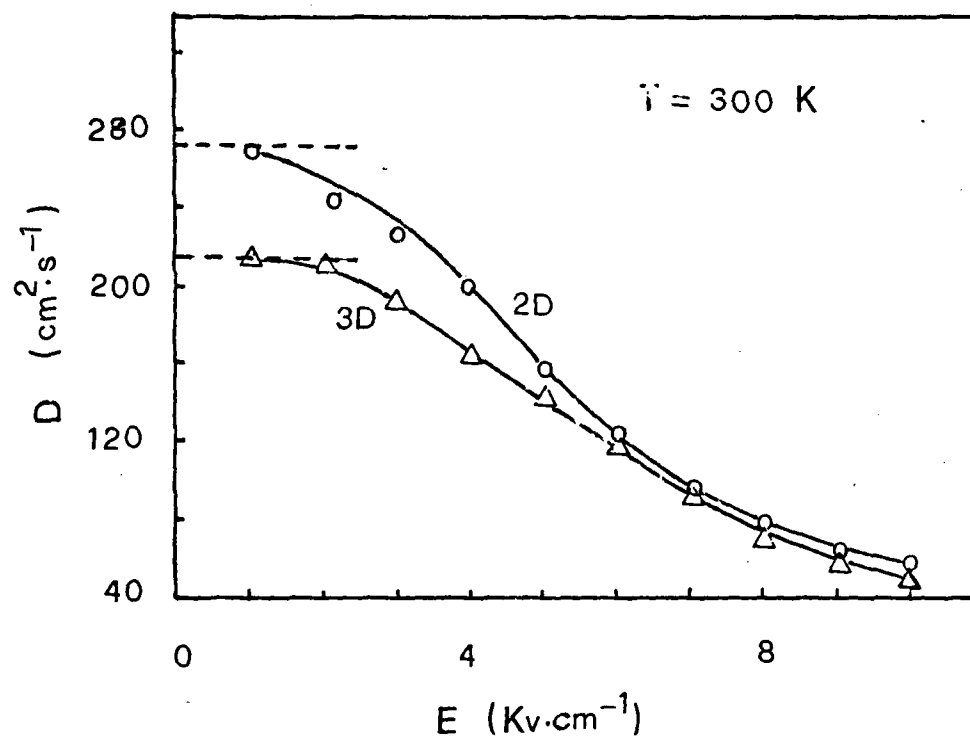


FIG. 3.4



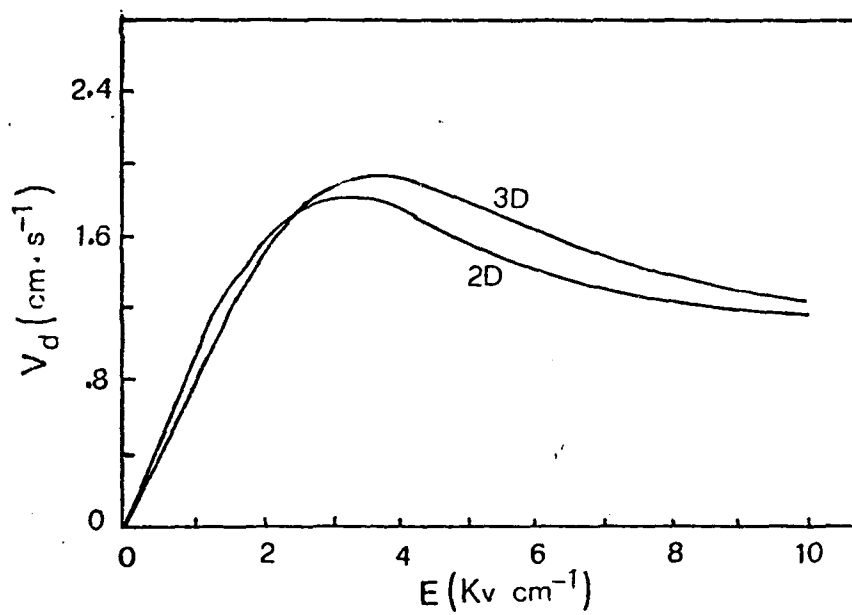


FIG. 3.6

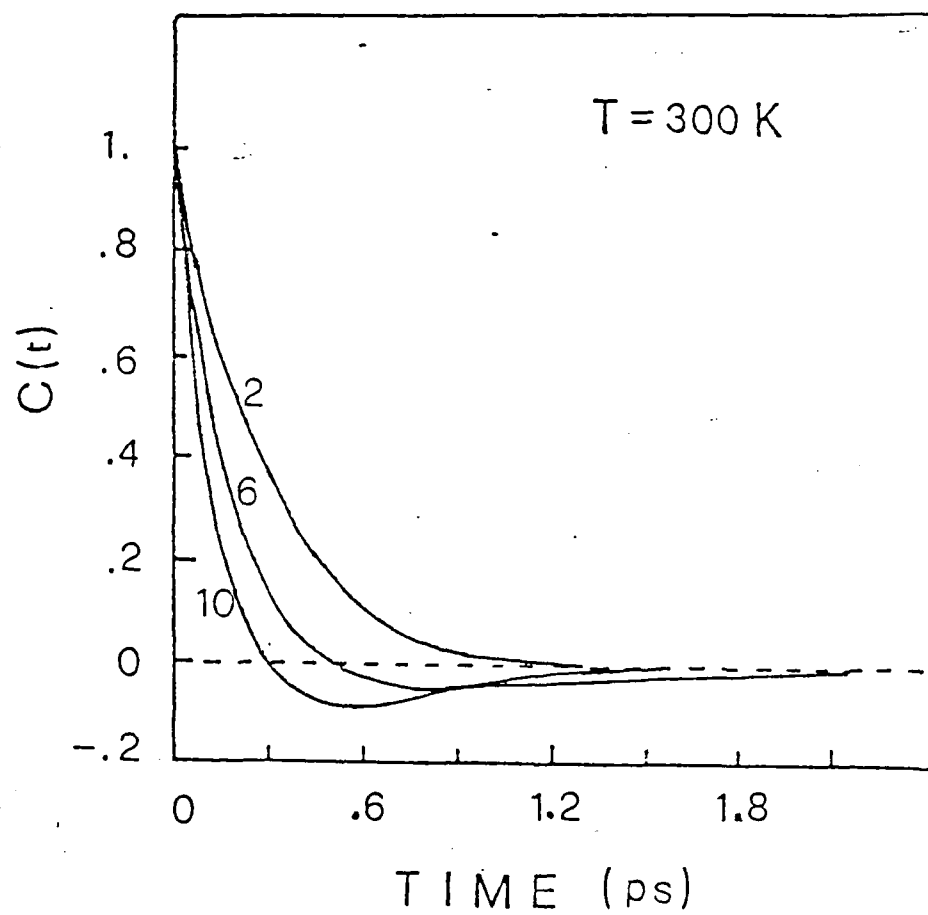
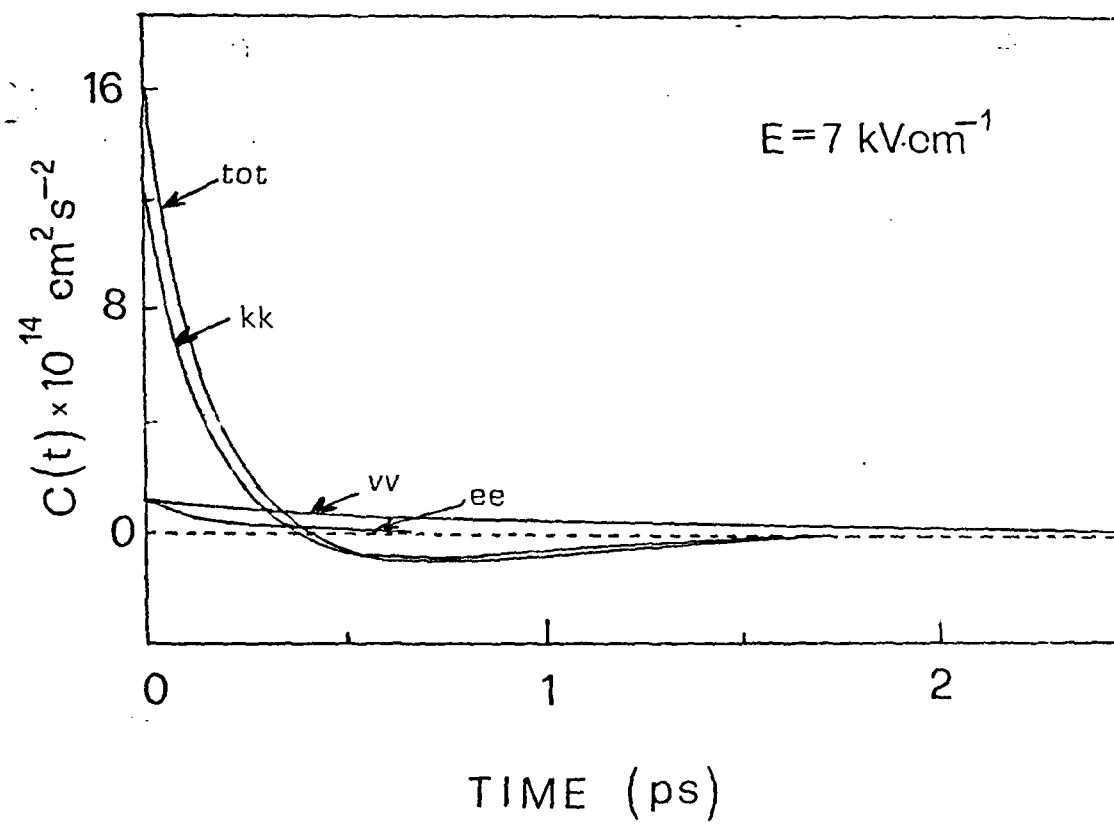


FIG. 3.7



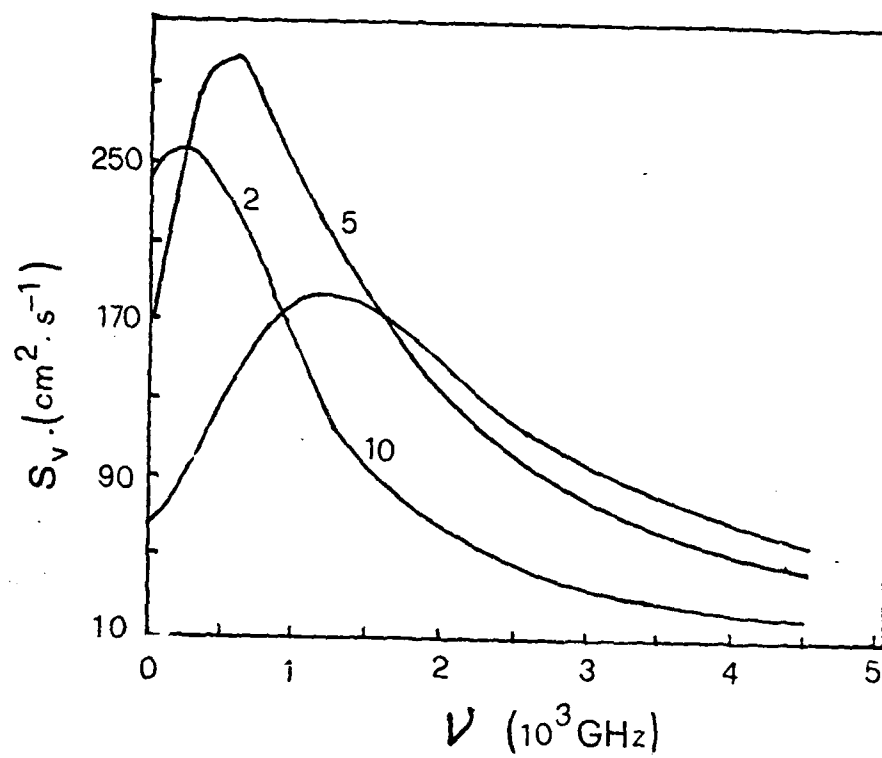


FIG. 3.9

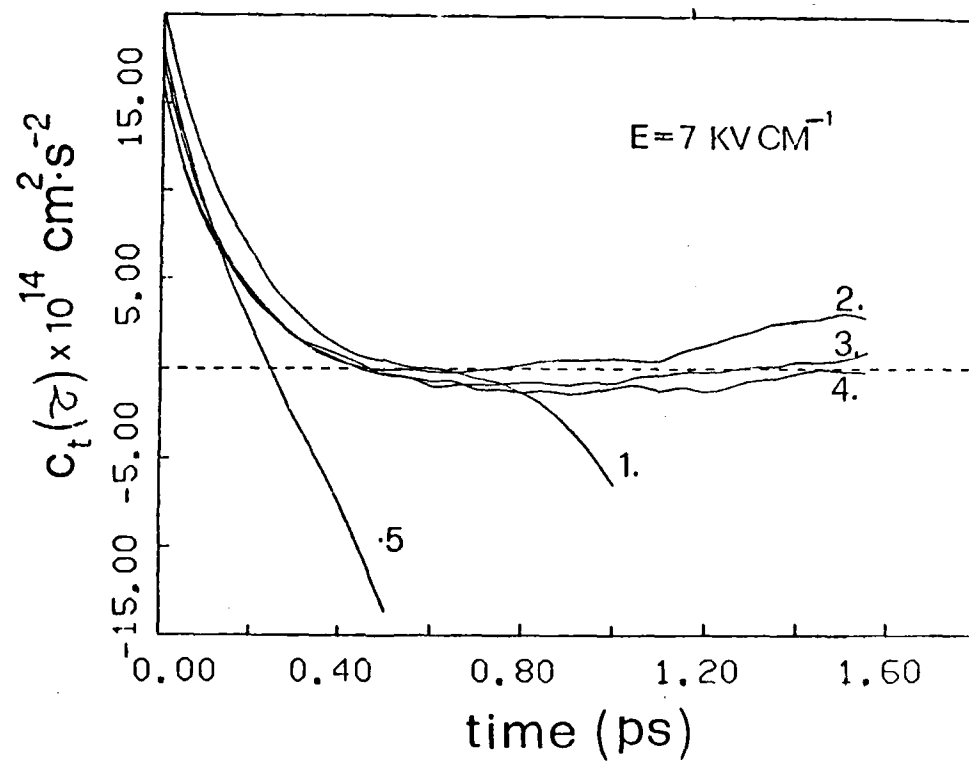


FIG. 2.10

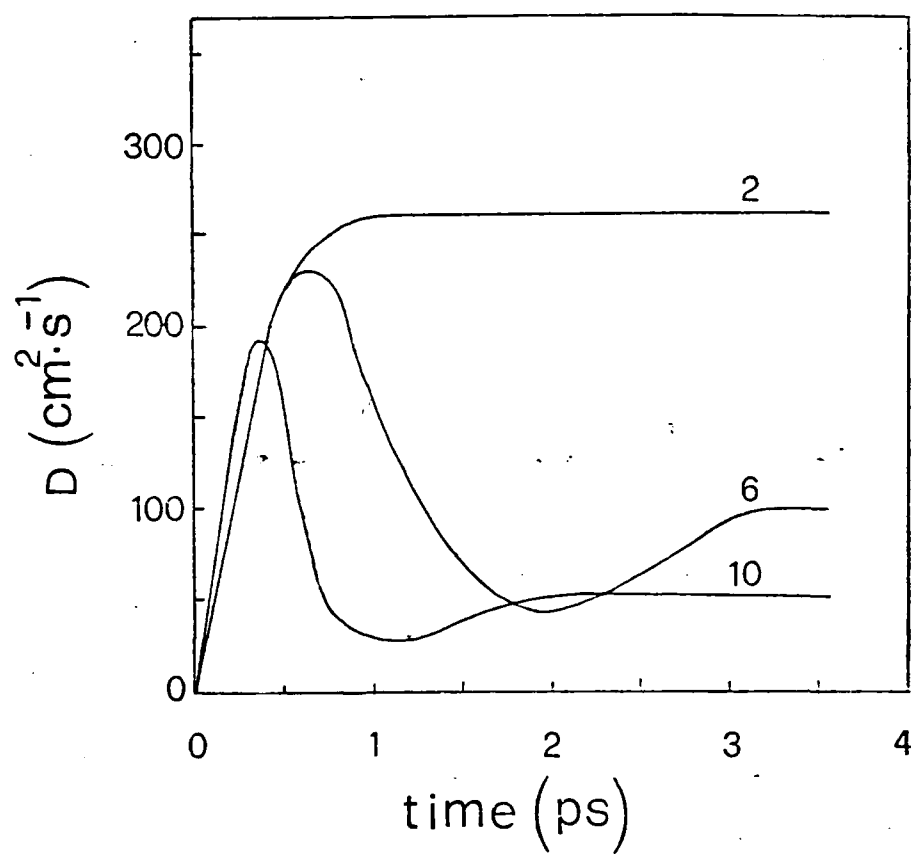


FIG. 3.11

4. MONTE CARLO STUDIES OF NON-EQUILIBRIUM PHONON EFFECTS

4.1 Introduction

In the presence of strong external perturbations (laser excitation, applied electric fields), the energy transferred to a semiconductor drives the carrier system out of equilibrium. Such a situation is usually referred to as hot carrier condition. If the main dissipation channel for the carriers is via phonon emission, then a non equilibrium (hot) phonon population can be found as a result of the energy transfer to the lattice. The presence of phonon amplifications will ultimately depend on the rate at which carriers supply energy to the phonons compared to the rate at which the phonons dissipate their excess energy to the thermal bath. The flux of energy in and out of the carrier system is schematically shown in Fig. 4.1. In general, both type of carriers (electrons and holes) can be present, and channels for energy exchange are provided by their mutual interaction, as well as by their interaction with the lattice. While Raman measurements have been able to detect hot phonon distributions for the case of picosecond and subpicosecond excitations, only indirect and non conclusive evidences exist today on the possibility for the phonon disturbances to feed back into the carrier systems and modify the overall energy transfer process. As the framework of semiclassical transport theory is well suited for the description of the transient dynamics of coupled nonequilibrium carrier-phonon systems, almost all theoretical work on hot phonons has hitherto considered the Boltzmann equation for the phonons with simplifying assumptions about the functional shape of the carrier distributions. The purpose of the present contribution is to circumvent such assumptions by directly solving the coupled Boltzmann equations for phonons and carriers by a Monte Carlo simulation. The advantages of the Monte Carlo technique are that it provides a very accurate

microscopic description of the physical processes, and it does not require any assumption on the electron nor on the phonon distribution functions. Furthermore, a direct evaluation of the characteristic times for the various scattering mechanisms involved in the interaction process is possible. The dynamics of the carrier-phonon system can be extremely complex. For instance, in the case of laser excitation in GaAs, six types of interacting carriers (Γ , L and X electrons, light, heavy, and split-off holes) might be present. Depending on the range of excited densities and on the lattice temperature, different scattering mechanisms can be of importance. Phenomena such as screening of the carrier-phonon interaction, carrier-carrier scattering are thought to dominate the dissipation process at high carrier concentration. Further complications might arise also as a result of plasmon-phonon coupling. It is clear that an exact theoretical treatment of such a system is today out of range, although a big effort is spent in this direction. On the other side, experimental measurements usually give an integrated view that might not allow to isolate the effects of specific phenomena. With this in mind, the present chapter will outline in Sec. 4.2 some of the theoretical approaches that have been pursued, together with the details of the Monte Carlo algorithm. The application of the Monte Carlo procedure to the case of laser excitation in bulk GaAs and GaAs/AlGaAs quantum wells will be discussed in Sec. 4.3. Throughout the chapter, the Monte Carlo analysis will only be limited to situations in which the adopted physical model is justified.

4.2 The Transport Model and the Monte Carlo algorithm

The dynamical evolution of the carrier phonon system can be adequately described by the coupled Boltzmann equations:

$$\frac{df}{dt} = \frac{df}{dt}\bigg|_{field} + \frac{df}{dt}\bigg|_{c-ph} + \frac{df}{dt}\bigg|_{c-c} + \frac{df}{dt}\bigg|_{c-impurity} \quad (4.1)$$

$$\frac{dN_q}{dt} = \left. \frac{dN_q}{dt} \right|_{ph-c} + \left. \frac{dN_q}{dt} \right|_{ph-ph} \quad (4.2)$$

where f and N_q are respectively the carrier and the phonon distribution functions. In the following, only electrons will be considered. Such an assumption is justified as long as the carrier densities are not too high, so that no efficient coupling exist between electrons and holes (electron concentrations always lower than $5 \times 10^{17} \text{ cm}^{-3}$ will be dealt with in the paper). In the same spirit, unscreened electron-phonon interaction will be treated. The time-dependent transport equations for carriers and phonons are coupled through the occurrence in the carrier-phonon collision integrals of both carrier and phonon distribution functions [4.1]. A decisive simplification of the phonon equation comes from the possibility to use a relaxation time for the phonon-phonon interactions, in the form:

$$\left. \frac{dN(q)}{dt} \right|_{ph-ph} = -\frac{N(q) - N_L}{\tau_{op}}, \quad (4.3)$$

where N_L is the thermal Plank distribution

$$N_L = (e^{\hbar\omega/k_B T_L} - 1)^{-1} \quad (4.4)$$

The relaxation time approximation is justified by the fact that the phonon-phonon interactions are dominated by the decay of the LO phonons into pairs of electronically non active phonons from zone-boundary modes. values of the phonon lifetime τ_{op} are generally of the order of 10 ps, with a weak temperature dependence [4.2].

Time-resolved phonon spectroscopy has yield a rather wide range of values for τ , between 7 ps [4.3] and 28 ps [4.4]. The reason for this spread of experimentally determined LO phonon lifetimes seems to have two sources. Firstly, the quality of the sample surface can strongly influence the decay dynamics within the thin light-absorption layer [4.5]. Secondly, the decay rate of a non thermal phonon population might contain strong contributions from the reabsorption by the photogenerated carriers of the initially excited phonons. This

point will be discussed in detail later. Our choice of τ equal to 7 ps at 77 K and 3.5 at 300 K is in agreement with the most recent experimental results [4.6,4.7]. Several theoretical approaches have been presented in the literature for the solution of Eqs. 4.1 and 4.2. Details about the various methods can be found in the references. Certainly one of the most interesting one is due to Collet and Amand [4.8] who directly solved the coupled transport equations through a discretization in q-space and in time to obtain the evolution of the carrier and phonon distributions and of the mean e-h plasma energy during and after 80 femtosecond laser excitation pulses of varying intensity. Another method, called the heated and drifted Maxwellian (HDM) model, is of particular interest here since it originated the Monte Carlo investigation of phonon perturbation. In the HDM approach, the carriers are assumed to be characterized by a heated and drifted Maxwellian distribution. In the first attempt to use a Monte Carlo technique in the study of phonon perturbations, it was assumed that the perturbed distribution function for acoustic phonons of wavevector \mathbf{q} was given by the asymptotic steady-state solution $\bar{N}_{\mathbf{q}}$ of the phonon Boltzmann equation in the presence of a HDM carrier distribution

$$\bar{N}_{\mathbf{q}} = \frac{N_c g_c + N_L g_{ph}}{g_c + g_{ph}}, \quad (4.5)$$

where

$$N_c = \left[\exp\left(\frac{\hbar\omega_{\mathbf{q}} - \mathbf{v}_d \cdot \hbar\mathbf{q}}{K_B T_c}\right) - 1 \right]^{-1} \quad (4.6)$$

a Planck distribution, heated to a carrier temperature T_c and shifted about \mathbf{v}_d . In Eq. (4.5), g_c and g_{ph} are respectively the inverse relaxation time for electronic and non electronic phonon transitions. At a given temperature $\bar{N}_{\mathbf{q}}$ depends basically on three physical parameters which describe the ensemble of the carriers, i.e.: the concentration n_c , the mean drift velocity \mathbf{v}_d and the temperature T_c of the carriers. These parameters contribute in different ways to the

determination of \bar{N}_q . An increase in n_c will lead to an increase of the phonon perturbation. Moreover an increase of v_d will increase the phonon perturbation for modes with wavenumbers within the forward-cone around v_d . An increase of T_c results in an overall increase of \bar{N}_q . Finally, lower lattice temperatures, via Eq.(4.5), also favour the phonon perturbation. To evaluate the effects of the phonon perturbation on the semiconductor transport properties, an iterative scheme was used. Starting a MC simulation with the equilibrium phonon distribution, the values of the carrier mean energy $\langle \epsilon \rangle$ and drift velocity v_d were determined and substitute in Eq. (4.1) to obtain the perturbed phonon distribution. The new scattering rates, accounting for the phonon perturbation, were then calculated numerically and the MC algorithm repeated until convergence was achieved. A semiconductor model parameterized for the case of holes in Ge was used. The effect of the phonon disturbance leads to an increase of both v_d and $\langle \epsilon \rangle$ at low fields and to a decrease of these quantities at higher fields. The reason of this behavior is associated with the competing roles of the anisotropic and of the isotropic contribution to the phonon amplification. When the anisotropic aspect prevails, the phonon-gas drags the carriers whose drift velocity and mean energy increase above their unperturbed value (directional effect of the phonons). When, on the contrary, the net isotropic amplification dominates, the phonon gas most effectively randomizes the motion of the carriers; therefore v_d and $\langle \epsilon \rangle$ are reduced with respect to their unperturbed values.

Fig. 4.2 shows the drift velocity and mean energy as functions of the applied electric field at 4.2 K with and without phonon perturbation.

The method just described was still lacking consistency, since it relied on the assumption of a HDM electron distribution. A full consistent Monte Carlo simulation was developed for the case of photoexcitation in GaAs. The novel procedure allows to follow the time evolution of the phonon distribution.

Preliminary results have been presented in [4.9].

A two-valley (Γ and L) model is used for GaAs (under the conditions considered here X valleys do not contribute significantly). The following scattering mechanisms are considered:

- acoustic phonons with deformation potential coupling ($D_{ac} = 7\text{eV}$), treated exactly according to the procedure given in [4.10];
- polar optical phonons, without screening;
- ionized impurities, treated in the Conwell-Weisskopf formalism;
- intervalley $\Gamma \rightarrow L$ phonons ($D_{iv} = 8 \times 10^8 \text{eV/cm}$); Throughout the paper, nominally undoped materials (with a residual impurity concentration of 10^{14}cm^{-3}) will be considered.
- electron-electron interaction between Γ -valley electrons have been included using the algorithm presented in Ref. 4.11. There, it was also shown that at the low injection densities examined in the present work (typically $5 \times 10^{16} \text{cm}^{-3}$), the effect of the carrier-carrier scattering is negligible.

The laser excitation is reproduced by adding particles to the simulation, distributed in time as the lineshape of the laser pulse, as shown in the insert of Fig. 4.3. The simulation is subdivided in time intervals Δt (with Δt typically much shorter than the average scattering time for the LO phonon scattering). At time $T = j\Delta t$, the number of Monte Carlo electrons is updated from the previous step according to the expression :

$$N(T) = N(T - \Delta t) + C \Delta t \cosh^{-1}(\omega T), \quad (4.7)$$

where ω and C are parameters related to the width and power of the laser pulse.

Electrons are excited in the conduction band centered around a given energy E_{inj} , with a small broadening depending on the width of the laser pulse. Since the excitation energies considered here are below the threshold for intervalley scattering (0.3 eV for Γ to L transitions), there is here no significant

transfer to the satellite valleys.

The LO-phonon distribution function is followed in its time evolution, and phonon-induced modifications to the relaxation rates of the electrons are considered. The disturbances of other types of phonons are negligible in the situation examined here. In a finite difference scheme, Eq. (4.2) for the phonon evolution can be written in the form:

$$N_q(n\Delta t) = N_q((n-1)\Delta t) + \delta N_q(n\Delta t) \Big|_{e-ph} - (N_q(n\Delta t) - N_0) \frac{\Delta t}{\tau_{ph}} ; \quad n = 1, 2, 3... \quad (4.8)$$

The procedure set up to account for the LO-phonon disturbances has the following features:

i) the time evolution of the LO-phonon distribution N_q is calculated as a function of wavevector q from the Monte Carlo simulation, by setting up a histogram h_q defined over a grid in q -space of mesh size Δq . After each scattering event involving an LO phonon, the histogram is updated. In the absence of external d.c. fields, because of the full spherical symmetry only the amplitude of q is relevant, thus reducing the complexity and the storage requirements of the simulation. Preliminary results for the field dependent case have been presented recently [4.12].

ii) At fixed times $T = j\Delta t$ during the simulation, N_q is calculated as

$$N_q(j\Delta t) = \bar{N}_q(j\Delta t) + [\bar{N}_q(j\Delta t) - N_0] \frac{\Delta t}{\tau} \quad (4.9)$$

Here, N_0 is the equilibrium Bose distribution and

$$\bar{N}_q(j\Delta t) = N_q((j-1)\Delta t) + A\Delta h_q. \quad (4.10)$$

The term $A\Delta h_q$ gives the dynamical contribution of the electronic processes to the phonon distribution during the time step Δt . There, A is a normalization

factor accounting for the density of states in q -space and for the concentration of excited electrons, given by

$$A = \frac{2\pi}{q^2 \Delta q} \frac{n}{N}, \quad (4.11)$$

where n is the electron concentration and N the number of simulated particles. The second term on the right hand side of Eq. (4.9) accounts for the phonon-phonon processes. The algorithm for the phonon counting can be viewed as a hybrid Monte Carlo solution of the phonon Boltzmann equation within a finite difference scheme.

iii) to account for the modifications induced by the phonon disturbance on the rate of electron-phonon scatterings, the integrated scattering probabilities for LO-phonons are calculated and tabulated at the beginning of the simulation using an artificially high value N_{max} for the phonon distribution. The choice of the final state of each scattering process involving an LO phonon is made using a rejection technique which compares the actual value of the differential scattering rate with the maximized one. In this way, we are able to discriminate between the scatterings that can be attributed to the enhanced phonon distribution versus those induced by the initial maximization (which are treated as self-scatterings in the simulation). In order to reduce the number of self scattering events , it is possible to recalculate the scattering rates at fixed times during the simulation. A numerical integration over the perturbed phonon distribution function gives the exact scattering rates at a given time, which can be used directly on the simulation.

The suggested procedure is a full Monte Carlo simulation of the dynamics of an interacting electron-phonon gas within the finite difference scheme indicated above, free of adjustable parameters. In the next section, the results of the Monte Carlo simulation in the presence of laser excitation will be presented. The application of the algorithm in the presence of an applied electric field will

be presented in a separate contribution. In that case, a two dimensional grid is used to describe the perturbed distribution.

4.3 Applications

The question of possible effects of nonequilibrium optical phonon distributions on the dynamics of optically excited charge carriers in semiconductors is becoming a widely investigated and debated topic. The main scientific motivation came from the rapid development of picosecond and subpicosecond laser spectroscopy, which allows to study even the fastest relaxation phenomena in solids and thereby also some fundamental hot carrier-hot phonon processes which might ultimately limit the switching efficiencies of ultrafast electronic devices. The algorithm described in the previous section has been applied to various situations to study the dynamics of the LO phonon, of the electron distributions, and their mutual effects. The time evolution of the perturbed phonon distribution is shown in Fig. 4.3 for an excited carrier density of $5 \times 10^{16} \text{ cm}^{-3}$. Electrons are excited at 0.25 eV above the bottom of the conduction band, corresponding to a photon energy of 1.8 eV. The lattice temperature is 77 K. The lineshape of the laser pulse is shown in the insert (halfwidth = 0.8 ps). The LO distribution is driven out of equilibrium even during the excitation, due to the fast power dissipation of the high-energy photoexcited electrons. The maximum is reached at a delay time of 1 picosecond for wavevectors of about $6 \times 10^5 \text{ cm}^{-1}$. The small q values that are amplified during and immediately after the excitation are due to the polar nature of the e-phonon coupling. At longer times, the phonon distribution relaxes towards its equilibrium value as a result of two distinct processes, phonon reabsorption and phonon-phonon interaction. The first one is due to the fact that the group velocity of optical phonons is very small (less than 10^3 cm/s), implying that the phonons cannot drift away

of the excitation volume during their lifetime. Therefore, if the phonon lifetime is long enough and the coupling with the carriers sufficiently strong, emitted phonons can be reabsorbed.

It is important to notice that modes of different wavevector evolve in time in different ways, as indicated in Fig. 4.4. Those with the smaller q ($6 \times 10^5 \text{ cm}^{-1}$) exhibit an exponential decay, immediately after the end of the excitation, with a characteristic decay time of 7 ps. At intermediate q 's (8 and $10 \times 10^5 \text{ cm}^{-1}$) the phonon distribution decay much faster at short times (up to 5 and 8 ps delay), approaching then the exponential behavior. The amplification of these large- q phonons is not as pronounced as that of the small- q ones.

The time evolution of the phonon distribution reflects the microscopic details of the cooling processes in the coupled electron-phonon system. While phonon-phonon processes are always active, and their effect is independent of wavevector, phonon reabsorption varies drastically as a function of time and wavevector. In fact, the very rapid changes in the electron distribution function (that will be examined below) modify the range of phonon transitions that are allowed by energy and momentum conservation. Fig. 4.5 shows the minimum q for LO-phonon absorption and emission as a function of electron energy in a parabolic band. At high energy, electrons can emit phonons with very small q , but as they cool the minimum allowed q shifts at higher values. Such a shift appears in Fig. 4.3, hidden though by the strong initial amplification. Furthermore, an electron will not be able to reabsorb the earlier emitted phonons once it goes below a certain energy.

This simple analysis explains why the phonons with small q -vector excited during the first stages of the electron relaxation (up to 2 ps delay time) cannot be reabsorbed, and decay exponentially via non-electronic processes.

On the other side, both the reabsorption and the phonon-phonon terms will contribute to the damping of phonons of larger wavevector in the first few

picoseconds, leading to their faster decay over this time interval.

The modification of the scattering rates for the electron-LO phonon interaction due to the phonon perturbation is presented in Fig. 4.6. There the total scattering rates for absorption and emission, obtained from a numerical integration over the perturbed distribution function N_q , are plotted at different time delays after the end of the laser pulse. Since at low temperature the value of the equilibrium phonon distribution is much smaller than unity, the emission probability is a few orders of magnitude higher than the absorption one. As the phonon population grows out of equilibrium, the absorption rate increases dramatically, relatively much faster than the emission one. The changes of the scattering rate with time reflect the temporal evolution of the phonon population. It is important to notice that even a few picoseconds after the pulse, a significant amount of phonons is still present and a considerable number of phonon reabsorptions are detected.

The time evolution of the electron distribution function, shown in Fig. 4.7, completes the previous analysis of the phonon amplification. The distinct peaks in the distributions at short time delays (0 and 1 ps) are due mainly to LO phonon emission which sets up already during the laser pulse (an average time of 160 fs for the emission of an LO phonon by electrons at the excitation energy is calculated from the simulation). At a time delay of 4 ps, the electrons mainly populate the low energy region below 100 meV. Many of them have an energy below the threshold for LO phonon emission. It will be seen later that in this case reabsorption can become very important.

As a last remark on the phonon dynamics, it is important to compare the previous considerations with the experimental results of Raman spectroscopy. The shaded area in Fig. 4.5 indicates the range of raman-active wavevectors for the data given in Refs. [4.6,4.13]. The Monte Carlo result for those modes (curve x in Fig. 4.4) are in good qualitative agreement with the findings of Kash et

al. [4.6], obtained for the same electron concentration but a higher excitation energy.

The effect of the phonon perturbation on the cooling of the photoexcited electrons is shown in Fig. 4.8. The electron relaxation rate is drastically reduced because of the presence of non-equilibrium phonons. The phenomenon is mainly due to the reabsorption of the LO phonons that have been emitted in the first stage of the relaxation without having had enough time to decay. The effect of phonon reabsorption grows with time as the electrons populate the low energy regions below the threshold for optical emission. It has also been found that the reduction in the cooling rate of the electrons is even larger at higher electron densities or higher injection levels.

The Monte Carlo algorithm presented here has been compared with the models of Ref. 4.14 and 4.5. At the low excitation energies used in Ref. 4.15, the phonon disturbance is reduced with respect to the case shown in Fig. 4.3., and reaches its maximum at higher q 's. The Monte Carlo result agrees quite well with ones of the more sophisticated model of Collet et al.

The temperature model of Ref. 4.14 assumes that the carriers (electrons and holes) are characterized by a Fermi-Dirac distribution at any time during and after the laser pulse, corresponding to a very fast thermalization within the photogenerated plasma. In order to verify the consistency of our results, we have performed a simulation by assuming that the carriers are initially distributed according to a heated maxwellian distribution. The Monte Carlo results obtained using the same parameters of Fig. 4.3 indicate in this case a much smaller phonon perturbation, with the maximum of the phonon distribution still reached at 1 picosecond delay time as in Fig. 4.3, but its value is reduced by a factor two. The reduction of phonon heating is related to the increased population of the low energy tails of the maxwellian distribution compared to the quasi monoenergetic distribution used before. The Monte Carlo

results agree very well with those of the temperature model, for a one component system. When both electrons and holes are considered, the temperature model (which assumes the same temperature for both carriers) shows a further reduction of phonon heating, which indicates a strong energy transfer from the electron to the hole system, which then dissipate mainly via TO emission. Although the latter result depends heavily on the assumptions of the model, it nevertheless shows that the e-h interaction can be very important. A preliminary step to combine the effect of e-h scattering and non equilibrium phonons has been recently presented [4.16]. The results just shown refers to the simple case of GaAs, where only the central valley is important. In general, especially if the excitation energy is sufficiently high, the population of the higher valleys (L and X) is not negligible. The influence of such effect on the phonon population can be very strong. Fig. 4.9 shows the minimum q for LO phonon emission as a function of electron energy for the Γ (same curve as Fig. 4.4) and the L valleys. Due to the higher effective mass of the satellite valley, the emitted LO phonons have a larger wavevector. Since the area of phase-space is increased, their contribution to the phonon population will be reduced. This is illustrated in Fig. 4.10, where an initial electron energy of 0.5 eV has been used (with a $\Gamma - L$ separation of 0.3 eV). The parameters of the simulation are the same as before. After 1 picosecond from the excitation, about 60 percent of the electrons are found in the L valley. The Monte Carlo histogram (Fig. 4.10a) confirms that the emission of LO phonons by L -valley electrons is concentrated in the large q region. The actual number of phonons reflects indeed the relative population of the two valleys. Nevertheless, the effect of those phonons on the perturbed distribution (Fig. 4.10b) is negligible. Furthermore, all of the L -valley phonon have q values too large to be detected spectroscopically. We can therefore expect that phonon amplifications experimentally detected would decrease when a relevant number of intervalley transfers is present.

Recent results obtained with time resolved photoluminescence have shown dramatically reduced energy relaxation rates for photo-excited electrons in GaAs-AlGaAs quantum wells [4.17 , 4.18]. It is still an open question whether the slow cooling rates are due to the presence of non-equilibrium phonons or to the effect of reduced dimensionality and screening [4.19,4.20]. The algorithm just presented has been applied to a single quantum well of GaAs-AlGaAs ($t_w = 150 \text{ \AA}$, $\phi_B = 0.28 \text{ eV}$), with subband energies given by the solution of the one dimensional wave equation for a square well potential. The bands are assumed parabolic. The scattering rates of the quantized 2D electrons with bulk unscreened LO-phonon (both intra- and intersubband) are calculated numerically without the use of momentum conserving approximations [4.21]. It has been shown [4.21] that, for wells larger than 100 Å, very little difference exist from the scattering rates calculated accounting for phonon confinement (slab modes) and the one obtained using bulk modes. Intervalley transfer to the L-valleys (also quantized) is included as well. 2D electron-electron scattering is introduced in the Monte Carlo simulation through a generalization of the self-scattering technique given in Ref. 4.22 to the multi-subband quantized system [4.23]. The various electrons are allowed to interact via a statically screened Coulomb interaction determined by the long wavelength limit of the two-dimensional Lindhard dielectric function. Degeneracy effects due to the Pauli exclusion principle are also considered [4.24]. In the present simulation we have neglected electron-hole scattering and recombination, which might be of importance in some of the reported experiments.

In order to include non-equilibrium LO phonons in the Monte Carlo simulation, we generalize to two-dimensional systems the procedure described earlier for bulk GaAs. The phonon distribution is given directly by a detailed balance of the emission and absorption events during the simulation on a grid in q-space with the excess LO phonon population in each mode decaying via a

phenomenological phonon lifetime of 7 ps. Since no direct measurement of LO phonon lifetime in quantum well systems is available at this time, the measured bulk value is used. In 2D, the component of the phonon wavevector in the direction of the well, q_z , is not conserved. For a square well, however, it has been shown that the q_z component is very peaked for wavevectors corresponding to the change in intersubband energy during the transition [4.14]. Therefore, the phonon distribution is tabulated for discrete q_z corresponding to the various inter- and intrasubband events, with the phonon wavevectors otherwise treated as two-dimensional.

The cooling of photoexcited electrons in an n-type GaAs-AlGaAs quantum well at low temperature (5 K) has been considered [4.25, 4.26]. A background density of $2.5 \times 10^{11} \text{ cm}^{-2}$ is used. The injected density is $5 \times 10^{11} \text{ cm}^{-2}$. The GaAs parameters are the same as for the bulk case. The width of the simulated laser pulse is about 1 ps, during which time carriers are added to the simulation with an initial energy of 0.25 eV above the bottom of the lowest subband. Fig. 4.11 shows the evolution of the electron total energy (kinetic plus potential) as a function of time during and after the pulse. The excited electrons lose energy mainly through the interaction with the background electrons and through the emission of LO phonons. Without hot phonons, the hot electrons are found to reach equilibrium in about 3 ps. In contrast with the case of an unperturbed phonon distribution, a much slower relaxation is found when non-equilibrium phonons are accounted for. The two cases in Fig. 4.11 correspond to different quantum wells. It is clear that no real dependence on well width has been found in the Monte Carlo result. The total electron energy plotted here is calculated as an ensemble average during the simulation. For degenerate systems, this quantity can vary considerably from the electron temperature, which can be rigorously defined only in the presence of a fermi distribution. the electron temperature calculated from the average energy, assuming the distribution function is fermi-

like, (dashed curve) correspond to the slope of the tail of the distribution. The reduction of the electron cooling rate is due to the reabsorption of non-equilibrium phonons which build up during the initial pumping and the first stage of the electron relaxation. This is evidenced by the time evolution of the phonon distribution at $q_z=0$ (intra subband scattering) shown in Fig. 4.12. The same, although reduced, features are found also at $q_z \neq 0$. LO-phonon emission during the pulse and immediately after creates a large population of phonons at small q 's. At longer times, phonon reabsorptions and phonon-phonon losses drive the distribution back to equilibrium. The secondary peak that develops at later times in the phonon distribution is due to phonon emission by electrons that have already relaxed to lower energy.

As pointed out before, the reduction in the electron relaxation rate is mainly due to reabsorption of the emitted LO-phonons. The effect is stronger when a considerable number of electrons have relaxed to the low energy region below the emission threshold.

Shortly after the end of the laser pulse ($t = 1.6$ ps), the strong intercarrier scattering creates a broad distribution where the subband minima (indicated by arrows) clearly appear. Within each subband, the distribution function starts to exhibit a Fermi-like appearance which is fully established at longer times as shown in the bottom curve.

4.4 Conclusions

In summary, a full Monte Carlo technique for the study of electron and phonon dynamics in bulk GaAs and GaAs-AlGaAs quantum wells has been presented. A strongly perturbed phonon distribution is found in the first picoseconds after the laser pulse, which is responsible for a reduction of the cooling rate of the photoexcited carriers. Good qualitative agreement with Raman data

is found.

References

- 4.1 E. Conwell, "High Field Transport in Semiconductors", Academic Press (1967).
- 4.2 P. G. Klemens, Phys. Rev. **148**, 845 (1966).
- 4.3 D. von der Linde, J. Kuhl and H. Klingenberg, Phys. Rev. Lett. **44**, 1505 (1980).
- 4.4 Mooradian and G. B. Wright, Sol. St. Comm., **4**, 431 (1966).
- 4.5 T. C. Damen, R. C. C. Leite, and J. Shah, Proc. X Int. Conf. Semicon., Eds. S. P. Keller, J. C. Hensel, F. Stern, (U.S. Atomic En. Comm., 1970).
- 4.6 J.A. Kash, J.C. Tsang and J.M. Hvam, Phys. Rev. Lett. **54**, 2151 (1985).
- 4.7 E. O. Gobel, private communication.
- 4.8 J. Collet and T. Amand, J. Phys. Chem. Solids **47**, 153 (1986).
- 4.9 P. Lugli, C. Jacoboni, L. Reggiani, and P. Kocevar, to be published in Appl. Phys. Lett.
- 4.10 C. Jacoboni and L. Reggiani, Rev. Mod. Phys., **55**, 645 (1983).
- 4.11 P. Lugli and D.K. Ferry, Physica **134B**, 364 (1983).
- 4.12 M. Rieger, P. Kocevar, P. Bordone, P. Lugli and L. Reggiani, to be published in Solid State Electron.
- 4.13 C. L. Collins and P. Y. Yu, Phys. Rev. **B30**, 4501(1984).
- 4.14 W. Poetz and P. Kocevar, Phys. Rev. **B28**, 7040 (1983).
- 4.15 J. Collet and T. Amand, J. Phys. Chem. Solids **47**, 153 (1986).
- 4.16 M. A. Osman, H. L. Grubin, P. Lugli, M. J. Kann, and D. K. Ferry, to be published in "Picosecond Electronics and Optoelectronics", Springer-Verlag (1987).
- 4.17 J. F. Ryan, R. A. Taylor, A. J. Turbefeild, and J. M. Worlock, Surf. Sci. **170**, 511 (1986)
- 4.18 Z. Y. Xu, and C. L. Tang, Appl. Phys. Lett. **44**, 692 (1984)

- 4.19 C. H. Yang, J.M. Carlson-Swindle, S. A. Lyon, and J. M. Worlock, Phys. Rev. Lett. **54**, 2045 (1986).
- 4.20 J. Shah, A. Pinczuk, A. C. Gossard, and W. Wiegmann, Phys. Rev. Lett. **54B**, 2045 (1985).
- 4.21 F. A. Riddoch, and B. K. Ridley, J. Phys. C: Solid State Phys. **16**, 6971 (1983)
- 4.22 R. Brunetti, C. Jacoboni, A. Matulionis, and V. Dienys, Physica **134b**, 369 (1985)
- 4.23 S. M. Goodnick, and P. Lugli, to be published in Phys. Rev. B
- 4.24 S. Bosi, and C. Jacoboni, J. Phys. C. **9**, 315 (1976)
- 4.25 S.M. Goodnick and P. Lugli, in 'High Speed Electronics', Eds. B. Kallbak and H. Beneking, p. 116, Springer Verlag, Berlin (1986)
- 4.26 S.M. Goodnick and P. Lugli, in Proc. of XVIII Int. Conf. Phys. Sem., Ed. O. Engstrom, p. 1335, World Scientific, Singapore (1986).

Figure Captions

Fig. 4.1 Schematic representation of the energy flux inside and outside a semiconductor.

Fig. 4.2 Drift velocity and mean energy as functions of the electric field strength for holes in Ge at 4.2 K for the indicated impurity concentration N_I . Dashed (continuous) curves refer to an unperturbed (perturbed) phonon distribution function.

Fig. 4.3 Non-equilibrium LO phonon distribution functions at three different delay times as a function of the phonon wavevector. The insert shows the shape of the laser pulse.

Fig. 4.4 Time evolution of four different modes as a function of delay time.

Fig. 4.5 Energy dependence of the minimum wavevector for absorption and emission of LO phonons, as a function of energy in a parabolic band. The shaded areas indicate typical Raman active phonon wavevectors.

Fig. 4.6 Absorption and emission scattering rates for LO phonons as a function of energy, at different times after the laser pulse.

Fig. 4.7 Time evolution of the electron distribution function, at different delay times.

Fig. 4.8 Average electron energy as a function of time with (continuous curve) and without (dashed curve) hot-phonons.

Fig. 4.9 Energy dependence of the minimum wavevector for absorption and emission of LO phonons, as a function of energy in a parabolic band for Γ and

L valley.

Fig. 4.10 Monte Carlo histogram and perturbed LO phonon distribution 1 ps. after the excitation ($E_{inj} = 0.5\text{eV}$).

Fig. 4.11 Average electron energy as a function of time during and after the laser excitation for two different excitation densities. The electron temperature is shown by the dashed line.

Fig. 4.12 LO Phonon distribution as a function of total parallel momentum (for $q_{\perp} = 0$) for times during and after the laser excitation.

Figures

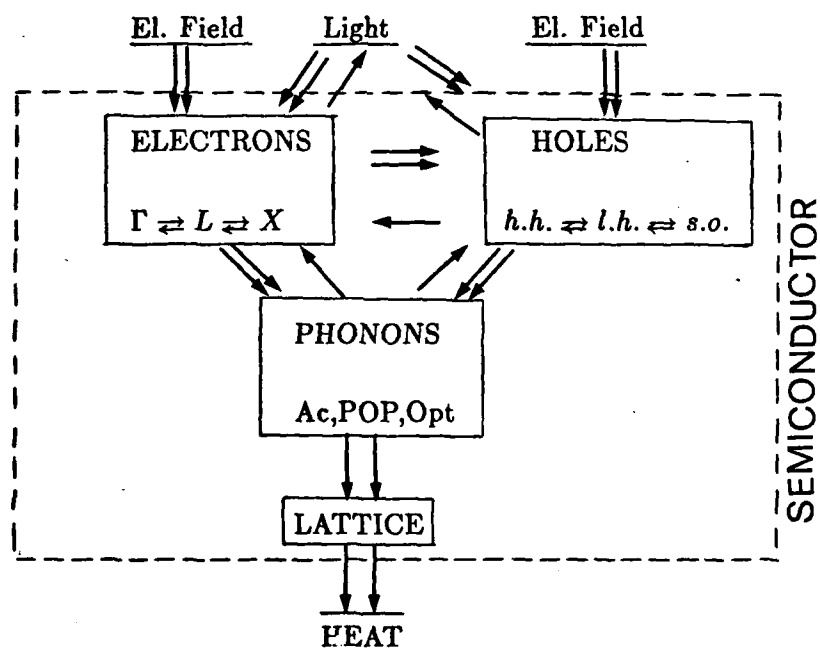


FIG. 4.1

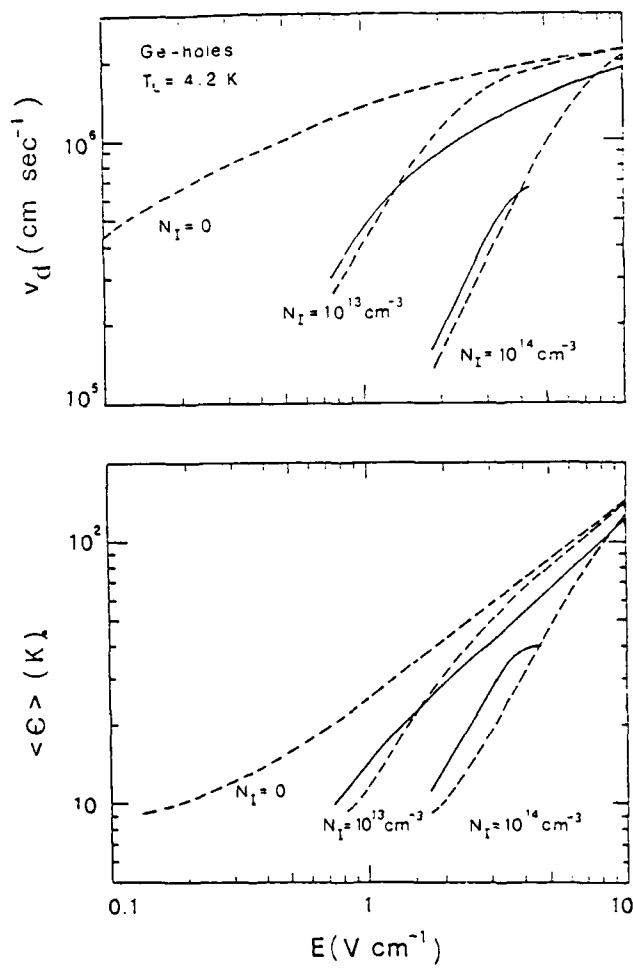


FIG. 4.2

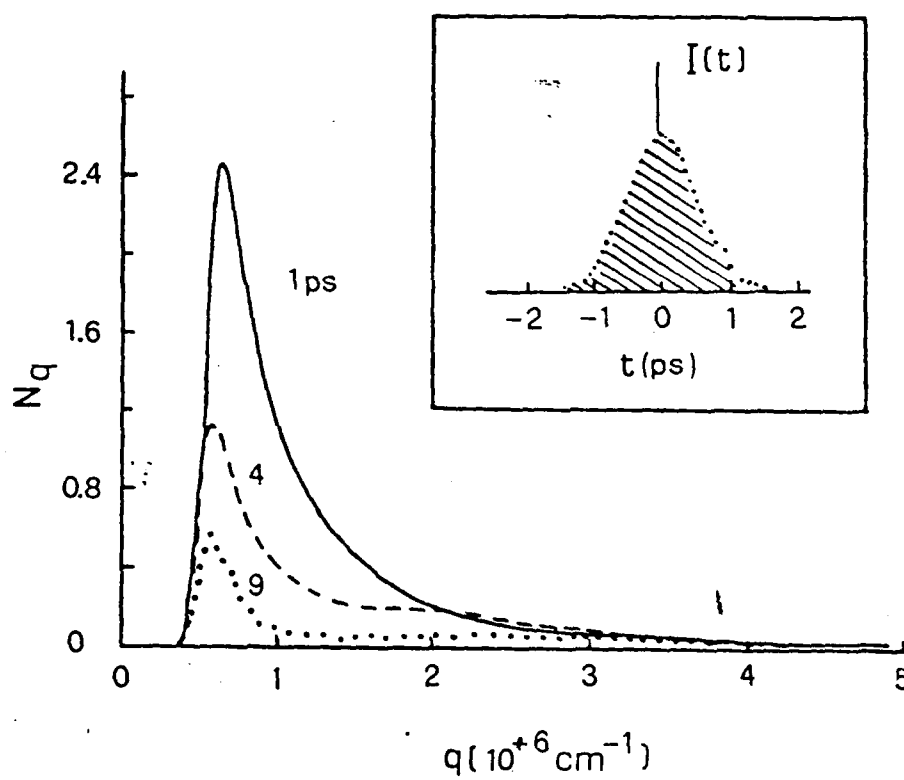


FIG. 4.3

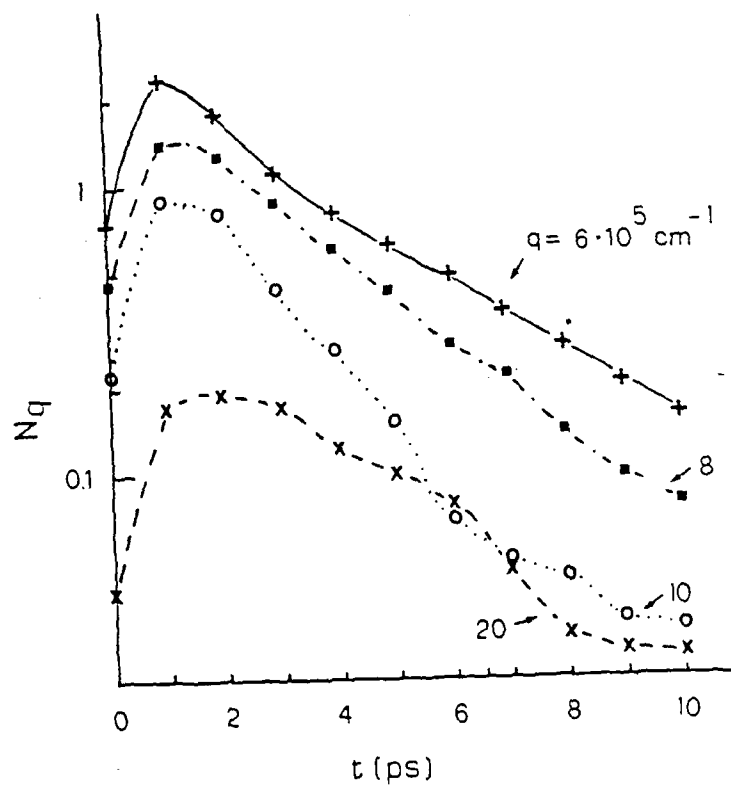


FIG. 4.4

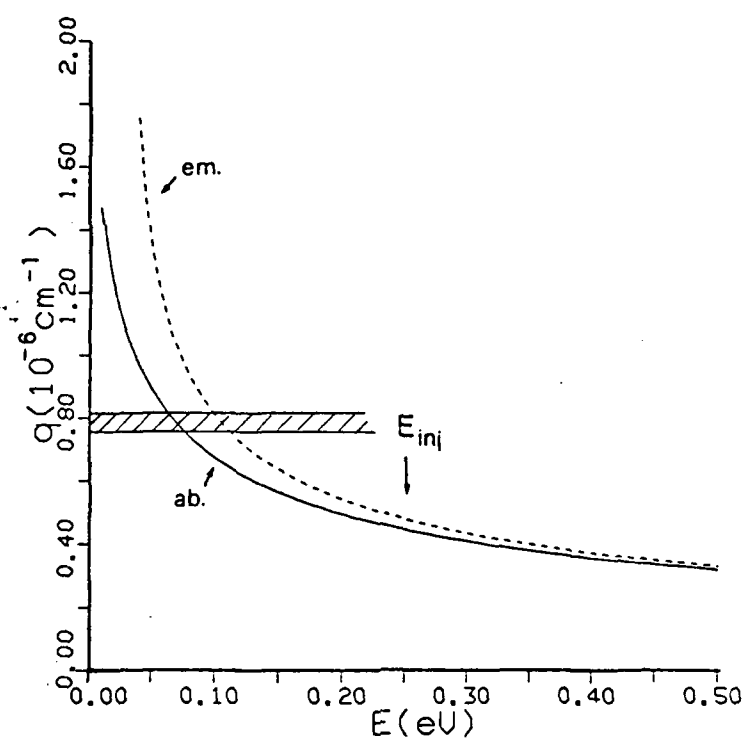


FIG. 4.5

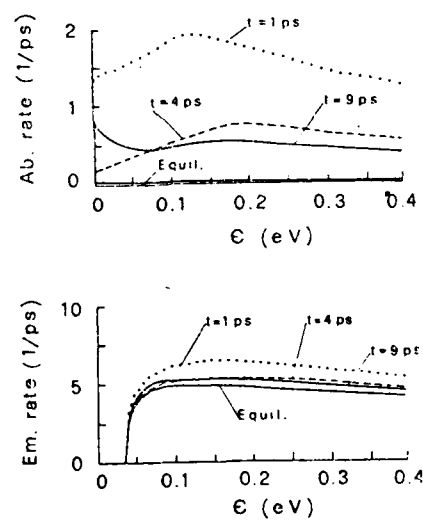


FIG. 4.6

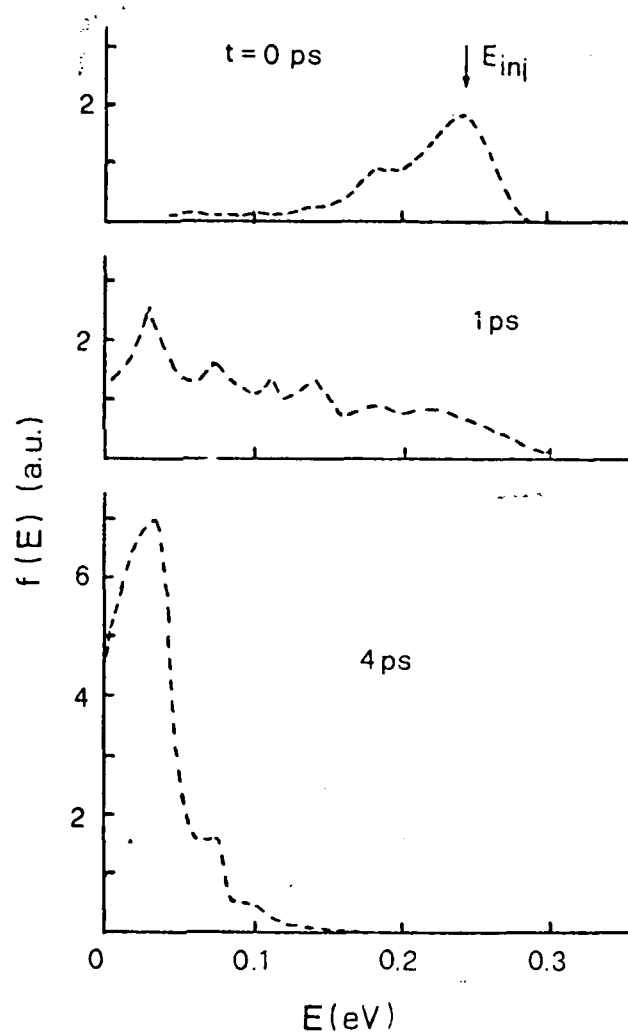


FIG. 4.7

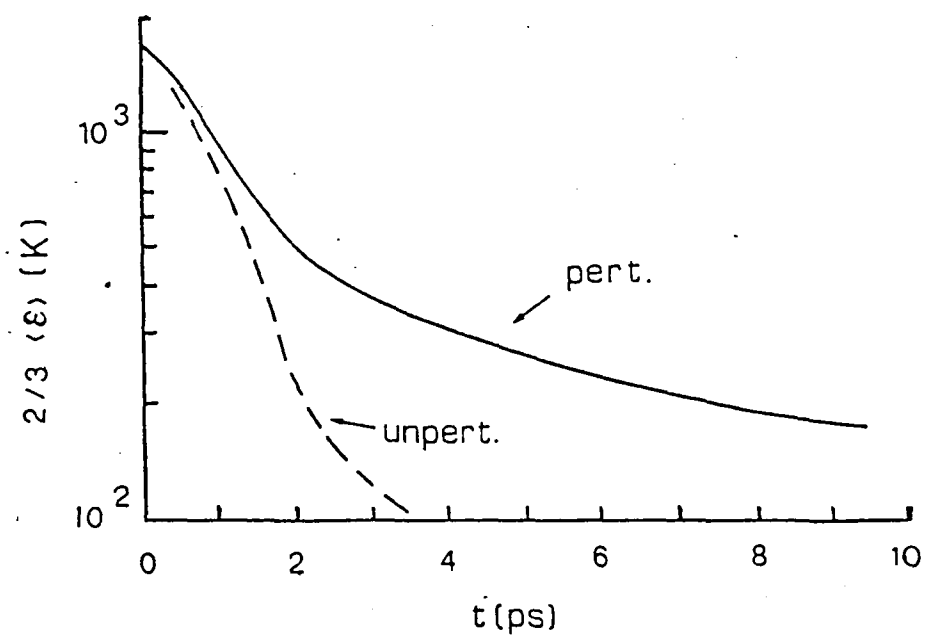


FIG. 4.8

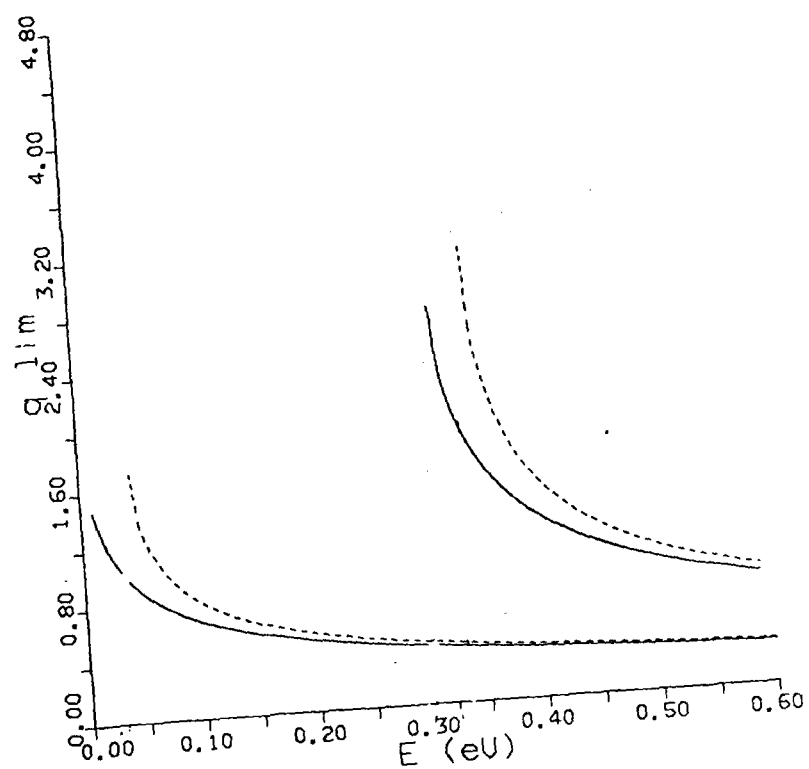


FIG. 4.9

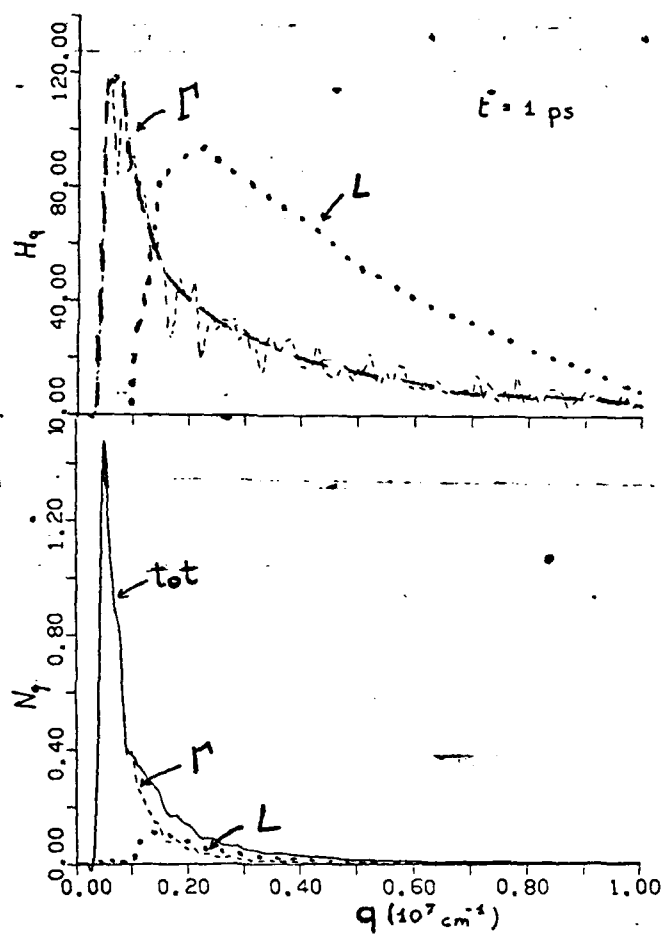


FIG. 4.10

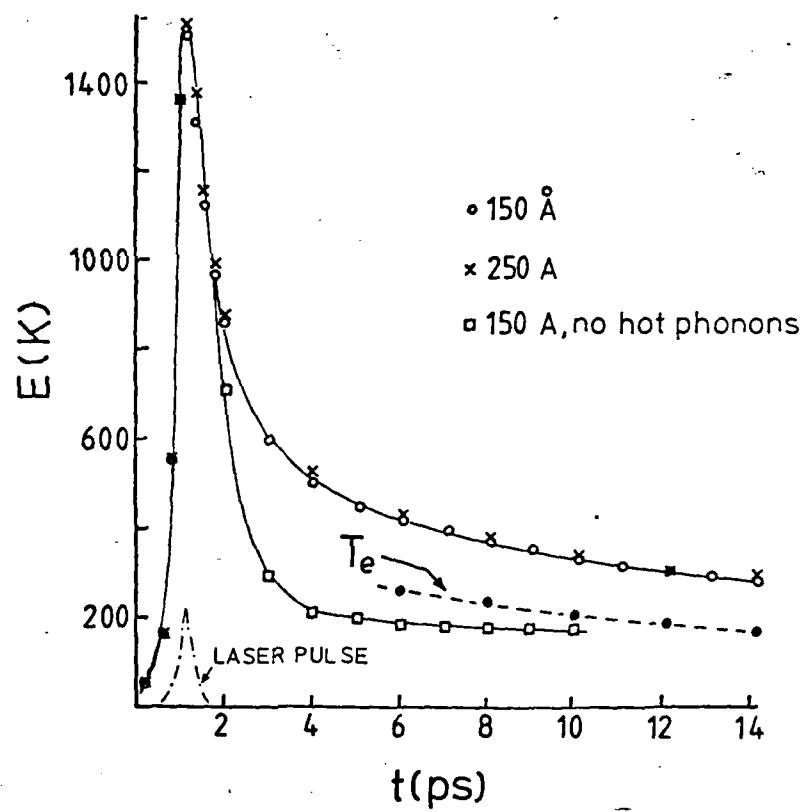


FIG. 4.11

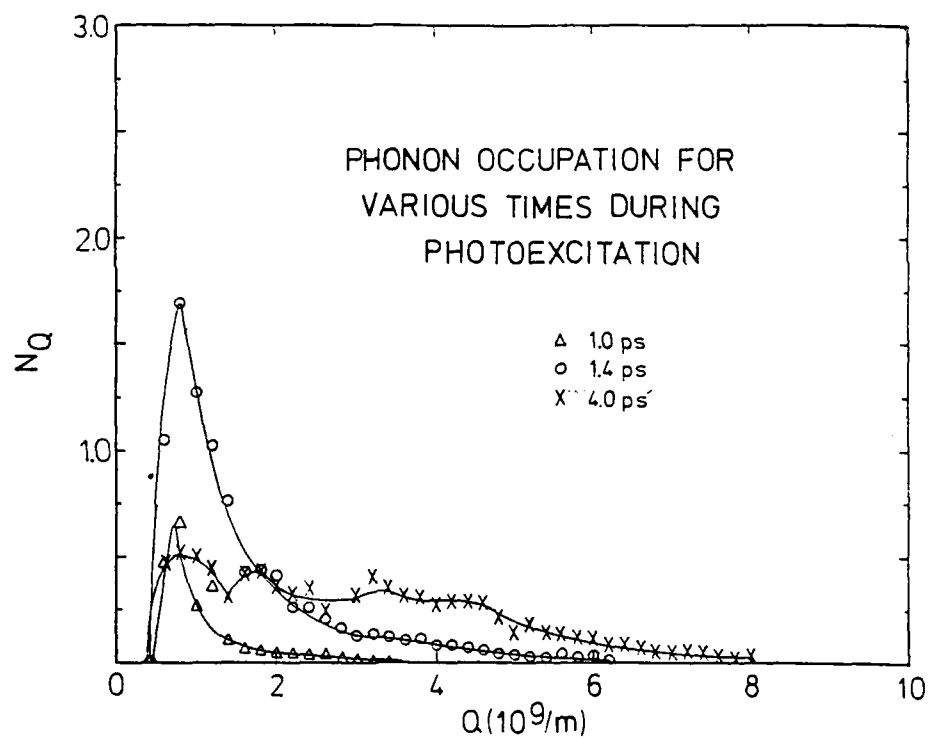


FIG. 4.12

END
DATE